2001

The magmatic evolution of the upper ~3450 Ma Hooggenoeg Formation, Barberton greenstone belt, Kaapvaal Craton, South Africa

MSc thesis
Karin L. Louzada
January 2003

Karin L. Louzada
Dept of Earth Sciences
Utrecht University
k.l.louzada@students.uu.nl

The magmatic evolution of the upper ~3450 Ma Hooggenoeg Formation

Abstract

This report presents new whole-rock geochemical data on 45 samples from the upper part of the ~3450 Ma Hooggenoeg Formation of the Barberton greenstone belt, Kaapvaal Craton, South Africa. The study attempts to constrain the magmatic evolution of the felsic upper part of the Hooggenoeg Formation.

Considerable controversy exists concerning the ideas pertaining to the origin and emplacement of Archaean felsic suites. Resolving these issues will contribute to the understanding of the evolution of Early Archaean greenstone belts, and in particular their tectonic settings and the role of subduction processes in Archaean geology.

Detailed mapping and geochemical sampling in a key area of the Buck Ridge on the western limb of the Onverwacht Anticline, was conducted in order to obtain an accurate overview of the different lithological units present in the upper part of the Hooggenoeg Formation. The Hooggenoeg Formation there is characterized by (ultra-) mafic massive and pillowed lavas; a trondhjemitic suite of silicified felsic intrusive and flow banded rocks; and sedimentary chert beds. Veins of felsic, chert and (ultra-) mafic material intrude the belt, in that order. The depositional environment is thought to be a shoaling shallow sea in which the Hooggenoeg Formation has been deposited in a west-block down, listric faulted, synsedimentary setting.

The Hooggenoeg Formation felsic rocks were divided into two groups: an **intrusive group** of interlocking and shallow intrusive rocks, and a **porphyritic group** of rocks from the veins, based on differences in immobile and incompatible element compositions, This subdivision was not contradicted by major elemental compositions, despite pervasive alteration. Lavas from the upper part of the felsic unit were too altered to be assigned to one of these groups. The **intrusive group** is related TTG-suite Stolzburg Pluton, which intruded along the southern margin of the Barberton greenstone belt. Melting of an amphibolite or quartz eclogite has been suggested as a probable origin for these high-Al_2O_3 felsic magmas. (Ultra-) Mafic rocks of the Hooggenoeg Formation were most likely not parental for the felsic rocks.

Subduction processes may have played a role in the generation of the felsic rocks, but a tectonic setting for the (ultra-) mafic rocks remains uncertain.

The felsic units of the Hooggenoeg Formation are very similar to those of the Panorama Formation of the Early Archaean Coppin Gap greenstone belt of Western Australia. Similarities in geological setting, petrography, and geochemical (trace element in particular) characteristics suggest a possible genetic relation between the two formations and support the theory that a combined continent Vaalbara existed ~3450 Ma.

The magmatic evolution of the upper ~3450 Ma Hooggenoeg Formation

Table of Contents

Chapter 1 – Introduction

The Barberton greenstone belt (Kaapvaal Craton, South Africa) is one of the best known and most studied mid-Archaean greenstone belts on Earth. It comprises a unique sequence of some of the best preserved and oldest rock suites known. The upper part of the ~3450 Ma Hooggenoeg Formation in the Onverwacht Group consists of a variety of rock types from ultramafic to felsic igneous rocks, as well as massive and sedimentary cherts, and pyroxene/amphibole porphyries. Based on observations from the Barberton greenstone belt, many statements have been made regarding the evolution of the Kaapvaal Craton and the continental crust in general. Some suggested settings for greenstone belts are volcanic arcs (Martin, 1999), oceanic plateaus (Cloete, 1999) and large collapsing calderas (Nijman, 1999). At the heart of the controversy lies the question of mantle pluming versus plate-tectonics (and related subduction). Recently, a possible shared evolution of the Kaapvaal Craton with the Pilbara Craton of Western Australia (Cheney, 1996; Zegers et al., 1998) has become a hot topic as well.

On the western limb of the Onverwacht Anticline of the Barberton greenstone belt the Hooggenoeg Formation is well exposed and stratigraphically intact along the east-west oriented Buck Ridge. It has been seen as an ideal location for observing lateral and vertical variations of rock types. Previous work on the western limb of the Onverwacht Anticline has been preformed by (among others) Viljoen and Viljoen (1969), de Wit (1987), de Ronde and de Wit (1994), Robb and Anhaeusser (1983), and Lowe (1999). The Barberton greenstone belt consists mainly of mafic and ultramafic igneous rocks, but the small percentage of felsic (~5 %) and sedimentary rocks can by no means be neglected. The latter have raised important questions about greenstone belt evolution, such as the implications of bimodal igneous rock assemblages and the depositional setting of greenstone sequences. These issues have been subject of heated debate and much of the geology of Archaean terrains is still not adequately constrained.

The objectives of this research are two-fold. First, a local problem will be concentrated on, in order to clarify the relations between in- and extrusive felsic rocks of the upper part of the Hooggenoeg Formation in the Buck Ridge area. Second, the data obtained are combined with data from the literature to interpret the magmatic, geological and tectonic evolution of the Barberton greenstone belt.

Specific questions addressed in this study are:

- *Can a boundary be drawn between intrusive and extrusive felsic rocks in the upper part of the Hooggenoeg Formation of the Barberton greenstone belt at the Buck Ridge?*
- *What are the relationships between the different (felsic) units in a key area identified in which vertical felsic, mafic and chert veins were observed along with intrusive and extrusive igneous units?*
- *Does a genetic relationship exist between the Hooggenoeg Formation felsic rocks and the tonalite-trondhjemite-granodiorite Stolzburg Pluton, and what are possible origins for these magmas?*
- *What is the tectonic setting of the upper Hooggenoeg Formation?*
- *How does the Hooggenoeg Formation compare with similar rocks of the Coppin Gap greenstone belt of Western Australia?*

In order to asses these problems, a field work was undertaken in the Buck Ridge area of the Barberton Greenstone Belt from May 11 to June 3, 2001. Detailed mapping of the a key area identified on the western limb of the Onverwacht Anticline was conducted in order to identify the different rock types present in the upper part of the Hooggenoeg Formation and their field relations. Whole rock geochemical analyses on samples from each group were performed at the XRF and ICP-MS facilities of the University of Cape Town. Thorough examinations of the results and interpretations based on comparisons between chemical characteristics of the different groups, and from other data obtained from the literature, were done in order to evaluate the problems stated above. The use of trace elemental chemistry (incompatible and immobile element ratios) was particularly helpful in identifying genetic relations and possible tectonic settings.

In this report, first, in Chapter 2, the geological setting of the Kaapvaal Craton and previous work done on the Barberton greenstone belt and the Hooggenoeg Formation are delineated. Next, in Chapter 3 the methods of investigation are described. Detailed description of the results of the fieldwork, and petrographical and geochemical analyses are presented per rock type identified in the field, and can be found in Chapter 4. The chapter concludes with a summary of the most important characteristics of each group. Chapter 5 is a discussion including interpretations pertaining to (1) genetic relationships between the felsic groups, (2) the origin of felsic magmas, (3) relations between other chert veins and sedimentary cherts, and between pyroxene/amphibole porphyries and the Kaap Valley Tonalite, and (4) the characteristics of the (ultra-) mafic rocks of the Hooggenoeg Formation. Finally, (5) the tectonic setting of the upper part of the Hooggenoeg Formation and (6) a comparison between the felsic upper Hooggenoeg Formation and the felsic units of the Coppin Gap greenstone belt (Pilbara Craton, Western Australia) are be discussed. In Chapter 6 a number of conclusions are drawn based on the new data presented in this study. Figures and tables can be found in appendices at the back of the report.

Since 1999, a number of researchers have been participating in the project entitled *Earth's Earliest Sedimentary Basins*, which has focussed on the geometry, architecture and structural settings of Archaean sedimentary basins in relation to syn-sedimentary deformation, in greenstone belts of the Kaapvaal and Pilbara Cratons in South Africa and Western Australia respectively (Nijman and de Wit, 1999). Detailed biological, sedimentological, volcanological, geochemical, and structural analyses were the tools envisaged for a multidisciplinary approach to understanding the evolution of the early Earth. The research presented here has been conducted in accordance with this EEB project.

Chapter 2 – Geological Setting

2.1 THE KAAPVAAL CRATON

The Kaapvaal Craton (KC), in which the Barberton greenstone belt is situated (figure 1a), is $1.2x10^6$ km^2 in size (de Wit *et al.*, 1992), and represents a continental fragment known to have been much larger, with parts of it embedded in the Antarctic continent. The Ancient Gneiss Complex of Swaziland and the Southern Barberton Terrain (and the slightly younger adjacent terrains to the north and south, whrains to the north and south, wh the KC) are regarded to represent the early nucleus (or 'shield') of the KC with an age of 3.64-3.5 Ga. The KC is bound by the Lebombo monocline in the east, formed during the break-up of Gondwana, and to the south and west by the Proterozoic Namaqua-Natal Mobile Belt. The northern boundary of the KC is less constrained; the original edge of the KC may be hidden under the Central Zone of the Limpopo Belt in the north (Brandl and de Wit, 1997).

The evolution of the KC can be divided into two phases. The first period (early to mid-Archaean) during which the continental lithosphere first separated from the mantle, terminated with a major pulse of accretionary tectonics around 3.2 Ga to form the Kaapvaal shield. During the late-Archaean the shield continued to evolve. Continental growth took mainly place through a combination of aggregation of crustal fragments and subduction-related igneous processes, expressed by the late Archaean granite-greenstone terrains in the western part of the KC and the tectonic juxtaposition of the Central Zone of the Limpopo Belt between the Zimbabwe and Kaapvaal Cratons along the northern margin of the KC (Brandl and de Wit, 1997).

2.2 THE BARBERTON GREENSTONE BELT

The Barberton greenstone belt (BGB) (in the Lowveld of the Province of Mpumalanga, South Africa) (figure 1b) comprises one of the best exposed and least metamorphosed Archaean volcano-sedimentary sequences known (Hunter and Stowe, 1997). It is a fold and thrust belt, extending for 6000 km^2 (Brandl and de Wit, 1997), and records a complex history of tectonothermal events spanning a period of nearly 500 Myr (de Ronde and de Wit, 1994). The greenstone belt represents at least two different volcanic-arc environments separated in time (by at least 200 million years) and in space (by the Saddleback-Inyoka fault system) (Brandl and de Wit, 1997)). The Southern Barberton Terrain comprises mostly of volcanic and plutonic mafic to ultramafic rocks between 3.49-3.46 Ga in age. Following this period of predominantly mafic igneous activity, an episode of intermediate tonalitic (trondhjemitic) plutonism and volcanism occurred along the southern boundary of the BGB, accompanied by deformation and metamorphism between 3453 and 3416 Ma (SACS, 1980) (felsic rocks make up less than 5% of the total amount of volcanic rocks in the BGB (Brandl and de Wit, 1997)). Renewed tonalitic plutonism and volcanism, again accompanied by deformation and metamorphism, took place along the northern boundary of the Northern Barberton Terrain between 3.3 and 3.2 Ga. Amalgamation of the three old terrains (the AGC and the Southern and Northern Terrains) took place during a period of major north-directed thrusting between 3.15-3.07 Ga (Brandl and de Wit, 1997).

The western limb of the Onverwacht anticline (in the Southern Barberton Terrain) has an east-westerly trend and is relatively continuous in the Buck Ridge Chert area. The Buck Ridge

Chert (complex) forms the topographical high of the limb. The Hooggenoeg and Kromberg Formations on the west limb of the Onverwacht anticline form an essentially vertical, north-younging stratigraphic succession of volcanic and sedimentary units almost 8000 m thick. (Lowe *et al.*, 1985)

2.2.1 Stratigraphy

The "Swaziland Supergroup" (or "Barberton Sequence" (SACS, 1980)) is the oldest stratigraphic unit in the Barberton Mountain Land; its base is nowhere exposed. On the basis of lithology, it has been divided into three separate groups; a dominantly volcanic lower Onverwacht Group, and a dominantly sedimentary upper assemblage comprising the fine grained clastic Fig Tree and the coarse grained clastic Moodies Groups. Figure 2 shows a stratigraphic subdivision of the Swaziland Supergroup. The Onverwacht Group has been divided into the Lower Ultramafic Unit (also known as the Tjakastad Subgroup) and the Upper Mafic to Felsic Unit (also known as the Geluk Subgroup), both containing three formations. The Tjakastad Subgroup is characterised by the widespread occurrence of unusual ultramafic rocks (peridotitic komatiites) and the Geluk Subgroup is characterised by the pronounced cyclic nature of the volcanicity in the two lower formations (the Hooggenoeg and Kromberg Formations) (SACS, 1980).

2.2.2 The Hooggenoeg Formation

On the western limb of the Onverwacht anticline, in its type area, the Hooggenoeg Formation attains a thickness of 4,847 metres and has suffered only a minimal amount of structural disturbance. The formation stratigraphically thins to the west, and to the east the regular and well developed stratigraphy becomes disturbed (Viljoen and Viljoen, 1969b).

The lowermost horizon of the Hooggenoeg Formation is the Middle Marker, which divides the Onverwacht Group into its two units or subgroups. This sedimentary horizon is a remarkably persistent cherty band that has been traced for 72 km and ranges in thickness from a mere parting to 9 m (Viljoen and Viljoen, 1969b and SACS, 1980). The mafic lavas overlying the Middle Marker consist predominantly of meta-tholeiitic basalts, which are more resistant to weathering than the magnesium-rich sheared volcanics of the lower formations. The basalts are massive, well jointed and rather fresh, and grade into zones where pillow structures are well developed. The mineralogies of the pillowed meta-basalts and of the massive basalts, are similar, although the pillows are usually fine grained, often with a doleritic texture due to a random array of slender plagioclase needles (Viljoen and Viljoen, 1969).

Viljoen and Viljoen (1969b) regarded a cyclic nature of volcanicity, in which large accumulations of basalt pass upwards into generally narrow zones of white-weathering dacitic to rhyodacitic lavas of varying thickness (up to 304 metres), as characteristic of the Hooggenoeg Formation. They described these felsic rocks to be massive and pillowed. Substantial black and white chert horizons were believed to terminate individual volcanic cycles, which are often preceded by interlayered lenses and bands of finely banded chert within the acid lava. The cycles may have been initiated by ultramafic volcanicity. However, Lowe (1999) and Lowe *et al.* (1999) did not find evidence of small scale volcanic cyclicity and suggested that felsic volcanism in the Hooggenoeg Formation was limited to an uppermost felsic unit (termed "H6" by Lowe (1999) and the "Volcano-sedimentary sequence (unit 1) of the Buck Ridge Chert complex" by de Vries (1999, Unpubl.)). This uppermost

cycle consists of a substantial sequence of felsic material topped by a zone of (chert) sediments, the Buck Ridge Chert, with a total thickness of 1,520 metres. The zone is also more resistant to erosion and forms a marked topographical feature (the Buck Ridge) rising steeply from the underlying basaltic hills. Lowe *et al.* (1985) regard the Buck Ridge Chert as the lowermost unit of the Kromberg Formation, because it appears to be equivalent to several thin cherts in the lower part of the Kromberg Formation in its type section on the Komati River. The felsic rocks belonging to this unit are mostly feldspar porphyries containing also euhedral quartz phenocrysts in a fine grained ground mass of feldspar, sericite and quartz. The Kromberg Formation conformably overlies the Hooggenoeg Formation and is only extensively developed in the southern portion of the Barberton Mountain Land (Viljoen and Viljoen, 1969b). The rock types of the Kromberg Formation are essentially similar to those of the Hooggenoeg Formation although the possible "cyclic" nature of volcanicity is not as apparent. Minor ultramafic horizons are present on the west limb of the Onverwacht anticline, although in the type area ultramafic rocks are never continuous over long distances and appear to constitute part of the stratigraphy or are cross-cutting dyke-like bodies.

Lowe and Byerly (1999) gave a complete review of recent work done on the stratigraphy of the west-central part of the BGB. Many others (see references in Lowe and Byerly, 1999) have reported the existence of major thrust faults and fold nappes indicating horizontal shortening of the belt and repetition of major portions of the sequence. Lowe *et al.* (1985) have suggested that rocks of the uppermost Onverwacht and Fig Tree Groups are stacked and repeated in a series of thrust nappes. If structural repetition did take place (indicated by recumbent folds, inverted stratigraphy, nappes and olisostromes according to de Wit (1983)), the total thickness of the upper Onverwacht and Fig Tree Groups would be ~3000 m or less, in stead of ~9000 m as proposed by Viljoen and Viljoen (1969b). Lowe and Byerly (1999) and Lowe *et al.* (1985) also found that the Komati, Hooggenoeg, Kromberg and Mendon Formations in the western limb of the Onverwacht anticline in the "Southern Domain" of the BGB, form an overall intact sequence with a thickness of ~9,300 metres. This Southern Domain is bound in the north by the Granville Grove Fault and by the Kromberg Fault in the east and contains large tight to isoclinal folds (such as the Onverwacht anticline, the Kromberg syncline and the Steynsdorp anticline) with vertical to subvertical axes.

2.3 GEOCHRONOLOGY

Van Niekerk and Burger (1969) first dated acidic lavas of the Hooggenoeg Formation at 3360 ± 100 Ma. The sample was of questionable origin taken near the Geluk trigonometrical beacon and dated using U/Pb ratios in sulfides and zircons.

Since then, developments in analytical dating techniques have made it possible to date Archaean rocks more accurately, with analytical errors as small as 0.1%, and over the past decennia many workers have dated numerous rocks from the BGB. Figure 3 shows a compilation of the most recent data gathered on the Hooggenoeg Formation and other units of the BGB, since van Niekerk and Burger's (1969) first measurement. The figure shows that not only the dates have become more accurate, but that the age presented by van Niekerk and Burger was an underestimated age.

A composite sample of the main felsic unit of the Hooggenoeg Formation, dated on U/Pb ratios in zircons by ion microprobe, yielded an age of 3445 ± 4 Ma (de Wit *et al.*, 1987).

The magmatic evolution of the upper ~3450 Ma Hooggenoeg Formation

A number of felsic flows from the Hooggenoeg Formation were dated by Kröner and Todt (1988) at 3451 ± 3 Ma and 3438 ± 6 Ma and were found to be identical to the detrital grains of meta quartzites and metavolcanic rocks.

Dacitic to dacite-andesitic rocks from a shallow-level felsic intrusion, which was locally associated with extrusive volcanic equivalents belonging to the Hooggenoeg Formation, were dated by Armstrong *et al.* (1990) and found to be 3445 ± 8 Ma. They also dated a thin, remarkably persistent, sedimentary horizon known as the Middle Marker, which separates the Lower from the Upper Onverwacht Group (in particular the Komati Formation from the Hooggenoeg Formation.) The Middle Marker was dated at 3472 ± 4 Ma.

Krüner *et al.*[1] (1991) dated dacitic tuffs of the Hooggenoeg Formation at 3445 ± 3 Ma from a 300-700 m thick unit of dacitic tuff at the top of the Hooggenoeg Formation, and found an age of 3416 ± 5 Ma for a dacitic tuffaceous sandstone, suggesting that felsic volcanism in the upper Hooggenoeg Formation lasted for some 30 Myr. They used $^{207}Pb/^{206}Pb$ single zircon evaporation ages.

Byerly *et al.* (1996) confirmed the age of the Hooggenoeg Formation once again and found an age range of ~3445-3452 Ma for a tuff in a thick massive to bedded dacitic volcanic rock sequence from the upper Hooggenoeg Formation.

By single zircon dating, using various techniques, Kröner *et al.* (1996) tried to resolve the stratigraphic and age relationships in the southern part of the BGB and found the following dates:

Moodies Group	> 3.22 Ga
Fig Tree Group	~ 3.26-3.23 Ga
Upper Onverwacht Group	~ 3.42-3.3 Ga
Lower Onverwacht Group	~ 3.48-3.45 Ga

The great variety in ages of zircon xenocrysts in the different felsic units of the Onverwacht and Fig Tree Groups (see figure 3), has been interpreted as being inherited from various sources during the passage of the felsic melts to the surface. These sources were possibly greenstones and granitoid rocks now exposed in the form of tonalite-trondhjemite plutons, or even older units, not exposed (Krüner *et al.*, 1991).

Krüner *et al.* (1991) have shown that many of the granitoids along the southern margin of the greenstone belt, which intrude the lower mafic and ultramafic units of the Hooggenoeg Formation, have similar ages (between 3490 and 3440 Ma) to that of the Onverwacht felsic volcanism (in particular the Stolzburg and Theespruit plutons). The Kaap Valley pluton, along the north-western margin of the belt, was found to be coeval with dacitic volcanism of the Fig Tree Group. De Wit *et al.* (1987), Armstrong *et al.* (1990) and Sylvester (2001) have suggested that the felsic units in the Onverwacht Group are high level equivalents of granitoid plutons that intrude the BGB at its southern extremity, based not only on geochronological data, but also on geochemical data.

The BGB had a prolonged history of development lasting up to 250 Myr, with a series of discrete events of magmatism and deposition (Krüner *et al.*, 1991). Felsic volcanism in the Hooggenoeg Formation lasted from ~ 3445 ± 8 to 3416 ± 5 Ma (a maximum duration of 42

[1] NB: Author's name misspelled in article: *Krüner* = *Kröner*. Reference listed under *Krüner*.

Myr) and was likely associated with the emplacement of the Theespruit, Doornhoek and Stolzburg trondhjemitic plutons along the southern margin of the BGB. A second period of felsic volcanism occurred during deposition of the Fig Tree Group and lasted 34 Myr.

2.4 DEFORMATION

Five periods of deformation are thought to have occurred in the "Southern Domain" of the BGB by Lowe *et al.* (1999). The first period of deformation (D_1) occurred during Onverwacht dacitic magmatism and the intrusion of the comagmatic tonalite-trondhjemite-granodiorite plutons. The deformation expresses itself by a crosscutting zone of shearing and block rotation up to hundreds of metres thick, situated below and extending laterally from the dacitic intrusion. This zone is bound at the bottom by the Geluk Fault, a south-dipping thrust or reverse fault. Normal faults in the Buck Ridge Chert are a local, and possibly widespread expression, of extension related to cooling and subsidence of the underlying felsic intrusion (or dome.) During middle Fig Tree to early Moodies D_2 deformation the large tight upright folds to steeply inclined parallel and similar folds (the Onverwacht anticline and Kromberg syncline respectively) formed. Also, unmetamorphosed greenstones were thrust over TTG complex and metamorphosed greenstone belt roof rocks along the Komati Thrust Fault. Uplift and deep erosion of the TTG suite exposed in the Onverwacht anticline along with reactivation of the Komati Fault occurred during Moodies D_3 deformation. During D_4 and D_5 deformation (late and post Moodies) tightening of the Onverwacht anticline resulted in the folding of Moodies Group around the Onverwacht anticline.

2.5 METAMORPHISM AND ALTERATION

The Barberton Mountain Land has only undergone greenschist facies regional metamorphism. In narrow zones along contacts with granitoids, the Onverwacht volcanics have been upgraded to the upper greenschist facies and locally to the amphibolite and granulite facies (SACS, 1980).

Studies on the metamorphism of the rocks of the BGB suggested that the hydrothermal fluid responsible for much of the alteration in the early BGB rocks was modified sea water. 'Black-smoker' activity may have been present on the seafloor (de Ronde *et al.*, 1994; de Ronde *et al.*, 1997). The rocks of the BGB were possibly covered by a sea as shallow as 60 m, consistent with the evidence of evaporite sequences, stromatolite occurrences, and coarse clastic rocks that outcrop in the vicinity of ironstone pods; the presumable hydrothermal smokers.

In addition, silicification has lead to extreme alteration of the BGB and numerous chert veins are located throughout the Hooggenoeg Formation.

CHAPTER 3 – Methods

3.1 FIELDWORK

A fieldwork was carried out from May 11 to June 6, 2001 in the western limb of the Onverwacht Anticline of the Barberton Greenstone Belt, South Africa (figure 1b).

3.1.1 Mapping

A lithological map of the area to be sampled was made on transparencies over enlarged black and white aerial photographs (1:6000) of the area. (Figure 4 is a rescaled picture of these photographs.) Where needed, observations and interpretations were taken from maps by de Vries and Houtzager (1999, Unpubl.) and Houtzager (2001, Unpubl.). During the execution of the field work, first transects were walked perpendicular to the stratigraphy in key areas II and I. After acquiring an overview of this part of the greenstone belt, a number of days (four) were spent in key area I for detailed mapping of the lithologies. Sampling was preformed after sufficient mapping was completed.

Distinctions between lithologies were made in:

- colour (felsic rocks are lighter in colour than mafic rocks),
- topographical relief indicating resistivity to weathering of the rocks (felsic rocks were often more resistive to weathering, along with silicified rocks, than for instance fine-grained basalts),
- outcrop shapes and patterns (such as bedding parallel trends for flow or sedimentary units, and bedding perpendicular trends for veins) and outcrop dimensions,
- grain sizes and textures visible to the naked eye (grain sorting, fabrics such as flow banding, and veining in the rock)
- density of the rocks (heavy rocks usually indicate a more mafic composition compared to the relatively lighter felsic rocks),
- mineral shapes and compositions, and
- sedimentary and depositional structures (such as layering).

For orientation purposes in the field the following were used:

- 1:50000 geological map of de Wit (1983),
- 1:250000 geological map of Anhaeusser *et al.* (1981),
- 1:250000 geological map 2530 Barberton, of Walraven and Hartzer (1986),
- 1:50000 topographic map 2530 DD Nelshoogte, of the Surveys and Land Information, South Africa (1984),
- 2 sets of enlarged black and white aerial photographs (1:5000 and 1:6000), and
- a hand held Global Positioning System instrument: the GPS instrument was used to precisely fix especially noteworthy locations on overlays, such as geochemical (and zircon) sampling locations, and as a standardising tool for possible digitisation at a later stage. GPS coordinates were noted by their UTM coordinates corresponding to the Cape grid used in topographic maps of the Geological Society of South Africa.

The colours indicating lithologies were kept standard and were chosen to correspond with the colours used in earlier publications of greenstone belts as much as possible. **Dark green** was chosen for the (ultra-)mafic intrusive rocks. (Ultra-)mafic fine-grained (basaltic) rocks were

coloured **light green**. When pillow shapes were obvious, this was indicated by a pillow symbol. Heavily silicified basalts were indicated by a dotted light green. **Orange** was chosen for felsic rocks. Symbols were added indicating flow banding, an interlocking texture or a porphyritic texture. **Purple** indicated sedimentary cherts, massive bedding parallel cherts and the Buck Ridge Chert complex. Black vertical chert veins were coloured **dark grey**. **Red** was chosen for the faults.

All measurable orientations (such as bedding and fractures) were noted in dipdirection/dip and were plotted in stereographic projections using the software GEOrient 8.0. The geological maps and figures were created using Adobe Illustrator 8.0 software.

3.1.2 Sampling

Figures 5a and b are datasheets showing the locations of mapping and sampling.

30 Samples were taken in key area I of all lithologies from bedding parallel units (flow-banded felsic rocks, sedimentary and fine-grained bedding parallel (ultra-)mafic outcrops.) Samples were also taken from bedding perpendicular units of (massive black) chert, (ultra-) mafic intrusions and felsic outcrops.
In key area II 7 samples were taken along a profile from south to north, starting with the interlocking felsic rocks in the south, and ending with felsic flow-banded lavas in the north. One sample was taken from the dolerite intrusion into the area.
The Stolzburg trondhjemitic Pluton is located to the south-east of the greenstone belt, outside the field area, and was sampled at the Kangwane Crushers Quarry (S26°01'25.4" E030°45'43.0"), where particularly fresh samples of the pluton were gathered, and along the road to Badplaas (S26°00'29.0", E030°43'17.5"). Figure 5c shows the relative position of the Stolzburg Pluton and sampling locations.
A number of samples falling outside of these categories were taken, these were bedding parallel intrusive pyroxene-amphibole porphyries and a number of samples termed *others* (see section 4.2.13 for petrographic descriptions).

Geochemical samples were taken from the freshest and most homogeneous outcrops available, using a sledge hammer and geo-pick. During sampling in the field and transport of the rocks, care was taken not to contaminate the samples by packing them in plastic. Volumes of rock taken per sample were always over a litre. Generally speaking, the coarser grained the rock, the greater volume of rock was taken for an accurate bulk analysis. A number of hand specimens, for thin section analysis only, were collected.

3.2 ANALYTICAL TECHNIQUES – Bulk rock analyses

In figure 6 the steps taken for preparation of the samples for the chemical analyses can be seen. First the samples were split into pieces of approximately 6 cm, using a hydraulic rock splitter, during which process the weathered rims of the samples were removed. The pieces were then crushed to gravel size using a mechanical carbon/steel jaw crusher. 80 g Of the samples was then milled in a carbon/steel 100 cc sieb mill into powder form.

3.2.1 Preparations for the XRF analyses

For the XRF-analyses fusion discs and powdered briquettes were made with respectively 20 and 6 grams of powdered sample. First, the carefully weighed out 20 grams of sample was placed in platinum and ceramic crucibles in an oven at 110 °C for approximately 4 hours, removing the water absorbed on to the sample powder (H_2O^-)[2]. After cooling in a desiccator for 30 minutes, the crucibles and sample were weighed again before roasting in an oven at 850 °C overnight. After roasting, the cooled crucibles and samples were weighed again. During the roasting step, the structural water and carbon dioxide were removed from the sample and its weight loss percentage constitutes the Loss On Ignition (LOI)[3] content of the rock.
Finally 0.7000 grams of roasted sample and 6.0000 grams of flux (LithiumTetraborate-LithiumMetaborate flux in the proportion of 57:43 from Sigma Chemicals[4]) were fused into discs at high temperature in a Mini-Prometheus fluxer[5] (Willis, 1999). The apparatus agitated the samples in order to speed up the dissolution process and achieve homogenisation of the melt, and poured the melts into moulds (according to the method of F. Claisse: reference in Willis (1999)). The flux was added as a releasing agent (or nonwetting agent) to facilitate transfer of the melt to the mould and the removal of the glass discs from the moulds (Lachance and Claisse, 1995, p.249).

Eleven major elements (Fe, Mn, Ti, Ca, K, S, P, Si, Al, Mg, Na, Ni and Cr) were determined in their oxide weight percentages, on the Claisse discs in a Philips PW1480 Wavelength Dispersive X-Ray Fluorescence (WDXRF) spectrometer.

For the powder briquettes 1 drop of MOWIOL® 4-88[6] per gram of sample was added to 6 grams of unroasted powdered sample. The mixture was then pressed into a casing of boric acid crystal at a pressure of 10 tons using a bench press.
The trace elements (Mo, Nb, Zr, Y, Sr, U, Rb, Th, Pb, Zn, Cu, Ni, Co, Mn, Cr, and V) were determined on the powder briquettes in a series of analytical runs using Rh, Mo/Sc and Au X-ray tubes in a Philips PW1480 WDXRF spectrometer.

3.2.2 Preparations for the ICP-MS analyses

50 mg Of unroasted sample was digested for 48 hours at 50-60°C in 4 ml of HF/HNO_3 solution, after which they were evaporated. The samples were then dissolved in 2 ml of HNO_3 solution and evaporated at 75°C. This step was repeated a second time. 4 ml Of an internal standard stock solution was added in which the samples were dissolved in an ultrasonic bath for 20 minutes. The samples were then dissolved up to 50 mg with internal standard stock solution again. The felsic samples were diluted another ten times. The solutions were analysed in an ELAN 6000 quardrupole ICP-MS for the following elements: Ga, Rb, Sr, Y, Zr, Nb, Cs, Ba, La, Ce, Pr, Nd, Sm, Eu, Gd, Tb, Dy, Ho, Er, Tm, Yb, Lu, Hf, Ta, Pb, Th, and U.

3.2.3 Standardizations and data reduction

---

[2] The calculation for H_2O^- is as follows: $H_2O^- = \frac{\Delta m_{drying}}{m_{originalsample}} \times 100\%$.

[3] The calculation for LOI is as follows: $LOI = \frac{\Delta m_{roasting}}{m_{driedsample}} \times 100\%$.

[4] http://www.sigma-chemicals.com
[5] http://www.claisse.com
[6] An anti-fading agent, mostly used in the biomedical industry for mounting cells on slides, produced by *Calbiochem®*.

Fusion discs made up with 100% Johnson Matthey Specpure SiO_2, were used as blanks for all elements except Si during XRF analyses. Fusion discs made up from mixtures of Johnson Matthey Specpure Fe_2O_3 and $CaCO_3$ were used as blanks for Si. Throughout the preparation for, and actual analyses by, ICP-MS, of the samples, one blank sample and one USGS standard sample (BHVO-1: Hawaiian basalt) underwent the same steps during the treatment of each batch to be analysed. All samples were analysed twice. Standardization and data reduction techniques have been described by Potts (1987) for XRF and ICP-MS analyses in general. Willis (1999) and a university website (http://web.uct.ac.za/depts/geolsci/icpms/lectures/shrtcrs.html) have published specific procedures applied at the geochemical facilities of the University of Cape Town, South Africa.

3.3 THINSECTIONS

Polished thin sections (40 μm thick) were made of each geochemically analysed sample. Covered thin sections (30 μm thick) were made of each hand specimen. Petrographic analysis of the polished thin sections by an optical microscope can be found in section 4.2.

Chapter 4 – Results

In this chapter, the results of the mapping, petrographic and geochemical analyses are set out. Due to the sometimes lengthy descriptions, an integrated summary of the results can be found in section 3.4.

4.1 GEOLOGICAL MAP – Guide to reading the geological map (Figure 7)

Figure 5a shows an overview of the western limb of the Onverwacht Anticline of the BGB, indicating the two key sampling areas. Figure 7 is a detailed geological map of key area I. It shows the different lithological units of the Upper Hooggenoeg. Table 1 shows all orientations measured per locality and table 2 all samples taken.

4.1.1 Lithostratigraphic units

The upper Hooggenoeg Formation at the Buck Ridge is characterized by mafic and felsic, predominantly volcano-sedimentary, sequences, intercalated with minor sedimentary chert beds. The lithostratigraphic units of the Hooggenoeg Formation that crop out in the map area are discussed in stratigraphic order, starting with the oldest in the south and ending with the youngest in the north.

4.1.1.1 *Basalt*

The lowermost and oldest lithology present in the map area is basalt. The rocks are characterized by smooth, grassy north-south oriented hills sloping to the south, with little or no outcrop, except for along the edges of the hills, where massive and pillow basalts crop out (e.g. at LV01-66). It was difficult to determine the bedding of the basaltic unit and only one relatively reliable orientation was determined at ON99-101 on a thinly laminated chert bed. It was found to be 025/82[7]. The bottom of the unit was not observed, therefore the minimum thickness of the unit in the field area was estimated at ~340 m.

4.1.1.2 *Felsic unit*

Overlying the basalt is a felsic unit consisting of small outcrops of:

1. *Interlocking felsic rocks in the lower part of the unit;* Outcrops of these interlocking rocks consist of large (often larger than 1 metre in diameter), nicely rounded boulders. They are slightly pink in colour with millimetre sized grains of quartz, plagioclase and smaller darker minerals. The rocks are particularly resistant to weathering.
2. *Quartz (and plagioclase) rich porphyritic rocks, in the upper part of the unit;* The felsic porphyritic rocks contain euhedral grains of quartz of several millimetres in an otherwise fine-grained matrix. The shapes of the outcrops are often elongated and perpendicular to the strike of the belt oriented in NNW-SSE and NNE-SSW direction, and are often broken up and pervasively veined by black chert van white quartz. Due to their high quartz and chert content, the quartz porphyries are also particularly resistant to weathering.
3. *Flow banded felsic lavas, in the upper half of the felsic unit in both key areas;* Felsic rocks with positively identified flow-banding or columnar jointing indicating a lava were characterized by a fine grained rock with mostly matrix and small, often euhedral, quartz grains, but in which the observation of flow banding or columnar

[7] All orientations are indicated dipdirection/dip.

jointing has lead to positive identification of an extrusive nature of the rocks. It should be noted that true flow-banding was only observed a few times.

The orientation of the felsic unit in key area I was determined using the measured orientations of the flow banded felsic rocks in the upper part of the unit, (only seven measured orientations). Figure 8a shows a stereographic projection of the bedding of these outcrops, and the preferred orientation of the upper part of the unit is 188/90. Even fewer reliable measurements were done in the lower part of the unit. However, the orientations of rock boundaries between basalt and felsic rock near localities LV01-30 and at LV01-31, south of LV01-93, and north of W01-3, between felsic outcrops more resistant to weathering (mainly porphyries) and less pronounced outcrops below (approximately half-way in the felsic unit) are inclined, presumably dipping to the E. The entire thickness of the unit is ~750 m in the west. The upper part of the unit (containing porphyritic and flow banded felsic rocks) has a thickness of ~310 m in the west and ~480 m in the east. In key area II the succession from interlocking intrusive felsic rocks in the south to flow banded felsic rocks in the north can best be seen. Towards the top of the unit, sedimentary chert beds become more numerous and consistent over longer distances (a few hundred meters). The sedimentary chert beds are thickest and most densely spaced in the east. This felsic volcano-sedimentary sequence was termed Unit 1 of the BRCC by de Vries (1999, Unpubl.) (also known as "H6" of the Hooggenoeg Formation after Lowe (1999) and Lowe *et al.* (1999)).

4.1.1.3 *Veins*

Figure 9a is a photograph showing the felsic, black chert and mafic veins (oriented NW-SE to N-S) from the area indicated by the box in the detailed geological map of key area I. The photograph shows a number of white (due to weathering) vertical outcrops of rock in an otherwise grassy slope. The felsic veins (in the east) appear to be wider and more blocky than the long, straight black chert veins. The longest black chert vein can be seen terminating in a bedding parallel sedimentary outcrop (although not all terminate in this horizon) and the felsic veins in the east are capped by a relatively smaller bedding parallel outcrop of felsic material. Immediately overlying this horizon are basalts again (pillow basalts). The geological map and figure 9b show the relation between the different veins. Generally speaking, the chert veins intrude higher into the stratigraphy than the felsic veins, but not as high as the mafic intrusions.

The preferred direction of the upper vertical black chert veins is 104/75 (figure 8b), which is consistent with the observation that the veins are predominantly N-S oriented in the upper part of the felsic unit. The veins are often a few metres wide and on average ~60 metres in length, but can be 100 meters long.

4.1.1.4 *Second mafic unit*

A ~240 m thick mafic unit overlying the felsic unit is expressed by a grassy slope with little or no outcrop. In the east, pillow structures were observed in the outcrops a few metres wide and extending bedding- parallel for a few tens of metres. The entire unit consists of basalts (some pillowed) and has some minor felsic and thicker sedimentary chert beds towards the top. Its lower and upper boundaries are bedding parallel (parallel to the top chert beds of the felsic sequence below). Thin and small pillow basalt flows observed in the east of area I, are subparallel to the top and thickest sedimentary chert. The preferred orientation of the basaltic unit (and the uppermost part of the felsic unit underlying it), was also determined by the orientations of numerous sedimentary chert units which are finely laminated and very reliable

indicators of bedding. Figure 8c shows a stereographic projection of the these measurements (a total of 10) and the preferred orientation is 201/87.
The upper part of the mafic unit is most probably a zone of silicification. It has a more pronounced outcrop and relief (more resistive to weathering) than the less silicified basalts, and an irregular lower boundary. It thickens to the east towards the listric faults. These silicified basalts can be found to the west as well at LV01-47, LV01-48 and LV01-49 (figure 5a).

4.1.1.5 *Buck Ridge Chert complex*
Units 2, 3 and 4 of the BRCC (de Vries, 1999, Unpubl.) form the highest topographical feature in the study area. They overly the basaltic unit and consist of a number of thick banded sedimentary cherts (often with small scale sedimentary structures) with mafic intrusions, bedding parallel pyroxene/amphibole porphyry intrusions and iron breccia rich zones. The boundary between this chert complex and the volcano-sedimentary sequence below in this study, was drawn at the transition from igneous rocks with minor sedimentary units to dominantly sedimentary deposits, which can be followed over hundreds of meters.

4.1.1.6 *Other intrusive rocks*
Mafic intrusive rocks (dolerites) cross-cut the stratigraphy through valleys oriented NNE-SSW, through the listric normal faults. These rocks were often heavier and coarser grained than their finer basaltic counterparts, with an interlocking texture. The mafic intrusions have irregularly shaped, 'finger-like' protrusions reaching to the north (the former surface) (see also figure 9b).

Bedding parallel pyroxene/amphibole porphyries intruded each unit present, from the felsic unit at W01-3 to high in the Buck Ridge Complex at SV01-1 and SV01-3. Preliminary geochronological measurements on SV01-3 indicated a much younger age (Fig Tree Group age) for at least some of the pyroxene/amphibole porphyries (de Vries, pers. comm.).

4.1.2 Structures

Figure 8d shows the stereographic projection of the measured fractures parallel to the chert veins at LV01-129 and the wide felsic vein at LV01-70. The figure shows, although based on few data, good coherence and a reliable preferred orientation of 058/74. Figure 8e shows the remaining measured fractures and faults which do not have a consistent preferred orientation. However, the two fault orientations measured at LV01-77b and LV01-98 (310/42 and 138/64 respectively), have a preferred strike of 049 (figure 8f), which is slightly oblique to the orientation of the NNE-SSW normal faults observed.

At least one major fault, other than the predominantly NNE-SSW oriented normal faults, appears to be present in area I and is oriented NW-SE. The direction of movement along the fault is difficult to determine due to the presence of a long felsic vein lying directly to the northeast of the fault.

4.1.3 Deformation, metamorphism and alteration

The upper boundary of the silicified basaltic zone is relatively flat and formed by longer sedimentary chert beds. Its lower boundary however, is irregular and is increasingly inclined towards the listric faults in the west, indicating that silicification was either 1) synsedimentary: occurring at some shallow stratigraphic level and therefore creating a kind of

rollover anticline, or 2) post-sedimentary: where silicification was most pervasive near the listric faults (and presumably related to the faulting). Other lithological unit boundaries are similarly inclined however, e.g. the lower boundary of the felsic unit and individual chert beds dipping south to southwest from west to east, implies that synsedimentary deformation was most likely present in the northern limb of the Onverwacht Anticline. However, black chert veins (and other veins) are indeed mostly present near the listric faults and not distributed uniformly throughout the felsic unit. Quite possibly these veins were the mechanism for silicification as well.

(Secondary) Alteration appears to be limited to chloritization and silicification, e.g. in LV01-102 and the silicified basaltic unit respectively, and in some places can be extremely pervasive. Chert veining has occurred on all scales, from millimetre sized veinlets (figure 10) to vertical veins up to a meter wide (figures 9a).

4.2 PETROGRAPHY – Results of the optical microscopy analyses

Due to the severe alteration and silicification of most of the rocks, identification of primary mineral phases was not easy. Often mineral crystals of mafic and feldspar phases were completely replaced with fine grained, cryptocrystalline material (either chlorite, sericite or quartz). Sometimes heavily silicified rocks (e.g. the silicified basalts) had small secondary quartz grains in them. However, usually the original texture of the rock was visible. Either by colour contrasts between altered minerals and a matrix, or by differences in birefringence characteristics between the alteration material and matrix in crossed-polarized light, grain boundaries could be identified and the original texture of the rock deduced.

Mineral phases were identified and described by their:

- crystal shapes (eu-, sub-, anhedral or skeletal),
- colours in plane-polarized light and pleochroism,
- relief,
- birefringence colours,
- internal structures and textures in the grains (e.g. twinning, zoning or cleavage), and
- crystal state (clear, porous, cryptocrystalline etc.).

When identifying textures, particular attention was paid to:

- the distribution of the grains,
- relative grain sizes, and
- relations between the grains (e.g. interlocking contact, matrix dominated etc.).

Results of analyses by optical microscopy are detailed below for each rock group.

4.2.1 Shallow intrusives from area I *(LV01-140, LV01-ON99-t1)*

The rocks belonging to this group were identified as interlocking in the field. However, microscopic analyses revealed the rocks do not have an interlocking texture. They contain more than 50% matrix with phenocrysts of plagioclase and quartz floating in it, and were identified as possible shallow intrusives of dacitic-andesitic composition.

LV01-140 contains up to 60% matrix, 25% plagioclase and 15% quartz. The plagioclase minerals are altered and porous. The quartz and plagioclase are distributed homogeneously

throughout the thin section with large rectangular, multiple-twinned, 2.6 by 3.6 mm plagioclase grains and smaller rounded or euhedral quartz grains, up to 1.2 mm in diameter. The matrix is brown and fine-grained. LV01-ON99-t1 ((figures 11a and b)) is very similar to LV01-140, although it contains less matrix, approximately 50%. The rock also contains less quartz phenocrysts than LV01-140 (less than 1%), although the very few grains present, are larger in size, up to 1.4 mm in diameter. Chlorite is present in the rock in small grains with rounded edges (0.24 to 1 mm in size). The rock consists mainly of rectangular simple- and multiple-twinned plagioclase grains of varying sizes (0.6 mm in length to 2.6 by 2.4 mm).

4.2.2 Consolidated ash or tuff from area I *(LV01-109B)*

LV01-109B consists of a fine, brown coloured groundmass, of which the grain size is too small to further determine the composition of the matrix (possibly sericite or microquartz) with grains of plagioclase and quartz floating in it. There are no distinct patterns or preferred orientations of the grains visible in the matrix. However, the distribution of grains in the matrix is slightly inhomogeneous; there exist clusters of grains on a cm scale. A photomicrograph of one of these slightly denser clusters can be seen in figures 12a and b. Along with these minerals, dark opaque material of anhedral shapes is present surrounded by lighter or darker matrix material, often in occurrences larger than 2 mm in diameter. The quartz grains are often smaller than the plagioclase grains (average of 0.2 mm) and are irregularly shaped. Plagioclase grains have an average size of 0.3 mm (up to 1 mm in length) and rectangular lath-shaped. They are often altered so that the plagioclase has been replaced with fine-grained sericite or quartz and the grains often no longer show twinning. In some instances even the centres of the grains have been replaced. In the photomicrograph the plagioclase grains are severely broken. The rock is dominated by matrix (~80%) and plagioclase.

4.2.3 Interlocking felsic rocks from area II *(LV01-11, LV01-13B, LV01-141 and LV01-142)*

Figures 13a through c show LV01-11, which is a truly interlocking rock with little ground matrix between the grains. The fine grain size suggests a shallow intrusive nature for the rock. The plagioclase and quartz grains are distributed homogeneously throughout the rock with more plagioclase (70%) than quartz (25%). The rock also contains minor dark chlorite (<5%) and opaque material. The quartz grains are irregularly shaped with an average diameter of 0.4 mm and a maximum size of 2.6 mm. The plagioclases are pink/red in colour due to alteration, and have an average size of 1.3 mm (up to a maximum of 2 mm). Chlorite has grown along cracks and in between grains as a secondary phase. The thin section is light in colour in which the interlocking texture and individual plagioclase grains and contrasting chlorite grains are clearly visible with the naked eye.
LV01-13B is very similar to LV01-11, but with more matrix (up to 20%) and more chlorite. The euhedral and rounded quartz grains are again distributed homogeneously throughout the rock. The chlorite grains are slightly more euhedral, lath-shaped, and have a clearer green colour (with lengths from 0.4 up to 1.2 mm). The rock contains approximately 10% quartz, 10% chlorite, 60% plagioclase and 20% matrix.
Samples LV01-141 and LV01-142 are similar to each other, in that they both contain less chlorite than rocks LV01-11 and LV01-13B. LV01-141 is more weathered than LV01-142, and has a reddish appearance. Both rocks have a homogeneous distribution of rectangular plagioclase laths with sizes between 0.4 and 2 mm and rounded, or slightly rounded, grains of 0.2 to 0.8 mm in size. The matrix content of the rocks was ~20% with ~65% plagioclase and

~15% quartz. Although these rocks have some matrix they were considered as intrusive rocks of dacitic composition, with a (semi-) interlocking texture, also due to their field occurrences.

4.2.4 Quartz porphyries from area I *(LV01-122, LV01-125A, LV01-125B, LV01-127, LV01-127C, and LV01-129)*

All quartz porphyries contain plagioclase phenocrysts as well.
Sample LV01-122 is a porphyritic rock characteristic for the BGB in this area, with large rounded phenocrysts of quartz up to 3.2 mm in diameter and plagioclase laths (now ghost structures) up to 4 mm in length (figures 14a and b). The phenocrysts are homogeneously distributed throughout the sample and float in a cryptocrystalline dark matrix. All grain edges are altered, except for the quartz grains. A seriate texture[8] of plagioclase exists. Along with quartz and plagioclase, which both constitute approximately 15% of the rock, a third mineral phase is present in the rock, possibly biotite or amphibole. The dark mineral is very altered, contains no visible cleavage and shows no clear birefringence colour. This third phase constitutes no more than 5% of the rock content. The rest of the rock (~65%) consists of groundmass material, probably microquartz or fine sericite.
The texture of LV01-125A is very similar to that of LV01-122, however with smaller quartz phenocrysts, only up to 1-1.2 mm in size. The quartz grains are rounded and the slightly larger ones are euhedral, sometimes broken or skeletal. Plagioclase grains are again altered, but can be seen in plane polarized light due to the slightly darker colour of the grains compared to the surrounding matrix, and their rectangular shape. Small plagioclase crystals are also present, but difficult to distinguish. All plagioclase crystals are smaller than 1 mm in length. The grains again float in a dark matrix (of which the colour varies). The rock contains slightly more matrix than LV01-122 (approximately 70%) and an equal amount of quartz and plagioclase.
LV01-125B has a slightly more heterogeneous composition than LV01-125A, it contains many angular grains and fragments homogeneously distributed throughout the rock, but with darker regions in the matrix containing plagioclase and quartz grains. (These heterogeneities are possibly due to secondary alteration of the rock.) The rock contains also slightly less matrix than LV01-125A with larger rectangular plagioclase (up to longer than 1 mm) and rounded and euhedral quartz (up to 2.6 mm) crystals. The content of plagioclase is possibly higher than that of quartz (~20% and ~15% respectively).
LV01-127 was sampled from a vertical felsic vein in area I. Approximately 80% of this light coloured rock consists of a dark matrix in which plagioclase and quartz grains float in an equal amount. The plagioclase grains, with sizes of 0.2-1.2 mm, have irregular shapes and are recognized by ghost structures. The grain size distribution of the quartz grains is fairly homogeneous with an average grain size of 0.2 mm. LV01-127C (figures 15a and b) was taken from the top of the same felsic vein. It is however an agglomerate, consisting of different fragments up to 1 cm in diameter. The fragments and single grains are now cemented by quartz. The different fragments contain varying quantities of plagioclase laths, quartz crystals and matrix in them. Again, the plagioclase grains are altered to a dark red-brown colour, which strongly contrasts with the lighter colour of the matrix.
LV01-129 is a very fine grained, slightly layered rock consisting for 90-95% of matrix and for 5-10% of very small quartz grains with an average size of 0.2 mm and no larger than 0.8 mm. Plagioclase grains can not be distinguished, possibly due to alteration of the probably similarly sized groundmass crystals. The rock does not have a very porphyritic texture, but was added to the group due to its occurrence in the field.

[8] A seriate texture is a complete gradation in size of crystals from phenocrysts through microphenocrysts to groundmass crystals. (MacKenzie *et al.*, 1982, p.14)

4.2.5 Felsic lavas from area I *(LV01-124C and LV01-128A)*

Felsic lavas were sampled in area I when flow-banding was positively identified.
LV01-124C is a very veined and altered rock, which is completely silicified and now consists of only quartz. The original texture of the rock is not visible. Sporadically a few, possibly plagioclase, grains with a low birefringence colour and lath shape (0.8 mm in length), are observed. The rock is light in colour and fine-grained. Quartz grains are 0.2 mm and up to 0.6 mm in size. Veins through the rock are darker in colour and fine-grained, with larger quartz grains up to 0.3 mm in the centres.
LV01-128A has been altered even more than LV01-124C and has a darker brown colour with a lot of opaque material in it. Many veinlets or fractures throughout the rock are darker and finer grained than the matrix material (possibly flow patterns: see figures 16a and b). No original grains other than quartz are visible. The quartz grains are generally small (0.2 mm in size) and have irregular shapes, often with rounded edges.

4.2.6 Felsic lavas from area II *(LV01-23 and LV01-144A)*

Again, the felsic lavas described here were collected in flow-banded outcrops.
LV01-23 and LV01-144A are both plagioclase and quartz rich porphyritic rocks with nice euhedral quartz grains and lath-shaped plagioclase. The quartz grains are often smaller than the plagioclase grains which are altered in both rocks, although more so in LV01-144A. The average size of plagioclase grains in LV01-23 is <1 mm. For LV01-144A, due to the extent of alteration, it is difficult to determine the average grain size of the plagioclase grains, but for both rocks the maximum size is approximately 1.5 mm. Quartz grains in LV01-144A are often hexagonal in cross section, in LV01-23 usually not (figures 17a and b). Anhedral opaque material is also present, but does not constitute for more than 1% of the rock. In both rocks matrix constitutes for approximately 65% of the rock in which the phenocrysts are distributed homogeneously. The more weathered rock, LV01-144A, contains also another phase, a brown secondary mineral present at the sites of former plagioclase grains. It is not pleochroic, and does not have a significant birefringence colour or extinction. Due to the cryptocrystalline state of the occurrences, the mineral phase can not be determined.

4.2.7 Stolzburg Pluton (Kangwane Crushers Quarry) *(LV01-131A, LV01-131B and LV01-132)*

The Stolzburg plutonic rocks have an interlocking texture as can be clearly observed in figures 18a and b. The quartz grains are often the largest grains in the rock (in e.g. LV01-131A). The rocks contain a significant amount of biotite grains, which are often strongly pleochroic and elongated in the cleavage direction with an average length of 0.5 mm. In LV01-131A, which has a slightly gneissose fabric, the biotite grains are often clustered and the plagioclase and quartz grains are aligned in the fabric layers, although this is better visible in a hand specimen than in thin section. In all samples, all grains, except for micas, are irregularly shaped. Microcline (a K-feldspar) was recognized by cross-hatched-twinning (figure 18c) and plagioclase (predominantly albite, also confirmed by microprobe analysis) by multiple- and single-twinning. LV01-131B (which is a later white intrusion into the Stolzburg Pluton and younger than 3445 ± 3 Ma (Krüner *et al.*, 1991) or 3460 +5/-4 (Kamo and Davis, 1994)) and LV01-132 contain minor amounts of chlorite, also cleavaged and strongly pleochroic (green) in ppl. Quartz grains in LV01-131A and LV01-132 are up to 2.8 mm in size, in LV01-131B they are smaller and only have a maximum size of 1.4 mm. Plagioclase

and feldspar grains are smaller in LV01-131B relative to LV01-131A and LV01-132, an average of 0.6 mm and sizes varying from 0.5 to 1 mm respectively. The Stolzburg plutonic rocks are fine-grained intrusive rocks of trondhjemitic composition.

4.2.8 (Ultra-) Mafic rocks *(LV01-56, LV01-68, LV01-82, LV01-94, LV01-124A, LV01-124D, LV01-128C, and LV01-143)*

4.2.8.1 *Fine-grained basalts*

Fine-grained mafic rocks are LV01-56, LV01-124A, LV01-124D and LV01-128C.

The thin-section of LV01-56 is green in colour and fine-grained. The rock has a slightly foliated cryptocrystalline texture with a very fine matrix with crystals too small to identify with an optical microscope (figure 19). The rock is very dark under crossed polars with many very small (<0.1 mm) white and grey (low order birefringence) spots. The grains are distributed homogeneously throughout the rock. Brown fine-grained material, often with clear centres (0.2 mm) and altered edges, is pleochroic and arranged in parallel layers, possibly representing a former flow direction. Matrix makes up approximately 50-60% of the rock.

LV01-124A is a much finer grained rock and very silicified. Optical microscope analyses confirmed the presence of quartz in the rock. Grains up to 0.4 mm of quartz were found in veins of the rock. Some show slightly undulose extinction and irregular subgrain textures. The borders of the quartz occurrences are dominated by the crystal faces of the euhedral and subhedral, cubic pyrite crystals with an average grain size of 0.5 mm. Smaller quartz grains <0.1 mm were observed throughout the rock. Many of these smaller quartz grains are porous and have solid rims of quartz with darker, finer grained rims. Small opaque laths of ilmenite (confirmed by microprobe analyses) are homogeneously distributed throughout the rock.

Secondary chlorite is not pleochroic, but cryptocrystalline and too fine to show interference colours. The original texture of the rock is no longer visible, but believed to be homogeneously fine-grained.

LV01-124D consists for roughly 75% of a brown matrix. The matrix is dark and cryptocrystalline, probably devitrified glass. Lighter material in the rock consists of degenerated sub- to anhedral, rectangular 0.2 mm lath shaped, porous grains. The grains have low birefringence colours (cryptocrystalline replacement phase), but no clear extinctions. This material is probably plagioclase in the groundmass of the rock. Other light material in the rock is sub- to anhedral quartz with low order birefringence colours and no twinning. Material with higher order birefringence colours, but slightly larger, and not as fresh as the quartz, is also present in the rock, possibly remains of other mafic minerals such as clinopyroxene. The chlorite occurrences in the rock had anhedral outlines and are slightly pleochroic. The chlorite has a radiate texture and shows 'fan extinction'. Anhedral and lath shaped opaque phases are 0.2 mm in size. Parallel veins of 1 to 2 mm wide are also present in the rock.

Grains of quartz float in the fine, dark, cryptocrystalline matrix of LV01-128C along with larger, 0.5 mm, occurrences of brown/green cryptocrystalline material. The groundmass probably consists of micro-plagioclase, clinopyroxene and devitrified glass. Skeletal and subhedral opaque grains of magnetite are 0.4 mm in size and plentiful. Small white quartz grains, 0.4-0.6 mm in size, with high relief and hexagonal/prismatic shapes have low birefringence colours and do not show any twinning or strain. The edges of the grains are dark and embayed. The nature of these, likely secondary, quartz grains is uncertain.

The possible nature of these green fine-grained rocks is a basalt.

4.2.8.2 *Coarse-grained dolerites*

Coarser grained rocks with an interlocking texture are LV01-68, LV01-82, LV01-94, and LV01-143.

LV01-68 is a dolerite with an interlocking texture and contains biotite and minor chlorite. It also contains sporadically 0.8-1.6 mm sized colourless minerals, severely cracked and rounded with low order birefringence colours varying in intensity from centre to edge of the grains. Higher (third) order birefringence and highly cleavaged colourless minerals are the dominant mineral phase in the rock. The rock has a slightly greenish colour in plane-polarized light. Brown fine-grained altered material is sometimes lath-shaped (rectangular) and visible under crossed polars. The size of the ghost-structures of the minerals (possibly feldspar) is 1 mm.
LV01-82 is a very altered medium- to coarse-grained green rock with originally an interlocking texture. It contains a high amount of mostly rectangular, skeletal magnetite grains, 0.5 to 1 mm in size. The rock owes its green colour to the presence of chlorite. In LV01-82 the chlorite is not pleochroic or cleavaged, the occurrences are anhedral and too fine grained to have an interference colour. Crystallites[9] of possibly secondary material are up to 0.1 mm in length. Transparent prismatic crystals (often subhedral having a partial hexagonal shape) with low order birefringence colours are clear with a high relief and no twinning. The nature of the 0.3 to 0.6 mm sized minerals, could be feldspathoid (nepheline, $NaAlSiO_4$) indicating an alkaline origin for the rock. Brown, secondary alteration material was observed in between and overgrowing the other grains in the rock. The material is cryptocrystalline with irregular boundaries, although sometimes in planar contact with e.g. chlorite.
LV01-94 is fresher than LV01-82, with an original interlocking texture consisting of many lath-shaped, simple-twinned feldspars (plagioclase) up to 1 mm in size, and chlorite crystals. The chlorite crystals are strong green pleochroic and cleavaged, and larger than those of LV01-82, namely 1.5 mm in length, often elongated in the cleavage direction. High order interference colours are observed in the chlorites. The magnetite grains are smaller and fewer than those in LV01-82, only 0.2 mm, and not skeletal.
LV01-143 has an interlocking texture as well, however with relatively small plagioclase laths and other larger phenocrysts. Some of the phenocrysts are zoned and single twinned, and often octagonal in shape. They are pale in colour, have a high relief and a maximum second order birefringence colour. Based on these observations, the phenocrysts were determined to be clinopyroxene crystals. Many of the clinopyroxene grains contain inclusions of chlorite in the form of thin needles embedded in the grains under 90° angles. Chlorite occurrences throughout the rock vary from anhedral fine-grained chlorite, only slightly pleochroic, to the very pleochroic needles embedded in phenocrysts. The occurrences of chlorite show the various processes of chloritization in the rock. A seriate texture exists for the clinopyroxene. Skeletal and square opaque minerals are often larger than 1 mm in size and distributed homogeneously throughout the rock. Another pale mineral phase, with slightly higher relief is present in the rock. This mineral phase does not show any twinning, zoning or chlorite incorporation, and has first order birefringence colours, possibly (secondary) quartz. The grains are anhedral and have an average size of 0.5 mm.

4.2.9 Silicified basalts *(LV01-47, LV01-48A, LV01-49, LV01-100B, LV01-100E, and LV01-100D)*

Both LV01-47 and LV01-49 consist predominantly of a dark cryptocrystalline groundmass with plentiful secondary quartz grains floating in it (figure 20a). Most quartz grains are anhedral, often cryptocrystalline, with low order birefringence colours, and a high relief. LV01-49 is slightly more greenish than LV01-47 and contains smaller quartz occurrences, with grain sizes ranging from cryptocrystalline to 0.4 mm and 0.8 mm (a maximum size of 1.6

[9] Crystallites are globular, rod-like and hair-like crystals, which are too small to show polarization colours; form of cryptocrystalline. (MacKenzie *et al.*, 1982, p.9)

mm was measured) respectively. Many of the quartz grains in LV01-47 are lath-shaped (0.6 mm), possibly replacements for plagioclase.
LV01-48A also has a fine, dark, cryptocrystalline matrix, however less matrix than LV01-47 and LV01-49, only approximately 30%. The original texture is clearly visible, despite pervasive alteration and silicification: approximately equal amounts of plagioclase laths (now weathered red-brown and cryptocrystalline) and quartz are present in the rock. The quartz in the rock is sub- to anhedral with 90° angles and generally smaller than the laths. The largest quartz grains however, are bigger than the largest, originally plagioclase, laths (maximum size of 1.4 mm). The rock is medium-grained and has a slightly greenish colour as well. Many of the quartz grains are degraded and have inclusions (of lower relief) in their centres.
LV01-100B is a very silicified, very fine-grained, pale rock with sporadic quartz occurrences. These quartz occurrences are rounded, anhedral and cryptocrystalline. Often the centres of the occurrences are coarser grained and show undulose extinction (figure 20b). The quartz is visible with the naked eye. This fine-grained extrusive rock of questionable origin contains no phenocrysts and consists completely of cryptocrystalline matrix (with crystallites).
The very fine-grained rock sampled at LV01-100E is also slightly greenish with a cryptocrystalline-crystallitic matrix. Thin needles (or crystallites) are often arranged in fan shape in a variolitic[10] fashion, and are visible to the naked eye. Many crystallites are up to 1 mm in size and light in colour. Anhedral porous quartz grains with internal subgrains are present in varying sizes up to 1 mm. LV01-100E is also a very silicified, fine-grained, extrusive rock of questionable origin.

The original texture of LV01-100D is not clear, but under crossed polars rectangular laths with a maximum length of 1.4 mm were visible. These are presumably plagioclase laths. Transparent, slightly greenish, but not pleochroic, anhedral and cryptocrystalline material, has a high relief and occurrences of approximately 0.6 mm. A significant amount of euhedral and subhedral opaque (Fe-oxide) magnetite is present in the rock, approximately 10%, and distributed homogeneously throughout the rock. Transparent, high relief material with dark edges and undulose extinction is possibly quartz. The birefringence colour of the grains is either first or second order, but difficult to determine. The rock could have had an originally interlocking texture consisting of plagioclase laths with possibly less than 10% of groundmass material. The rock has been significantly silicified and chloritized.

All rocks belonging to this group are fine- to medium-grained with matrix making up for most of its content, and contain a significant amount of secondary anhedral quartz occurrences. The green colouration (most likely from chlorite) suggests a mafic origin for the rocks.

4.2.10 Sedimentary cherts *(LV01-62 and LV01-128B)*

Samples LV01-62 and LV01-128B represent the sedimentary cherts of the area. LV01-62 was taken at the top of a vertical black chert vein, and LV01-128B from a bedding parallel sedimentary outcrop, both in area I. The first is a fine- to medium-grained, dark, layered rock in which the original rounded grains are visible with the naked eye. Fine black, white and grey layering is present, but does not indicate a top. Many transparent cracks, some containing chlorite, are present in the rock. On microscopic scale a fine network of quartz acts as cement between the grains. The former grain boundaries are no longer visible due to the severe silicification. Minor chlorite occurrences are no larger than the width of the cracks (0.1 to

[10] "Variolitic texture is a fan-like arrangement of divergent, often branching, fibres; usually the fibres are plagioclase and the space between is occupied by glass or granules of pyroxene, olivine or iron ore." (MacKenzie *et al.*, 1982, p.56)

0.6mm) and are clear, showing cleavage and straight extinction. The lighter layers in the rock consist of more transparent microquartz, and less anhedral opaque occurrences than the darker layers. Layers in the rock are up to 1 mm thick.
The sample LV01-128B is more varied than that of LV01-62, with a very finely layered fine-grained part, a completely microcrystalline part, and a coarser grained part (figure 21). The fine-grained layered part of the rock is black and grey with layers as thin as 0.01 mm. The layers are made up of now cryptocrystalline material with very small scale structures (which may be sedimentary). The coarser grained part of the rock consists of angular and shard like fragments of beige/brown colour and a lot of opaque material (in places up to 50%). Possibly these 0.1-1 mm sized fragments were originally porphyritic material. Thin veins in the rock are again of microquartz, wider veins however contain larger interlocking quartz grains in their centres (up to 1 mm in size).

4.2.11 Massive cherts *(LV01-97 and LV01-133C)*

Samples LV01-97 and LV01-133C were taken from vertical black chert veins in area I, LV01-133C (figure 22) from the vein capped by the sedimentary chert unit LV01-62. LV01-97 is a fine-grained grey/black rock riddled with crosscutting quartz veins and inhomogeneous patches of darker chert. Lighter areas in the rock are fragments of former host rock, and have also been fractured and veined. The matrix of the rock consists of cryptocrystalline microquartz and is light in colour. The angular fragments of host rock, often larger than 1 cm, are fractured *in situ*, with many quartz veins running through them. The fragments are less homogeneous than the matrix with different coloured grains (more brown and opaque material) and darker in xpl than the matrix. Matrix in the fragments makes up over 50% of the rock, in which grains up to 0.5 mm float. Quartz veins vary in width with maximum widths up to 3 mm and quartz grains up to 0.3 mm in the centre. Some veins are microcrystalline and some very coarse-grained (perhaps indicating different stages or phases of silicification).
LV01-133C is also glassy, and very dark, riddled with fractures and veinlets. Many of the white veins contain angular fragments of varying colours (light to dark brown), often being lighter in colour near the white quartz grains. The fragments are also cryptocrystalline, finer grained than the veins, and show rounded spots with an average size of 0.4 mm, which are possibly former grains, but are presently cryptocrystalline.

4.2.12 Pyroxene/amphibole porphyries *(W01-3, SV01-1, SV01-3, and SV01-46)*

W01-3 (figure 23a) has a porphyritic texture with grains floating homogeneously in a fine matrix. Porphyritic crystals are dark thin needle-shaped laths, altered brown hexagonal in shape and more equidimensional laths. The first grains have an average length of 0.6 mm, are finer cryptocrystalline than the matrix, and oriented in no particular preferential orientation. The more equidimensional laths are much larger than the needles, however not as numerous. They are often single-twinned and have first order grey birefringence colours. The largest of these presumably plagioclase grains, was 2.2 mm in size. Brown, not pleochroic, but cryptocrystalline hexagonal grains contain lighter inclusions in them, are large in size and often nicely euhedral (between 0.5 and 2 mm). These grains were presumably originally pyroxenes or amphiboles.
The grains are not brown, but often transparent and degraded, with darker and finer centres than edges in SV01-1. Large subhedral single crystals of singly twinned plagioclase were again found sporadically throughout the rock, up to 1.6 mm in size. In SV01-1 the edges of the hexagonal grains are slightly rounded and the grains are smaller than those of W01-3, with an average size of 0.4 mm. The rock is pervasively chloritized, throughout the matrix and in

the veins and cracks, and has a dark green colour. Matrix constitutes up to 75% of the rock content in both samples.
SV01-3 contains minor amounts of opaque material (possibly magnetite) and less matrix than W01-3 and SV01-1, about 25%. The grains touch each other but the texture is not yet interlocking. The rock is also much coarser grained than the other pyroxene/amphibole porphyries. The hexagonal grains are largest in this rock (an average size of 1.2 mm and up to 2.8 mm in size) and either brown or green in colour. They are eu- to subhedral and now cryptocrystalline. Elongated plagioclase laths are altered brown and usually smaller than 1 mm.
SV01-46 is also porphyritic but with less matrix than W01-3 and SV01-1. The hexagonal grains are again altered brown and very cracked, up to 1.5 mm in size (figure 23b). Darker brown needles are slightly smaller than the hexagonal grains and also cryptocrystalline. Pyrite in a white quartz vein is observed with skeletal, hollow, cubic pyrite remains up to 1 mm in size. In between the different porphyritic grains are small anhedral occurrences of quartz, no larger than 0.01 mm. High relief material now makes up the matrix.
The rocks do not contain primary quartz.

4.2.13 Others *(SV01-35, SV01-39 and LV01-102)*

A coarse-grained interlocking dark rock was sampled at SV01-35. It contains biotite grains, nicely cleavaged and very pleochroic up to 1 mm. Many larger crystals (often larger than 3 mm) are severely cracked with clear and slightly pleochroic pink centres and completely altered along edges and cracks. The grains show second order birefringence colours (blue to yellow). The possible mineral phase of the grains is hornblende. Small, but present in great quantities, sub- and anhedral occurrences of opaque material were found throughout the rock, often aligned to or incorporated into the cleavage of pale biotite grains. A lot of transparent material is present between the grains of the rock, possibly quartz.

SV01-39 is a very fine-grained, green, igneous rock consisting almost completely of matrix. The rock is slightly foliated and contains anhedral occurrences of quartz, often elongated in the direction of the foliation, up to 1.2 mm long. Opaque minerals in the rock are anhedral; 0.7 mm in size.

LV01-102 was taken from a bedding parallel outcrop of a green and white pervasively veined rock. The rock has been completely silicified and altered and the original texture has been completely obscured, but is presumed to originally have been fine-grained. Cubic pyrite skeletons are 0.4 mm in size and sporadically found in clusters. Quartz is present in the form of coarse-grained and cryptocrystalline material. Sporadically 0.6 mm sized opaque needles are present in the rock. The appearance of the rock is quite green.

4.3 GEOCHEMISTRY – Results of the geochemical analyses

Tables 3a through c, showing the results of all the geochemical analyses, can be found in Appendix B.

Igneous rocks are classified based on their major elemental compositions. The major elements constitute more than about 1.0% of the rock and determine important properties of a rock such as phase relations, melting points, densities, and viscosities. Minor elements (elements constituting between 0.1 and 1% of the rock) form accessory minerals in a rock. Trace

elements normally constitute less than 0.1% of the rock. Because they are not essential to the stability of the phases involved, they play a relatively passive role, but their concentrations are effected by magmatic processes. Because they have such low concentrations, they substitute for major elements in mineral phases in the rock (Philpotts, 1990, p.88).

Figure 24a shows the relation between SiO_2 and H_2O^-. There does not appear to be a general trend in the graph. Most of the samples are low in H_2O^-. Figure 24b shows a plot of SiO_2 versus LOI for all samples analysed. The graph shows a general decrease in LOI with an increase in SiO_2. Generally speaking, the LOI content is highest for the coarse- and fine-grained (ultra-) mafic rocks (although very variable between 2 and 5.5 wt%), and between 1 and 4.5 wt% for the silicified basalts and most of the pyroxene/amphibole porphyries. The porphyritic felsic rocks form a more consistent group with 1–2 wt% LOI. The groups that contain the lowest LOI content are the Stolzburg Pluton (with an LOI content between 0 and 0.5 wt%) and the sedimentary and massive cherts (~0 wt% LOI). The LOI content of the other felsic groups are very variable as well. Table 3a shows the results of the H_2O^- and LOI determinations.

The Total Alkali Silica (TAS) diagram (after Le Bas *et al.*, 1986) in figure 25 shows the first real classification of the samples. The diagram is officially only to be used to classify fresh unmetamorphosed volcanic rocks, as alkalis are mobile during weathering and metamorphism, and care should be taken when reading the plot (Le Bas *et al.*, 1986). The effects of alteration (mainly silicification) can be clearly seen: e.g. the basaltic samples have been displaced along the horizontal axis to the right into the basaltic andesite field[11]. The *silicified basalts* are now situated in the dacite and rhyolite field. The *quartz porphyries* plot to the right of the rhyolite field, most other *felsic groups* (including the *Stolzburg Pluton* samples) plot in the rhyolite (and dacite) field as well. The plot also shows all samples are subalkaline, according to the classification by Irvine and Barager (1971). The terms felsic, intermediate and mafic have been used throughout this report, however the distinction between the three is based on SiO_2 content (a.o. Le Bas *et al.*, 1986.) Due to the often severe silicification, both observations from petrography and SiO_2 contents were used.

The SiO_2 content of the rocks is low and very variable for the (ultra-) mafic groups at 45 to 55 wt%, and extremely high for the silicified basalts between 50 and 70 wt% SiO_2, almost as siliceous as the shallow intrusives and consolidated ash from area I, and the interlocking felsic rocks from area II. At around 75 wt% SiO_2 the Stolzburg trondhjemites, overlap the last three groups. The quartz porphyries have the highest SiO_2 content of all the felsic groups at 75 to 85 wt%. SiO_2 content of the felsic lavas ranges from 75 to 95 wt%, due to severe alteration by silicification in some cases and weathering in others (see sections 5.1.2 through 5.1.4). The cherts (sedimentary and massive) have almost 100 wt% SiO_2, which is consistent with the petrographic observations (sections 4.2.10 and 4.2.11). The pyroxene/amphibole porphyries plot between 60 and 70 wt% SiO_2.

[11] Sample LV01-100D, which is less silicified than the other samples belonging to the group *silicified basalts*, plots in the andesite field, while the *fine-grained basalt* LV01-124D plots far into the dacite field. It appears these samples were both better assigned to each others groups, however, have not been due to their occurrence in the field.

In the AFM plot (figure 26, after Irvine and Baragar, 1971) most of the felsic groups[12] plot on the lower left side (near the alkali apex) of the plot in the calc-alkaline field. The Stolzburg Pluton is also particularly rich in alkali. The two lavas from area I plot as ferro-basalts in the AFM diagram (possibly due to alteration). The (ultra-) mafic rocks plot near the FeO* apex of the diagram, in the tholeiitic field.

In this section of the results, the geochemical analyses are discussed per rock group (except for the group termed *others*). The groups were based on the above mentioned classification and kept the same as those used in the description of the petrographic characteristics. Harker diagrams of SiO_2 against the major elements TiO_2, Al_2O_3, Fe_2O_3, MnO, MgO, CaO, Na_2O, K_2O, and minor elements P_2O_5, NiO and Cr_2O_3, can be seen in figures 24c through m. The trace element contents[13] of the rock groups are shown in a number of scatter plots of trace element concentrations plotted against SiO_2 and other elements (figures 27a through r). Chondrite-normalized Rare Earth Element (REE, lanthanides) diagrams, are shown in figures 28a through j. The average chondrite elemental concentrations were taken from Nakamura (1974). Spider diagrams, normalized to Primordial Mantle after Wood *et al.* (1979), are shown in figures 29a through j. The spider diagrams of Wood *et al.* were chosen because compositions of Archaean mantle and crust are uncertain.

4.3.1 The felsic groups *(These groups include the shallow intrusives from area I, consolidated ash or tuff from area I, interlocking felsic rocks from area II, quartz porphyries from area I, and felsic lavas from both areas.)*

Major element characteristics

All groups generally show decreasing major element contents with an increase in SiO_2. They are all low in TiO_2, Fe_2O_3, MnO, MgO, P_2O_5, NiO, and Cr_2O_3, and have variable Al_2O_3 contents, between 10 and 18 wt%. In particular the *quartz porphyries* show a nice linear trend in Al_2O_3 content.

Figures 24e'and g' show details of the Fe_2O_3 and MgO versus SiO_2 plots. Both show that the *quartz porphyries* are depleted in Fe_2O_3 and MgO relative to the other felsic groups, but they also show that the porphyries have variable amounts of Fe_2O_3 (0.5–1.5 wt%) and relatively constant low concentrations of MgO (<0.5 wt%), while the other felsic groups are variable in both Fe_2O_3 and MgO, 1–2.5 wt% (one of the lavas has an exceptionally high amount of almost 6 wt% MgO) and 0.5–2.5 wt% respectively.

The *quartz porphyries* and all *lavas* are extremely low in CaO and Na_2O (below the detection limit of the XRF, and therefore not plotted in the graph), although the *interlocking* and *shallow intrusive felsic* rocks do have measurable quantities of CaO, up to 4 wt%, and comparatively high Na_2O contents, up to ~6 wt%.

K_2O amounts in the felsic groups are in average higher for the *quartz porphyries* (3–5 wt%, with one rich sample at 8.5 wt%), *lavas from area II* (~6 wt%) and the *consolidated ash from area I* (~7 wt%), than for the *interlocking felsic rocks from area II* (0.5–2 wt%, also with one rich sample at ~6 wt%) and *lavas from area I* (0.5 and 2.5 wt%).

---

[12] The *interlocking felsic sample from area II*, LV01-142, is relatively enriched in FeO* and depleted in SiO_2, and plots in the upper corner of the AFM-plot. The *quartz porphyritic felsic sample*, LV01-127C, plots near the other *quartz porphyries*, but in the tholeiite field.

[13] A number of trace elements were determined by both XRF and ICP-MS techniques (Rb, Sr, Y, Zr, Nb, U and Th) For some of the elements however, the detection limits of the XRF mass spectrometer were too high for many of the samples. Therefore the concentrations presented here of the above mentioned elements, are those determined by the ICP-MS. (See Appendix C for comparison of output.)

Trace element characteristics

All felsic groups have low concentrations of V, Cr, Mn, Co, Ni, and Cu. Sample LV01-140 is anomalously rich in Cu, with a concentration of around 75 ppm. The *shallow felsic intrusives and consolidated ash from area I* have higher Zn contents than the *interlocking felsic rocks from area II* and *quartz porphyries of area I*. The *quartz porphyries* on the other hand have lower concentrations of Ga (between 12 and 18 ppm) than all the other felsic groups (around 21 ppm).

Y concentrations lie between 2 and 10 ppm for all the felsic groups. Zr and Nb levels range from 60 to 130 ppm and 2.5 to 3.5 ppm respectively. On average, the *quartz porphyries* have smaller quantities of Zr and Nb.

Mo levels are below the detection limit of the XRF for most of the samples, except for a few of the *quartz porphyries*, *interlocking felsic rocks* and *felsic lavas*, for which they are between 0.65 and 0.9 ppm.

The *quartz porphyries* (and *consolidated ash*) have the lowest Sr concentrations of all the felsic groups. The *interlocking felsic samples* show an increase in Sr in the following order: LV01-142, LV01-141, LV01-13B and LV01-11. Concentrations of Rb and Cs have similar trends decreasing from approximately 140 and 5.7 ppm to approximately 13 and 0.5 ppm respectively. Ba levels do not show a significant increase or decease between the samples of the *interlocking felsic rocks*. In the logarithmic plots (figures 27p, q and r) the groups plot in two clusters. Rb/Sr, Cs/Sr and Ba/Sr ratios are 0.05-7, 0.001-0.3 and 0.7-20 respectively, for the *interlocking felsic rocks* and *shallow intrusives from area I*. For the other felsic groups the ratio ranges are 5-60, 0.1-2 and 10-40 respectively.

The *lavas* generally lie in the vicinity of the *quartz porphyries*.

From figure 28a it can be stated that the *shallow intrusives* and *consolidated ash or tuff from area I* have very similar REE-trends. They show inclined trends decreasing for the LREE and MREE from La to Dy, and a flat trend from Dy to Lu. All three trends are smooth and show no obvious anomalies, except for a slight negative anomaly at Ce. The *interlocking felsic rocks* (figure 28b) also have decreasing trends from La to Dy and relatively flat HREE trends. The sequence of samples from least to most enriched is LV01-13B, LV01-11, LV01-142 and LV01-141. LV01-13B and LV01-142 both have small positive Eu anomalies, the first one being slightly larger than the last.

Similar enrichment factors can be observed in the *quartz porphyries*, as well as significant positive Eu anomalies (figure 28c). The samples appear slightly more variable in the HREE contents than the first groups. One *felsic lava* from each area shows a strong negative Ce anomaly (LV01-124C and LV01-144A, their alteration has been previously mentioned in sections 4.2.5 and 4.2.6). Sample LV01-128A is enriched in HREEs relative to all other felsic lavas and rocks, although it still has a decreasing trend from La to Dy. The most significant anomalies shown in the spider diagrams of the felsic groups (figures 29a through d) are negative Ba anomalies, positive anomalies at K and negative anomalies at Sr and P of varying degree, and negative Ti anomalies of similar degree for all groups, relative to Primordial Mantle. Some exceptions do exist however: samples LV01-11 and LV01-13B, have slight positive Sr anomalies, and sample LV01-142 has positive anomalies at P and Ti. Generally speaking, the trends of the felsic groups are all very similar, however the *consolidated ash or tuff from area I*, *quartz porphyries from area I* and *felsic lavas from both areas*, have the most extreme anomalies.

Two of the *quartz porphyry* samples plot near the *interlocking felsic* rocks in the Hf versus Ta (figure 27l) and Zr and Nb versus Y plots (figures 27i and j). Pb, Th and U levels have similar ranges for all the felsic groups, except for sample LV01-ON99-t1, which is not indicated in

figure 27m (its Pb level is ~70 ppm). The Pb concentrations are however slightly higher on average for the *interlocking felsic rocks from area II.*

4.3.2 Stolzburg Pluton

Major element characteristics

Samples from the Stolzburg Pluton plot near those of the felsic groups, in the TiO_2, Fe_2O_3, MnO, MgO, P_2O_5, NiO, and Cr_2O_3 graphs. With an Al_2O_3 content of 13–17 wt%, and CaO and Na_2O contents of 0.5–2 wt% and 4.5–5.5% respectively, the Stolzburg Pluton behaves as the interlocking felsic rocks and shallow intrusives. The samples plot in between the higher K_2O quartz porphyries, lavas and ash, and the lower K_2O interlocking felsic rocks and lavas with K_2O amounts of 2.5–3 wt%.

The intrusion into the trondhjemite (LV01-131B) was particularly rich in K_2O, at ~6.5 wt%, and low in Na_2O, at ~2.8 wt%, relative to the regular Stolzburg samples.

Trace element characteristics

Most of the trace element concentrations are low in the Stolzburg Pluton samples, similar to the felsic groups presented above (e.g. V, Cr, Mn, Co, Ni, Zn, and Cu). Ga was an exception with very high concentrations of over 40 ppm for LV01-131A and -131B.

Low Rb/Sr, Cs/Sr and Ba/Sr ratios (0.1-0.5, 0.002-0.007 and 1-7) are characteristic for the Stolzburg tonalites, and they plot to the upper right of the interlocking and shallow intrusive fields, as they are enriched in all four elements relative to the felsic groups. The Y, Zr and Nb concentrations of the Stolzburg Pluton are lower than the felsic groups, while the Mo concentrations are higher than the most enriched of the quartz porphyries.

Overall concentrations of REEs in the Stolzburg Pluton are lower than those of the other felsic groups. Especially LV01-131A has a very strong positive Eu anomaly (figure 28e). Their trends are not as smooth as those of the other felsic groups, but they are characteristically felsic. Spider diagram trends of the Stolzburg Pluton samples (figure 29e) are very similar to the felsic groups, except that the plots on average lie slightly lower, and the Stolzburg Pluton samples show positive Ba and Sr anomalies.

Ta levels are similar to the lower of the quartz porphyries, and on average the Hf concentrations are slightly lower. The Stolzburg Pluton is rich in Pb with concentrations between 9 and 14 ppm. The group contains less Th and U than the felsic groups, except for the intrusion into the Stolzburg Pluton (LV01-131 B) which is particularly high in Th (at >4 ppm). This sample is also richest in Pb with 16 ppm.

4.3.3 (Ultra-) Mafic rocks

Major element characteristics

The (ultra-) mafic rocks have variable concentrations of the major elements TiO_2 (between 0.8 and 2.1 wt%), Al_2O_3 (6–18 wt%), Fe_2O_3 (14–25 wt%), and K_2O (0–3.5 wt%) and are extremely variable in P_2O_5 (0.08–0.2 wt%), NiO (0–0.3 wt%) and Cr_2O_3 (0–0.75 wt%) content, independent of the mode of occurrence of the rocks. That is, whether they are fine-grained basalts or coarse-grained dolerites.

There does appear to be a subdivision of the rocks possible, based on MnO, MgO, CaO and Na_2O concentrations. The rocks most enriched in these elements are coarse-grained doleritic intrusions. The MnO content of the entire group varies between 0.07 and 0.23 wt%, with a high fine-grained exception at 0.48 wt% (LV01-124A). One coarse-grained dolerite (LV01-

68) was also exceptionally rich in MgO, with 18 wt%, compared to the 3–7 wt% range of the other mafic rocks.
The distinction between the two could best be seen in the CaO and Na_2O content, at 9–10 wt% and 3–4 wt% respectively for the coarse-grained dolerites, and fine-grained basalts plotted around 0 wt% or below the detection limit.

Trace element characteristics
Trace elemental concentrations vary enormously for this group, with ranges as large as for example 0 to 8000 ppm, as is the case for Cr in coarse-grained mafic rocks (see figure 27b). The mafic rocks have approximately the same range in Zr content as the quartz porphyries. Mo was only detected in one sample (LV01-124D) and found to be 1.5 ppm. Rb/Sr, Cs/Sr and Ba/Sr ratio ranges are ~0.2-40, 0.004-0.6 and 0.5-100 respectively.

Generally flat trends from HREEs to LREEs are typical for the mafic groups, along with negative Eu anomalies. The graph in figure 28f does not show a significant difference between the fine- and coarse-grained mafic rocks. On average the coarse-grained mafic rocks are slightly richer in all elements than the fine-grained groups. However, this is not indicative of a fundamental difference between the two, because the groups were only based on the grain size observed in the petrographic analysis. Spider diagram trends of the (ultra-) mafic rocks (figure 29f) are definitely more flat lying than those of the felsic groups, but not without significant anomalies, with low levels of Th and U, strong K anomalies and generally strong negative Sr anomalies.

Th and U concentrations were low and did not show much variation. Pb ranges are similar to those of the quartz porphyries.

4.3.4 Silicified basalts

Major element characteristics
The silicified basalts show variable TiO_2 (0.8–2.0 wt%), Al_2O_3 (7–13 wt%), Fe_2O_3 (0.5–14 wt%), MnO (0.01–0.11 wt%), and MgO (>0–6.2 wt%) amounts and very low NiO and Cr_2O_3, amounts, similar, although often slightly depleted, to those of the other fine- and coarse-grained mafic rocks. CaO and Na_2O concentrations are very low as well. K_2O and P_2O_5 amounts are higher in the silicified basalts relative to the other mafic rocks with ranges from 0 to 4.5 wt% and from 0 to 0.42 wt% respectively. Sample LV01-100D was very enriched in MgO, its green colour (observed and noted in section 3.2.9) was also an indicator of its more mafic nature.

Trace element characteristics
V levels are scattered similar to the mafic groups, Cr and Ni levels are low (except for LV01-48A), Mn concentrations are on average higher than the felsic groups, and Co levels are less variable than those of the mafic rocks (ranging between 0 and 50 ppm). LV01-100E has a high Cu content and the Zn concentration is around 100 ppm for all the samples except LV01-100D and LV01-47 (around 20 ppm). Ga levels are relatively high at 15-25 ppm, similar to the interlocking and shallow intrusive felsic rocks.
In the logarithmic plots of Rb, Cs and Ba versus Sr the silicified basalts plot in the vicinity of the majority of the mafic samples. A wide range of Y concentrations exists (just as for the mafic group). On average, the silicified basalts are slightly richer in Zr than the mafic rocks, but have similar Nb amounts. Mo was only present in a measurable quantity in LV01-100B, approximately 0.8 ppm.

Figure 28g shows REE patterns for the silicified basalts and confirms the group's relation with the mafic rocks by it's flat trends. The group on average seems slightly enriched in all elements relative to the mafic groups. LV01-48A has an abnormal looking trend, with a decreasing trend finally climbing for the heaviest of the HREEs. Negative Eu anomalies are also present, as in the other mafic groups. As for the mafic groups some of the rocks have depleted La (and Ce) concentrations and/or slight depletions at the ends of the trends. Spider diagram trends of the silicified basalts (figure 29g) are very similar to those of the (ultra-) mafic samples describe above, also with strong positive K anomalies and strong negative Sr anomalies. Again LV01-48A has an abnormal trend, which is less enriched in almost all elements relative to Primordial Mantle, and has a strong negative P anomaly.

Hf levels are more variable for the silicified basalts than for the mafic rocks and Ta levels were similar to the felsic groups. Pb, Th and U concentrations were again similar to the mafic group.

4.3.5 Sedimentary and massive cherts

Major element characteristics

The sedimentary and massive cherts are depleted in all major elements, except SiO_2, and plot in the lower right corner of all plots, near 100 wt% SiO_2. Often the concentrations of major elements were even too low to be detected for some, or all, of the samples, e.g. for MgO and CaO.

Trace element characteristics

Generally speaking, all chert samples are depleted in all trace elements. The sedimentary chert LV01-62 is an exception, as it is enriched in V, Cr, Mn, Co, Ni, Cu, and Zn. The massive black chert LV01-133C is also enriched in Cu (~LV01-62) and even more so in Zn (>200 ppm).

Mo levels in the massive cherts were too low to be detected. In the sedimentary cherts however they were high enough to be detected and found to be ~1.5 ppm. Sr levels were relatively constant at <2 ppm, as well as Rb/Sr, Cs/Sr and Ba/Sr ratios at ~2, ~0.1 and ~20. The four samples plot in elongated clusters in the Sr versus Rb, Cs and Ba plots (see figures 27p, q and r).

Very depleted and fluctuating REE trends are characteristic for the chert groups. Their trends are unpredictable, usually showing higher LREE contents than MREE, and sometimes increasing in HREE (figure 28h). Sedimentary and massive cherts have similar spider diagram trends in figure 29h, and show positive U and K anomalies and negative Sr and Ti anomalies.

The groups show variability in Pb content (0-5 ppm).

4.3.6 Pyroxene/amphibole porphyries

Major element characteristics

The pyroxene/amphibole porphyries generally plot near the felsic groups, in particular close to the quartz porphyries in the Na_2O and CaO plots, although their TiO_2, Fe_2O_3, MnO, and MgO are often slightly higher and more variable. Especially K_2O and P_2O_5 concentrations are higher in the pyroxene/amphibole porphyry group, between 2 and 10.5 wt% and around 0.1

wt% (nearer to the shallow intrusive and interlocking felsic group) respectively. Just as the felsic rocks, the group is depleted in NiO and Cr_2O_3.

Trace element characteristics

Overall the pyroxene/amphibole porphyries behave as the felsic groups. They do have higher amounts of V and Mn than the felsic groups, but similar Zn and Ga levels to the shallow intrusives (and interlocking felsic rocks). The porphyries are particularly rich in Zr (up to approximately 350 ppm) and relatively rich in Nb. Their Y contents are higher than those of the felsic groups. Sr concentrations are very variable leading to ratio ranges which are quite large: Rb/Sr=0.1-~20, Cs/Sr=0.002-0.4 and Ba/Sr=2.-30. The pyroxene/amphibole fields partially overlap both of the felsic clusters in the logarithmic plots.

The REE-trends of the pyroxene/amphibole porphyries (figure 28i) are reminiscent of the felsic groups, although they do not all show a distinct kink in the graphs at Dy. Negative Eu anomalies can also be identified. W01-3 has a strong negative Ce anomaly. SV01-1 is extremely enriched in all elements (especially the LREE) and has a steeper trend than the other groups. It often plots in the upper right corner of the scatter plots. With the exception of SV01-1, the pyroxene/amphibole porphyry spider diagram trends (figure 29i) are very similar to those of the felsic groups, with similar anomalies and levels of enrichment or depletion relative to Primordial Mantle.

On average Hf levels are higher for the porphyries, Ta levels do not differ much from the interlocking felsic group. Pb, Th and U levels are similar to those of the felsic groups.

4.4 SUMMARY

The most significant differences in field occurrences, and petrographic and chemical characteristics of the rock groups, are summarized here and in figure 30. The felsic groups are emphasised.

The felsic unit of the Hooggenoeg Formation at the Buck Ridge is characterized by interlocking felsic rocks, quartz and plagioclase rich phenocrytic porphyries and flow banded felsic rocks. These rocks appear to crop out from south to north, although the nature of emplacement of the rocks is uncertain, and it is most likely that the interlocking felsic rocks are intrusives. Towards the top of the felsic unit chert beds become more numerous and longer. Under- and overlying the felsic unit is a mafic unit containing elongated bedding parallel outcrops of small pillow basalts in an otherwise grassy slope. The upper part of this mafic unit has a more pronounced relief and irregular bottom boundary. The rocks have become more resistant to weathering due to intense silicification. Sedimentary horizons and the boundaries of the felsic and the mafic units are slightly inclined to the ESE, towards normal listric faults oriented NNE-SSW, through which mafic (or ultramafic) igneous rocks have intruded. The inclinations are greatest in the lower parts of the succession, creating wedge-shaped units and are the expression of synsedimentary deformation of the greenstone belt along the normal faults. Numerous vertical black chert veins (terminating in bedding parallel chert beds) and felsic veins (terminating at some level in the felsic unit) are present in the upper part of the felsic unit of the Hooggenoeg Formation, oriented NW-SE to NE-SW. The uppermost unit exposed in the Hooggenoeg Formation of the BGB at the Buck Ridge is the predominantly sedimentary Buck Ridge Chert complex.

Cas and Wright (1987, p.78) have stated that flow foliation in ancient andesitic and dacitic lavas can sometimes be confused with dense welded tuff textures. However, lavas should have euhedral and regular crystals aligned to form a sheeted structure, whereas crystals in pyroclastic rocks are broken and fragmented (as was observed in LV01-109B, figure 12a and b, section 4.2.2) indicating that pyroclastic rocks are also present in the Hooggenoeg Formation. Dacitic lavas are also known to have steep flow layering which is flow folded.

The similarity between the different felsic rock groups should be noted and explicitly brought to attention. Felsic rocks of the Hooggenoeg Formation often consist of a porphyritic nature with euhedral plagioclase and quartz grains floating in a fine cryptocrystalline matrix. Groups were termed lavas or ashes only when flow structures were positively identified in the field (or in thin section), and the mode of the other unassigned felsic rocks remains uncertain after petrographic analysis, ranging in options from shallow intrusives (either bedding parallel or in veins) to extrusive lavas or ashes. This will have to be determined by combining all observations.

All felsic rocks are oversaturated with quartz constituting for more than 10% of the rock. All contain plagioclase and little or no feldspar, except for the Stolzburg trondhjemites, which show high amounts of microcline feldspar. The felsic rocks belonging to the Hooggenoeg Formation are dacitic/tonalitic in composition, and those of the Stolzburg Pluton are granitic (trondhjemitic in particular according to the definition based on major elemental content, by Barker (1979)[14]).

The results showed the mafic groups were silicified to different extents as well. The samples belonging to the group *silicified basalts* were the most silicified with large anhedral quartz occurrences in them. However, the fine-grained texture of the rocks remained visible, indicating an extrusive origin of the rocks, and the green colour, presumably due to the presence of chlorite, a mafic nature of the rocks. Quartz replaced most of the minerals in the most silicified samples, and it appears alteration took place not only in cracks and veins, but also by *site to site* replacement of original mineral phases.

The main differences between the *interlocking* and *shallow intrusive felsic rocks* and the *quartz porphyries*, are the higher SiO_2 content in the last and higher CaO and Na_2O content in the first two groups. Along with the higher amounts of plagioclase grains observed in the thin sections of the samples (see sections 4.2.1 and 4.2.3), this all suggests the involvement of Ca- (and Na-) bearing mineral phases in the interlocking and shallow intrusive felsic rocks. The CaO and Na_2O levels are comparable to those of the *Stolzburg Pluton*. K_2O concentrations are similar for the *quartz porphyries, consolidated ash (from area I)* and the *intrusion into the Stolzburg Pluton*, but higher than in the other felsic groups. Finally, the *interlocking* and *shallow intrusive felsic rocks* are richer in MgO than the other felsic groups and the Stolzburg samples. The *felsic lavas* are the most variable of all the felsic groups. The *pyroxene/amphibole porphyries*, generally speaking, behave as the felsic groups in plots involving major elements. They are however, more variable and the group is on average slightly enriched in many elements relative to the felsic rocks. Based on major elemental

[14] Barker's (1979) definition of a trondhjemite is based on the major element characteristics of the rock, which include: (1) SiO_2>ca. 68%, usually <75%; (2) Al_2O_3 typically >15% at 70% SiO_2 (for high-Al_2O_3 trondhjemites) and <14% at 75% SiO_2 (low-Al_2O_3 trondhjemites); (3) (FeO*+MgO)<3.4%, and FeO*:MgO commonly is 2-3; (4) CaO ranges from 4.4-4.5% in calcic trondhjemite to typical values of 1.5-3.0%; (5) Na_2O typically is 4.0-5.5%; and (6) K_2O<ca. 2.5% and typically <2%. The author considers trondhjemites as a specific type of low K/Na ratio and low (FeO*+MgO) abundance, calc-alkalic rock.

compositions, no distinctions can be made between the *interlocking* and *shallow intrusive felsic rocks* so far.

Shallow intrusives and *interlocking felsic rocks* have lower Rb, Cs and Ba/Sr ratios than the other felsic groups (*felsic lavas* not included) and show decreasing trends of Rb and Cs with increasing Sr. The *Stolzburg Pluton* samples plot near the *shallow intrusives* and *interlocking felsic rocks*, although relatively enriched in all elements, particularly in Sr. *Quartz porphyries* have lower Ga contents, and (on average) Nb, U, Pb, and Ta than the other felsic groups (again not including the lavas.) The *pyroxene/amphibole porphyry* group is relatively enriched in V, Y, Zr, and Nb and plot near the felsic groups in most trace element plots. In trace element contents the group does not show a distinct correlation with a particular felsic group. Apart from a few exceptions, the *silicified basalts* behave as the *mafic groups*.

In order to illustrate the different REE-trends of the groups, two elements at either end of the lanthanide range, that do not show major anomalies in the REE-plots, (figures 28a through j) were plotted against one another. The elements chosen were Sm and Yb. Their ratios with chondritic abundances are shown in figure 31[15]. Rocks with steep REE trends will have high $Sm_{sample}/Sm_{chondrite}$ ratios and low $Yb_{sample}/Yb_{chondrite}$ ratios, and those with relatively flat trends plot around the line: $\frac{Yb_{sample}/Yb_{chondrite}}{Sm_{sample}/Sm_{chondrite}} = 1$. Furthermore, the distance of the points to the origin of the graph is a measure of the average enrichment of the elements, in other words: the elevation of the REE trend in the REE-plots. The graph shows that the trends are steepest for the *pyroxene/amphibole porphyries* and *Stolzburg Pluton* with ratios between 0.06 and 0.25. The *Stolzburg Pluton* samples are less enriched than the *pyroxene/amphibole porphyries*. Felsic groups have *'Yb/Sm'* ratios between 0.17 and 0.5 and form a relatively tight group. On average the *quartz porphyries* lie closer to the origin of the graph than the *interlocking, shallow intrusives* and *felsic lavas*. The *mafic groups* and *silicified basalts* plot between the 0.5 and 1 ratio lines. Both groups cover a significant area in the graph, indicating a range in the average total enrichment factors and inclinations of REE patterns. The *cherts* plot very near the origin due to their depletion in all elements. Slight positive Eu and slight negative Ce anomalies, and a kink in the REE-plots at Dy, characterize the *felsic groups*. The *mafic groups* are characterized by negative Eu anomalies. The *Stolzburg Pluton* and *pyroxene/amphibole porphyries* have similar REE trends despite a positive Eu anomaly in the first and a very small, negative Eu anomaly in the second.

Spider diagrams (after Wood *et al.*, 1979) show many similarities between all the *felsic groups* (figures 29a through d). They all show negative anomalies at Ba, Sr, P and Ti and a positive anomaly at K relative to Primordial Mantle. Generally speaking, the anomalies are greater for the *consolidated ash or tuff from area I,* the *quartz porphyries from area I* and for the *felsic lavas from both areas.* The *Stolzburg trondhjemitic samples* have very similar spider trends, however some significant differences do exist: positive Ba and Sr anomalies. Spider diagram trends of the *(ultra-) mafic* and *silicified basaltic* samples are identical to each other, with more flat lying trends and strong positive K and strong negative Sr anomalies. Both the *sedimentary* and *massive cherts* have positive U, and negative Sr and Ti anomalies and samples LV01-62 and LV01-133C both have negative P anomalies. The *pyroxene/amphibole*

[15] Sample SV01-1 was excluded from the graph; it's high enrichment in Sm, around 160 ppm, plots to the far right of the graph $\left(\frac{Yb_{sample}/Yb_{chondrite}}{Sm_{sample}/Sm_{chondrite}} \approx 0.06\right)$.

porphyries also have spider trends almost identical to those of the felsic groups, showing the same anomalies.

From the results of the petrographic and geochemical analyses it is obvious that many of the samples have been altered by secondary processes. This should be taken into consideration when interpreting the data.

Chapter 5 – Discussion

In this chapter, the combined data presented in the Results, will be interpreted in terms of geological, magmatic and tectonic settings. Furthermore, a comparison between the Hooggenoeg Formation and data from another greenstone belt in Western Australia, will be made

5.1 FELSIC GROUPS

5.1.1 Field relations

The quartz porphyritic rocks were sampled from vertical (oriented perpendicular to the bedding) felsic outcrops (e.g. LV01-127 and LV01-127c). Due to the numerous NNE-SSW oriented faults in the area, it was difficult to establish if a vertical outcrop was indeed a vein, or an outcrop fault-bound on one or both sides. However, at LV01-127 and LV01-124 veins were positively identified and it is reasonable that more vertical felsic veins exist. These veins were not observed beginning in, or sprouting from, shallow intrusive or interlocking felsic outcrops, neither was a direct termination into a flow banded or massive felsic extrusive outcrop observed. The veins did terminate at shallow stratigraphic levels in the felsic unit, and flow banded felsic rocks were observed at the same stratigraphic level elsewhere (e.g. at localities LV01-128 in area I and LV01-23 in area II). Because the field relations do not clearly indicate a genetic relation between the interlocking and shallow intrusive rocks, the quartz porphyritic veins, and the flow banded lavas, this will be investigated below, by comparison and interpretation of the geochemical data.

5.1.2 Silicification (and chloritization)

Indications that severe alteration of the samples has occurred are obvious in both the petrography of the samples (section 4.2) and the results of the (major) whole-rock chemical analyses (section 4.3). The most obvious effect is that of the silicification and many of the samples from the *porphyritic* group have an SiO_2 weight percentage of over ~77 wt %, which is unrealistic for naturally occurring felsic rocks.

Plots showing the SiO_2 weight percentages versus the concentrations of the incompatible elements Rb, Ba, Zr, Nb, Hf, and La (figures 33b, d, e, f, g, and h) all show linear relations with negative slopes (indicated by the black lines in the graphs) for most of the felsic rocks. On average 4 to 6 samples do not lie on the line; however, most of these were found to be unrepresentative of their groups (see section 5.1.4). If silicification caused an increase of SiO_2 from ~75 to ~85 wt% in some of the quartz porphyries (e.g. LV01-125B, LV01-127, LV01-127C and LV01-129), an increase of 13%, would imply that the e.g. original Zr and Hf concentrations were 13% higher than at present at ~85 and ~1.7 ppm respectively. This would place the samples still well below the other felsic samples on the line.
Not only silicification, but also chloritization has probably modified the major elemental compositions of the interlocking intrusive felsic rocks. Chlorite ($(Mg,Fe,Al)_6[(Si,Al)_4O_{10}](OH)_8$) is produced during low grade metamorphism of greenschist facies and occurs as an alteration product of ferromagnesian minerals in igneous rocks.

5.1.3 Possible groups based on major elemental compositions

Disregarding the obvious effects of alteration, the samples might still be divisible into new groups on the basis of major elemental compositions. It is clear that the major elemental compositions no longer represent original magma compositions, but systematic differences may be identified between the different groups.

The most significant major elemental differences between the different groups are the relative amounts of CaO, Na_2O and K_2O, Fe_2O_3 and TiO_2. Overall, the *shallow intrusive* samples and the *interlocking felsic intrusives* are particularly rich in Na_2O, CaO, Fe_2O_3 and TiO_2, compared to the *quartz porphyries* and the *consolidated ash or tuff*, while the latter are relatively rich in K_2O (figure 32). The lava samples are very variable and most will be omitted from genetic relationship considerations, for a number of reasons, further on in the Discussion (see section 5.1.4). On the basis of these chemical differences, two groups could be identified: a first group to which the shallow intrusive rocks and the interlocking felsic intrusions belong and a second group to which the quartz porphyries and consolidated ash or tuff belong.

The sampled rocks are not suitable to explore models based on their major chemical characteristics. More reliable statements on genetic relationships are therefore based on the incompatible and immobile element characteristics of the different groups.

5.1.4 Samples considered not to be representative of their groups

A number of samples can be omitted (due to severe alteration or other eccentricities). Sample **LV01-142** (a *shallow intrusive from area II*) shows unexpected and unexplainable discrepancies between the major and trace elemental characteristics compared to the other samples belonging to the same group, despite obvious likenesses in petrography. It is deviant in most major elemental compositions (including SiO_2) and has deviant major elemental anomalies (such as P and Ti) in the spider diagram trends (figures 27, 28 and 29b). **LV01-141** (another *interlocking intrusive* sample) was excluded even though it often plots near LV01-11 and LV01-13B (or nearer to LV01-11 and LV01-13B than to LV01-142), but more often in plots involving incompatible immobile elements it does not. Both the felsic lavas from area I are excluded: sample **LV01-124C** has an SiO_2 content of over 90 wt% and **LV01-128A** is anomalously enriched in Ti, Fe and Mg. The *consolidated ash or tuff from area I* (**LV01-109B**) is also omitted because of the nature of the rock. Ashes are composed of various proportions of vitric, crystal or lithic particles of juvenile, cognate or accidental origin[16] and are often reworked by aeolian or fluvial processes (Fisher and Schmincke, 1984, p.90-91). Finally extreme care was taken when the *quartz porphyry* **LV01-122** was interpreted because geochronological studies by de Vries (pers. comm.) found the sample not to be representative for the quartz porphyritic group with an inconclusive age. *Quartz porphyritic* sample **LV01-125A** is situated in many plots involving incompatible immobile elements nearer to LV01-122, than to the other four porphyritic samples, which usually form a better cluster. These samples are all excluded from the following discussion.

5.1.5 Interpretation of incompatible and immobile element data

[16] Juvenile particles are derived directly from the erupting magma and consist of particles of chilled melt or pyrogenic crystals. Cognate particles are fragmented comagmatic volcanic rocks from previous eruptions of the same volcano. Accidental particles are derived from the subvolcanic basement. (Fisher and Schmincke, 1984, p.90)

Philpotts (1990, p.269) stated that the ratios of strongly incompatible elements (elements which have very low distribution coefficients ($K^{s/l}_D$ <<1)) can be used to test for common lineage in suites of igneous rocks. As incompatible elements cannot substitute into early-crystallizing minerals because of their high ionic charge and/or large ionic radius, the ratio of two incompatible elements remains virtually the same regardless of the degree of fractionation of the minerals crystallizing, and can only be changed by the assimilation of country rock or a magma with a different ratio, and the appearance of a new primary phase for which the distribution coefficients differ. Some incompatible elements are P, K, Ti, Rb, Sr, Zr, Cs, Ba, the REEs, Hf, Ta, Th, U. The REEs are particularly useful trace elements for studying igneous petrogenesis. Because of their identical charge and similar ionic radii, all of the REEs are incompatible in most early-crystallizing minerals, and chemical processes do not discriminate strongly between the various REE. In the case of discrimination, it varies systematically; the LREEs have larger ionic radii than the LREEs and are therefore slightly more incompatible. Immobile elements are those elements that belong to the group of large high-valency cations (U, Th, Ta, Nb, Zr, Hf, Ti, Y, and Yb), which are also preceived to be alteration resistant (Wilson, 1989, p.138.) In particular, the immobile incompatible elements in conjunction with other incompatible elements are used to investigate genetic relations between rock suites (this section), and to discriminate amongst different tectonic settings (section 5.4.2.).

The similarities in most major elements, REE and spider diagram trends, between the different felsic groups have already been discussed in Chapter 4. In figure 34, the REE trends of all the felsic samples (except for those considered not representative) were plot together. The samples of the *interlocking intrusive* rocks and those of the *quartz porphyries* have similar enrichment factors and trends. Those of the *shallow intrusives* are more enriched in both LREEs and HREEs than the first two groups. The *felsic lava* from area II, sample LV01-23 is slightly enriched in LREEs and slightly depleted in HREEs compared to the first two groups. Sample LV01-144A is very weathered, with a negative Ce anomaly but has a similar trend to LV01-23, although relatively enriched in all REEs. The Nd/Sm ratios (figure 35a) of all the samples are similar though.

Most samples also have similar Hf/Ta (figure 35b) and U/Th (figure 35c) ratios (again LV01-23 has deviant ratios). However, some differences do exist. The *shallow intrusive* rocks have lower U/Th ratios than the other felsic groups. Also, the *shallow* and *interlocking intrusive* samples have higher concentrations of most of the immobile elements than the *quartz porphyritic* rocks. In general they have significantly higher Sr, Zr, Hf, Ta and Nb amounts than the other felsic groups (figures 33 and 34). (It is also for these groups that significant and detectable amounts of CaO are present (figure 24h).) Plots involving Ba do not show good agreement of the data between the different felsic groups (e.g. figure 33d of SiO_2 versus Ba). Most of the *interlocking intrusive felsic rocks from area II* and *shallow felsic intrusives from area I* show similar K_2O/Ba ratios (figure 35d) (as well as the *felsic lavas from area I*), which are much lower than those of the other felsic groups. The K/Rb ratios however, are similar for most of the felsic samples, but as mentioned before, the Rb/Sr and Ba/Sr are much higher for the *porphyritic group*, *lavas* and *consolidated ash or tuff* (figures 35e and f). Figure 35g

shows a graph of Sr versus Eu/Eu*[17] for the samples of the felsic groups. The *interlocking felsic* samples still have significant positive Eu anomalies, the *shallow felsic intrusives* do not. The *lavas* from area II have no or negative Eu anomalies, while the *quartz porphyries* seem to have the most divergent Eu anomalies, both positive and negative.
Finally, figure 33a shows a plot of SiO_2 versus TiO_2 for the felsic groups. This graph also shows a negative linear relationship.

5.1.6 Genetic relations between the felsic groups – One group or two?

On the basis of major elemental characteristics two groups were suggested: group 1 consisting of the shallow intrusive felsic rocks from area I and the interlocking intrusive felsic rocks from area II, and group 2 consisting of the quartz porphyries from area I. This distinction was also noticeable in the Rb, Sr, Cs, Ba, and U concentrations.

The *shallow intrusive felsic rocks from area I* and the *interlocking intrusive felsic rocks from area II* are very similar to each other in their incompatible and immobile element characteristics. With similar concentrations of elements and ratios. They only differ in the REE patterns, where the first are uniformly enriched in all REE, and in the U/Th ratios. It is therefore believed that the two groups are genetically related. The *quartz porphyritic* samples usually plot in a nice cluster and have lower concentrations of all immobile trace elements.

Unfortunately the felsic lava samples from area I were found to be unsuitable (section 5.1.4) and the felsic lava sample from area II LV01-23 was deviant in many plots involving immobile and incompatible trace elements. The other felsic lava sample from area II (LV01-144A, which plots near the shallow and interlocking intrusive groups in most graphs) was found to be weathered and therefore possibly less reliable. We believe therefore that there is insufficient lava data to state if there is a genetic relationship between the other felsic groups and the felsic lavas. On the basis of major elemental data and petrography, it seems as though the lavas could be similar to the quartz porphyries, REE patterns are steeper however. As stated before, the major elemental compositions no longer accurately resemble original magmatic compositions, due to alteration processes.

On the basis of the immobile chemical characteristics of the felsic rocks, two new felsic groups can be identified: 1) **an intrusive group**: the *interlocking intrusive felsic rocks of area II* and the *shallow intrusives*, and 2) **a porphyritic group**: the *quartz porphyries from area I*. It is striking that despite the pervasive alteration this subdivision is not contradicted by the division based on the major elemental compositions (section 5.1.3). In figure 32 once again the distribution of the two new groups and their major and immobile chemical characteristics are shown. The two groups are not identical. Figures 33a through h, used to discuss the effects of silicification, indicated that the effects of silicification are most likely insufficient to

[17] The magnitude of the Eu anomaly (Eu/Eu*) can be quantified in the following manner:

$$Eu^* = \left(\frac{\left(\frac{Sm_{observed}}{Sm_{chondrite}} + \frac{Gd_{observed}}{Gd_{chondrite}} \right)}{2} \right) \times Eu_{chondrite}$$ is the expected Eu concentration if no fractionation or enrichment were to have taken place; and $Sm_{chondrite}$, $Gd_{chondrite}$ and $Eu_{chondrite}$ are the average concentrations of Sm, Gd and Eu in oridinary chondrites. The average concentrations of Sm, Eu, and Gd in ten ordinary chondrites are 0.203, 0.0770 and 0.276 (ppm) respectively (Nakamura, 1974). If $Eu_{sample}/Eu^* > 1$ then the anomaly is positive, if $Eu_{sample}/Eu^* < 1$ then the anomaly is negative.

account for the observed linear negative trend observed in the SiO_2 versus immobile element plots. Green (1980) stated that the presence of Ti indicates that fractionation of Fe-Ti oxides (such as ilmenite or titanomagnetite) has occurred; possibly the crystallization of accessory minerals (e.g. ilmenite ($FeTiO_3$), sphene ($CaTiSiO_4$), and zircon ($ZrSiO_4$)), played a major part in element fractionation between the felsic samples. However, since the extent of silicification cannot be accurately quantified, it is believed that a mathematical model of crystal fractionation involving the common mineral assemblages occurring in igneous rocks of dacitic to rhyolitic compositions (quartz, feldspars, pyroxenes, biotite and amphibole), cannot be successful.

5.1.7 Other new data

New geochronological data by de Vries (pers. comm.) has shown that the different felsic rocks of the Hooggenoeg Formation have (within error) the same age: 3451 ± 5 Ma. This was based on SHRIMP-data from samples taken from the interlocking felsic intrusive at locality LV01-113 and a massive felsic lava flow at locality LV01-23, both in area II. (The sample from locality LV01-122, a small vertical outcrop of porphyritic material in area I, unfortunately did not produce a single conclusive age.) This would indicate that even if the **intrusive** and **porphyritic** groups do not share a common lineage, they were certainly emplaced at the same time.

5.2 ORIGIN OF THE FELSIC MAGMAS

5.2.1 Comparison with tonalite-trondhjemite-granodiorite suites

The geochronology (section 2.3) has shown that felsic magmatism in the Hooggenoeg Formation is contemporaneous with the emplacement of a number of large granitic plutons belonging to the TTG suite of the BGB. These plutons are some of the thirteen discrete gneiss bodies that have been identified in the south-western region of the BGB by Robb and Anhaeusser (1983). The 1.5 to 25 km diameter sized plutons are elliptical or irregularly shaped (referred to as "cells" by Robb and Anhaeusser, 1983) and incorporate large greenstone remnants. The plutons vary from hornblende-bearing tonalites to more leucocratic biotite-bearing trondhjemites and their contacts with the BGB are generally characterized by parallel, subvertical foliation in the plutons and few magmatic intrusive features (tonalitic veins, apophyses etc.), although some are clearly intrusive (e.g. the Theespruit Pluton) and some contacts are sheared (e.g. the Kaap Valley and Doornhoek Plutons). De Wit *et al.* (1987) stated that Hooggenoeg felsic rocks are high crustal level equivalents of the tonalite-trondhjemite terrain and it is quite possible that the felsic rocks of the Hooggenoeg Formation and the Stolzburg Pluton are related and share a common origin. This will be examined in the following sections.

5.2.2 The Stolzburg samples compared with Stolzburg data from literature

The Stolzburg samples collected from the BGB (see figure 5c) will be compared to other chemical data on the Stolzburg Pluton from literature.
Major, Rb, Sr, (and Ba) elemental data were obtained for three trondhjemitic Stolzburg gneisses by Anhaeusser (published in Viljoen and Viljoen (1969a)), Anhaeusser (1974) (an average of four samples reference in Anhaeusser and Robb, 1983) and Anhaeusser and Robb

(1983). Other samples, which included REE data as well, were from Condie and Hunter (1976) (an average of two samples) and from de Ronde *et al.* (1991).
The K/Rb ratios for the Stolzburg samples in the literature are between 260 to 660, their Rb/Sr ratios are ~0.1, and their Ba/Sr ratios are below 1 (no Ba data was available for the Stolzburg sample of Viljoen and Viljoen (1969a)). Figure 35f shows that the Stolzburg samples presented here have similar Rb/Sr ratios and that K/Rb ratios lie in the previously mentioned range, sample LV01-132 also has a Ba/Sr ratio below 1. The other Stolzburg samples have higher Ba/Sr ratios (similar values as for the shallow intrusive samples, figure 35e). The REE trends of all available Stolzburg samples are plotted in figure 36a. The trends are similar, often with significant positive Eu anomalies. The new data presented here however are slightly depleted in HREE and LV01-131A has significantly lower ΣREE. Even though the total data set is limited, the similarities are obvious and the samples from this research are believed to be representative of the pluton as it is presented by other researchers.

5.2.3 Felsic (upper) Hooggenoeg Formation compared with the Stolzburg Pluton

Many authors (e.g. Barker and Arth, 1976; Robb and Anhaeusser, 1983; Martin, 1993) have investigated the characteristics and possible origins (see section 5.2.4) of the tonalite-trondhjemite-granodiorite suites (TTG) from South Africa and other Archaean terrains.
Barker and Arth (1976) showed that the TTG from various provenances have K-Ca-Na trondhjemitic affinities. Unfortunately silicification has made the major elemental data unreliable for the Barberton Mountain Land and a similar trend cannot be reproduced. Robb and Anhaeusser (1983) found that a low Rb/Sr, high Ce_N/Yb_N (indicating a steep differentiation trend), low ΣREE subtype of tonalite-trondhjemites is dominant in the BGB (including the Stolzburg Pluton). The authors found the Stolzburg Pluton to have distinctive Na_2O contents of >5.25 wt% and chondrite normalized traces that are relatively LREE enriched (50-70 x chondrites), HREE depleted, and have no significant Eu anomaly. Martin (1986 and 1993) identifies Archaean TTG also by their REE enrichment and differentiation trends (Yb_N and $(La/Yb)_N$).

The data presented in the REE plot (figure 36b) include the **intrusive group** and all available REE data on the Stolzburg Pluton and show that the samples have LREE enrichments of 9-50 x chondrites and are very depleted in HREE, but the Stolzburg samples have slightly more negative trends than those of the intrusive group. However, unfortunately the Stolzburg samples of Condie and Hunter (1976) and Robb and Anhaeusser (1983) did not include measurements of all HREE. Figure 37 shows that the Stolzburg Pluton and both felsic groups of the Hooggenoeg Formation plot in the Archaean TTG field of Martin (1993). Figures 35a through c show that the Stolzburg Pluton samples (LV01-131A and LV01-132) have similar Nd/Sm, Hf/Ta and U/Th ratios, despite the fact that the REE trends appear slightly different as mentioned above (as the felsic groups of the Hooggenoeg Formation) but often plot below the negative trends of the SiO_2 versus La, Zr, Hf, and Nb plots, but the effect of silicification has not been assessed properly for the individual Stolzburg samples, and might well be less prominent. The plots of K/Rb versus Ba/Sr and Rb/Sr show that the Stolzburg trondhjemites plot in the vicinity of the felsic **intrusive group**. Eu anomalies are positive. Finally, the Stolzburg Pluton has similar major elemental contents (that is, in particular, detectable CaO amounts) (figure 24h) as the **intrusive group**. (Care should be taken when looking at sample LV01-131B because it is a (later) intrusion into the Pluton.)

The data (in particular immobile and incompatible element ratios) has shown that the **intrusive group** of the felsic Hooggenoeg Formation strongly resembles the Stolzburg Pluton

and other TTG, and most likely they are genetically related. The **intrusive group** is most likely indeed a high-level equivalent of the Stolzburg trondhjemites.

Before, the quartz porphyry samples were found to belong to a separate group, the **extrusive group** (section 5.1.6), and a genetic relation between this group and the **intrusive group** (and now the Stolzburg trondhjemitic pluton) was not established. The **extrusive group** is therefore probably not a direct equivalent of the Stolzburg trondhjemite. The group however, does belong to a TTG suite according to figure 37 and the group's origin and setting may be the similar.

5.2.4 Origin of TTG suites

The Stolzburg Pluton and felsic Hooggenoeg Formation belong to the uncommon high-Al_2O_3 fractionation suites of TTG (or trondhjemite-tonalite-dacite "TTD") according to Drummond and Defant (1990)) with (1) high Sr (>300 ppm ranging up to >2000 ppm), very low Rb/Sr ratios of <0.15, (2) enriched LREEs, depleted HREEs, and no Eu anomaly or only a slight positive or negtavie one, (3) low Y (<15 ppm), (4) low to moderate K/Rb, mostly below 550, and (5) low Nb (<10-11 ppm). Figure 38 is a schematic diagram showing the different possible origins envisioned for low-Al_2O_3 and high-Al_2O_3 trondhjemitic magmas[18] (from Barker and Arth, 1976). It shows that high-Al_2O_3 trondhjemitic-tonalitic liquids may form by either fractionation of a wet basalt or partial melting of a basaltic parent which has inverted to either amphibolite or quartz eclogite. Drummond and Defant (1990) suggested that the distinction between low- and high-Al_2O_3 TTG types may be due to lack of hornblende involvement and initial hornblende extraction in TTD genesis, respectively.

The most prevalent hypothesized means of producing high-Al_2O_3 TTG in the Precambrian is by partial melting of amphibolite or quartz eclogite (although melting from eclogitic assemblages to create Archaean TTG is debated by some on the grounds that there exist only scarce outcrops of eclogite in all granite-greenstone terrains; eg. Barker and Arth, 1976). This mechanism seems plausible for the BGB-TTG as well. HREE-depletion and steep negatively slopes of the REE patterns have been attributed to high-pressure garnet and/or hornblende extraction (Drummond and Defant, 1990). Drummond and Defant (1990) have attempted to determine the relative portions of garnet versus hornblende by evaluating the general shape of the REE patterns (pure hornblende extraction would yield concave-up REE pattern, due to the strong affinity of hornblende for the middle REE) and by determining the degree of aluminum saturation in the rock (TTG magmas derived from a basaltic parent with hornblende-rich, garnet-barren refractory, at 5-8 kbar, are strongly peraluminous). The involvement of a strongly peraluminous phase, such as garnet, may have lowered aluminum saturation levels in many high-Al_2O_3 TTG. Positive Eu anomalies may be caused by the effective removal of garnet amphibolite or eclogite restite, although Eu signatures could be a function of several processes (see Drummond and Defant (1990) for a detailed digress). Low K/Rb values are thought to be a function of hornblende extraction because of its greater affinity for K relative to Rb.

[18] Barker and Arth (1976) placed the boundary between the low- and high-Al_2O_3 TTG at ~15 wt% Al_2O_3. The Al_2O_3 content of the Hooggenoeg Formation felsic rocks and the Stolzburg Pluton samples from this study is approximately ~15 wt%, or slightly below. However, it is believed that their original contents, before silicification, may have been higher. Their trace elemental contents are also more comparable with the high-Al_2O_3 suites as described by Drummond and Defant (1990).

Barker and Arth (1976) suggested a model involving partial melting of amphibolite under wet conditions for the genesis of trondhjemitic liquids in Archaean grey gneiss terrains. They proposed mantle upwelling and basaltic volcanism (probably in rift zones) led to the formation of a thick pile of which the lower parts metamorphosed to (hornblende – plagioclase ± quartz) amphibolite with the necessary water coming from interstitial sources. Wolf and Wyllie (1991) calculated that amphibolite begins to melt below 850 °C, because multicomponent amphibole begins to break down about 200 °C below its upper temperature stability limit, releasing vapour to cause H_2O-saturated melting elsewhere in the rock. (In lineated amphibolites the boundaries between elongated grains can become pathways for the migration of liquid or the diffusion of components during partial melting.) Partial melting of the amphibolite at less than 10 kb total pressure would have yielded trondhjemitic-tonalitic liquids which ascended and extruded into the upper crust before the fraction of melting of the parental amphibolite exceeded about 40% (before the liquid phase became andesitic). The residue of partial melting would have been transformed to anhydrous, refractory assemblages and mantle upwelling and basaltic volcanism continued as trondhjemitic-tonalitic liquids were being extruded.

The origin of the felsic melts of the **intrusive group** (and possibly the **extrusive group**) of the Hooggenoeg Formation is likely the same as those of the Stolzburg Pluton and other TTG suites. Melting of amphibolite or quartz eclogite is the most probable means of producing these rocks. Melting of a hydrous MORB source, leaving an eclogitic to amphibolitic residuum, in young subduction zones (<20-30 Ma) has been suggested as a possible site for Cenozoic high-Al_2O_3 TTG generation (a.o. Drummond and Defant, 1990; Martin, 1993) (see section 5.4 for more on possible tectonic settings of TTG).

5.3 OTHER VEINS AND INTRUSIONS

5.3.1 Cherts

De Vries (1999, Unpubl.) and other authors (cited in de Vries 1999, Unpubl.) have described the nature of the sedimentary and structureless black chert veins of the felsic volcano-sedimentary sequence (unit 1). De Vries (1999, Unpubl.) concluded that the majority of the Upper Onverwacht Group cherts were of secondary origin, based on the fact that often sedimentary structures and/or textures were still visible, and that gradations from clastic sediments to chert existed both across and along strike. De Vries (1999, Unpubl.) also concluded that the depositional environment of the volcano-sedimentary sequence, in which these cherts were sampled, was a subaerial to shallow water one. Stromatolitic sedimentary textures, cracked bedding plane biofilms and the presence of evaporite minerals (gypsum, calcite and halite) and a thick resistant biofilm in cherts sampled more to the East in the BGB, led Westall *et al.* (2001) to conclude that the cherts were deposited in a shallow environment as well, periodically subaerially exposed, e.g. in tidal flats or sabkhas, in an otherwise deep depositional environment of basalts. The presence of tourmaline, the general silicification of the rocks, the excellent preservation of fossils, and oxygen isotopic studies on fluid inclusions, were believed to indicate that the rocks have been overprinted by hydrothermally circulated, modified seawater of evaporitic origin, no warmer than 200°C. De Vries (1999, Unpubl.) suggests that the circulation of crater-lake water could have taken place.

In order to test if silicification of the Buck Ridge Chert complex occurred via the vertical black chert veins, chemical data from both rock types should be compared. In the field, a

relation between samples LV01-62 and LV01-133C could be observed. The first was taken from a vertical vein, and the second from the bedding parallel sedimentary chert unit capping the vein. REE patterns (figure 28h) are not identical for the two, however the spider diagram trends relative to Primordial Mantle (figure 29h) are virtually identical, including similar negative P anomalies, which the two other chert samples do not have. Granted, this is too small a number of samples to base any conclusions on regarding silicification processes, however it does indicate that future research would benefit greatly from a more detailed analysis of geochemical data from these and other chert samples.

5.3.2 Pyroxene/amphibole porphyries

Dyke and sill stock works of the pyroxene/amphibole porphyries have been described by de Vries (1999, Unpubl.) and Houtzager (2001, Unpubl.) and have not been observed intruding higher into the stratigraphy than the Lower Buck Ridge Chert (unit 2 of the Buck Ridge Chert complex after de Vries, 1999, Unpubl.) (de Vries, pers. comm.). New, unpublished geochronological data (de Vries, pers. comm.) from sample SV01-3 was found to be 3227.8 ± 2.5 Ma, which is significantly younger than that of the Hooggenoeg Formation, and equal, within error, to that of the Kaap Valley Tonalite (see figure 3). De Ronde *et al.* (1991) suggested a co-magmatic relationship for other porphyritic sills (the Mudpools and Ironstrone porphyries) in the central region of the Barberton Greenstone Belt.

Geochemical data, including REEs, from the Kaap Valley Tonalite have been presented by Robb and Anhaeusser (1983), Condie and Hunter (1976) (an average of five samples) and de Ronde *et al.* (1991). Robb and Anhaeusser stated that the potash-rich batholiths of the second magmatic cycle, and in particular the Kaap Valley Pluton (see figure 5c), are more mafic than the biotite-bearing trondhjemites (with up to 25 % hornblende and biotite). They are said to have Rb/Sr ratios of 0.3-0.4. The ratios of the pyroxene-amphibole porphyries vary two orders of magnitude, but on average are indeed higher than the ratios of the TTG of the first magmatic cycle. Figure # shows a plot in which the REE trends of the four pyroxene/amphibole porphyries presented in this study, along with the Kaap Valley Tonalite sample from the literature, are plotted. The data do not clearly indicate a relationship between the two rock types: ΣLREE values are similar for the samples W01-3, SV01-3 and SV01-46 (SV01-1 was already found to be deviant in many aspects, see section 4.3.6) and the Kaap Valley samples, but the latter appear to be slightly less depleted in HREE than the pyroxene/amphibole porphyries, in other words: their differentiation trends are different.

5.3.3 (Ultra-) Mafic rocks

The petrographic analyses of the coarse-grained (in particular but also the fine-grained) (ultra-) mafic rocks have shown great diversities in mineral content and states of alteration. Almost all have proven to be tholeiitic basaltic in composition (section 4.3) (except two of the six silicified basalts) and all REE differentiation trends (figures 28f and g) are similar.

Cloete (1999) has reported extensively on the (ultra-) mafic units of the Komati and Hooggenoeg Formations on the western limb of the Onverwacht Anticline. The majority of the mafic flows of the Hooggenoeg Formation are massive, with less than 15 % of the area underlain by pillows. Komatiitic basalts[19] comprise ≤ 30 % of the formation (excluding the ≤2

[19] Komatiitic basalts are essentially magnesian basalts and are classified as komatiitic basalts because of their spatial relationship to komatiites and their petrographic features including olivine or pyroxene spinifex textures (Cloete, 1999, p.14).

km thick felsic units of the Hooggenoeg Formation, termed "Buck Ridge rhyodacitic sill" by Cloete (1999)) occurring in the central part. The latter are intimately interleaved with tholeiitic basalts. Isolated clusters of pillows occur in the formation, which are larger towards the top and grade upwards into the massive flows containing vesicles. The increasing degree of vesiculation and upward increase in frequency of chert horizons, were interpreted to reflect a shoaling shallow sea depositional environment (with episodic drowning of the lava platform) for the Hooggenoeg Formation.

The continuance of the Hooggenoeg Formation flows across the entire length of the western limb of the Onverwacht Anticline for ≥ 15 km, its ~3.5 km thickness (a similar thickness exists for the Komati Formation), a platform architecture without steep palaeoslopes, and predictions of high extrusion rates, were found consistent with the observations of the dominance of sheet-flooding versus pillow formation. Sheet-flood flows propagate radially away from overflowing lava fissures and all parts of the flow fronts are progressive and dynamic (see references in Cloete, 1999). A depression-free topography is essential, because topographical features allow hotter parts of flows to propagate more efficiently than cooler parts, thereby effecting viscosities and flow speeds. No primary fissures crop out on the western limb of the Onverwacht Anticline, so if large fissures existed, they were spaced at relatively large intervals, or oriented subparallel to the present erosion surface.

Cloete (1999) concluded that the volcanics of the Komati and Hooggenoeg Formations do not resemble typical MOR-type crust, but are more like the lavas in the upper parts of oceanic plateaus of modern oceans. Oceanic plateaus are anomalously thick volcanic piles, typically elevated to between 2-3 km above the oceanic crust, and ranging in thickness from 20-40 km, which is two to five times thicker than standard oceanic crust; examples of modern oceanic platforms are the Otong-Java Plateau, the Caribbean Plateau and the plateau on which Iceland stands. They are thought to from cataclysmically when the bloated heads of emerging mantle plumes invade the base of the lithosphere and are associated with the outpourings of several times more lava than those extruded in the continental flood basalts of the Deccan Traps, in only a few million years time. Oceanic plateaus are relatively buoyant and inclined to resist block subduction; during collision they accrete or uplift onto adjacent arcs and it is believed that the Onverwacht Oceanic Plateau was tectonically emplaced along the major thrust at the base Komati Formation between 3453 ±6 and 3445 ± 8 Ma (Cloete, 1999). This was immediately followed by the main surge of trondhjemitic magmatism in the south western part of the BGB. The sudden tectonic loading of the Theespruit arc-trench may have been the direct cause of melting of amphibolitic assemblages to produce the TTG and **intrusive** (and possibly **extrusive**) **group** rocks of the Hooggenoeg Formation. This would imply that the basaltic rocks of the Hooggenoeg Formation are not the direct parental material for the felsic rocks. The REE trends of the (ultra-) mafic rocks and those of the felsic rocks of the Hooggenoeg Formation also do not show many similarities: neither rock types show significant anomalies in their REE trends, except a slight negative Eu anomaly for the (ultra) mafic rocks and slight positive Eu anomalies for the felsic rocks. Their spider diagram patterns are different as well (figure 29), except for positive K and negative Sr anomalies in all.

Thrusting of the Onverwacht Oceanic Plateau over the Theespruit Formation, before deposition of the Buck Ridge Chert complex, and subsequent felsic magmatism, does not account for the second period of felsic TTG igneous activity during the deposition of the Fig Tree Group.

5.4 TECTONIC SETTING

5.4.1 Plate-tectonics in the Archaean?

It has been suggested by many authors (e.g. Drummond and Defant, 1990; de Wit, 1998; Martin, 1986 and 1999) that plate-tectonic processes, although most likely in a slightly different form, have operated in Archaean time: e.g. de Wit (1998) stated that back arc spreading may not have been as prominent in the Early Archaean. Although not everyone agrees with this consensus: e.g. Vlaar *et al.* (1994) believe recycling of basaltic crust into the mantle through its high-pressure phase eclogite, and the consumption of latent heat upon solidification of renewed pressure-release melt and advective cooling through magma migration, were sufficient to cool the early Archaean mantle by several hundred degrees. Hamilton (1998) fiercely opposes plate-tectonics in the Archaean as well by stating that granite-and-greenstone terrains have no modern analogues at all due to the lack of relationships between distinctive accretionary wedges, forearc assemblages, magmatic arcs, and backarc complexes, and the fact that rifts and continental-margin wedges of shelf have not been identified.

The commonness of high-MgO komatiites in Archaean terrains, which were believed to be emplaced at temperatures of 1600 °C (lithosphere temperatures in modern constructive plate margins were estimated at 1200-1250 °C (see references in Martin, 1993)), and which are absent from the lower Proterozoic on, have in the past been used to argue the probable different nature of plate-tectonism in the Archaean (Martin, 1986). They were believed to be produced at high melting temperatures deep in the mantle by mantle plumes like those responsible for volcanism in Hawaii and Iceland today (Arndt *et al.*, 1998 and Walter, 1998; references in Parman *et al.*, 2001). However, in a paper published in 2001 by Parman *et al.*, it was stated that Phanerozoic boninites are chemically and petrographically very similar to Barberton basaltic komatiites and that the high-MgO boninites are produced exclusively in subduction zones by hydrous melting at shallow depths. This is possible due to the high concentrations of H_2O in the rocks and mantle production temperatures are now estimated at 1400-1500 °C (Parman *et al.*, 2001). Kröner and Layer (1992) even go on to state that numerical calculations and available paleomagnetic data (although based on a very limited dataset, often with data points only once every 200 Myr) suggest that plate velocities have not changed much trough geologic time and were presumably 17 mm/year (references in Kröner and Layer, 1992) between 3.5 and 2.4 Ga. Vertical accretion through plume-induced magmatic underplating in an Iceland-type setting, could account for the extraordinarily high crust production rate in the Archaean, and the extensive shortening and thrusting observed in many Archaean cratons was explained as "crumpling" or the sideways motion of lithospheric fragments above mantle plumes. Others have claimed that plume magmatism cannot account for the additional water needed for melting of amphibolite (see section 5.2.4), and that thrusting tectonics indicate that rigid plates existed in the Archaean (de Wit *et al.* 1987).

It has been suggested by Martin (1993 and 1999) that Archaean TTG suites are formed when geothermal gradients along the Benioff plane are very high, leading to melting of the subducting slab at shallow depths before dehydration occurs and plagioclase could be a residual phase. TTG magmatism has been suggested to occur in subduction related settings today (Barker, 1979; Drummond and Defant, 1990) and Martin (1999) proposed that

adakites[20] may be modern day equivalents of **Late** (Smithies, 2000; Martin and Moyen, 2002) Archaean TTG. Adakites are exclusively found in subduction zone environments, where the subducted slab is young (<20 Ma) as in Southern Chile. Because Early Archaean TTG are poorer in Mg, Ni and Cr than adakites, mantle-magma interactions were less efficient, probably due to the shallower depth of slab melting (Martin, 1999 and Martin and Moyen, 2002). Longer ridge systems and more numerous plates associated with a larger number of triple junctions, were envisioned as a more efficient way of dissipating the higher amount of heat produced (Lagabrielle *et al.*, 1997), such as those in the North Fiji Basin where more than half of the total length of the present spreading boundaries are not directly controlled by the kinematics of the major subduction.

The ideas concerning plate-tectonics in the Archaean are still very controversial and subject of heated debate. Therefore the felsic and (ultra-) mafic rocks of the Hooggenoeg Formation will be tested to see if they show geochemical signatures which are indicative of (modern) subduction zone settings.

5.4.2 Chemical indications of tectonic setting – Discrimination diagrams

In figure 40, after Irvine and Baragar (1971) and Wilson (1989), the classification of common volcanic rocks can be seen with their specific tectonic settings. Interpretation of the samples based solely on major elemental characteristics (in particular total alkalis). The classification indicates that the felsic rocks of the BGB are calc-alkaline dacites and rhyolites. Modern calc-alkaline suites form volcanoes near convergent plate boundaries (in subduction zones) where the depth to the Benioff zone exceeds 100 km, provided that the subduction angle is greater than 25°. The proportions of various rock types depend on e.g. the types of plates involved in convergence, the angle of subduction, and the rates of convergence (Philpotts, 1990, p.282). The principal rock type is a two-pyroxene andesite with about 59% SiO_2, and the eruptions tend to be more explosive than those of island-arc tholeiite association, with pyroclastic fall and flow deposits (Philpotts, 1990, p.282 and Fisher and Schminke, 1984, p.20-21). It is very well possible that more of the Hooggenoeg Formation consists of pyroclastic rocks, like those observed at LV01-109B, which are now no longer recognizable, e.g. due to silicification.

A number of discrimination diagrams are used here to investigate possible tectonic settings. It should be noted that as fractionation of accessory minerals may have taken place in the felsic rocks of the Hooggenoeg Formation (section 5.1.6), trace elemental compositions (including incompatible and immobile elements) may have been effected. Pearce *et al.* (1984) constructed diagrams based on trace elements, which indicate the nature of the source regions of granitic magmas, that in conjunction with geological constraints, may add information about post Archaean tectonic settings. They stated that the discrimination between granites of different tectonic settings is most effective in Rb-Y-Nb and Rb-Yb-Ta space, but that for Archaean granites a diagram of Y versus Nb is more appropriate (see Pearce *et al.*, 1984). In the granitic classification diagram in figure 41a, all felsic samples of the Hooggenoeg Formation, Stolzburg Pluton and the pyroxene/amphibole porphyries were plot. All samples (except SV01-1) plot in the *volcanic arc granite* field. The setting of these granites range from

---

[20] "Adakites are intermediate to felsic volcanic rocks, andesitic to rhyolitic in composition (basaltic members are lacking). They have trondhjemitic affinities (high Na_2O contents and K_2O/Na_2O ~ 0.5) and their Mg no. (0.5), Ni (20-40 ppm) and Cr (30-50 ppm) contents are higher than in typical calc-alkaline magmas. Sr contents are high (> 300 ppm, until 2000 ppm) and REE show strongly fractionated patterns with very low heavy REE contents (Yb <= 1.8 ppm, Y <= 18 ppm)." (Martin, 1999)

oceanic to continental and their compositions range from tholeiitic to calc-alkaline to shoshonitic. A shortcoming of the diagram is that it does not geochemically discriminate for post-collision granites, since their characteristics depend on the thickness and composition of the lithosphere involved in the collision event and on the precise timing and location of magmatism (Pearce *et al.*, 1984). The geochemistry of associated basalt suites from the BGB are tested for geochemical indications of subduction as well.

Pearce and Cann (1973) devised a classification scheme for basic volcanic rocks based on trace element concentrations of Zr, Ti and Y, which are believed to be insensitive to processes of alteration. All mafic and ultramafic samples are plot in figure 41b and lie in the fields B, C and D. (All coarse grained rocks lie in field B, except for LV01-143). Tthat tholeiitic to alkalic ocean-floor basalts plot within fields D and B. Calc-alkali basalts (volcanic arc basalts) within fields C and B; the first being characteristic of divergent plate boundaries, and the second of convergent plate boundaries. Wood *et al.* (1979) constructed a diagram based on the incompatible elements Th, Hf and Ta, to supplement the Zr-Ti-Y diagram of Pearce and Cann (1973) in order to discriminate between silicic magmas derived from E-type MORB or within plate basalts and those associated with destructive plate margins or remelted continental crust. Both the felsic and (ultra-) mafic samples are shown in figure 41c. The felsic samples, Stolzburg trondhjemite and pyroxene/amphibole porphyries plot in field D (magma series erupted at destructive plate margins) and the (ultra-) mafic samples plot in fields A and B (N- and E-type MORB respectively). N-type MORBs are MORBs erupted at normal ridge segments and E-type MORBs those erupted at ridge segments with positive residual gravity depth and heat flow anomalies, often associated with "hot spots" (Wood *et al.*, 1979).

Additional information can be obtained by comparing spider diagram trends of the (ultra-) mafic rocks with those of present day basalts from known tectonic settings (e.g. after Thompson *et al.*, 1984). The (ultra-) mafic rocks of the Hooggenoeg Formation of the BGB are clearly different from modern basalts as can be seen in figures 42a and b. The patterns show positive Rb, K and (slight) Ta anomalies and significant negative Sr anomalies. Alkalic ocean island basalts are characterized by enrichments in Nb (and Ta), island arc calc-alkaline basalts by positive K anomalies and depletions in Nb and Ta (Thompson *et al.*, 1984). The relatively flat trend of the spider patterns also indicates that the rocks are not derived from a depleted mantle like the one from which Mid Ocean Ridge Basalts are generated. Subduction-related basalt spider patterns are spiked as a consequence of the components added to the mantle source of the basalts by subduction-zone fluids (Wilson, 1989, p.21). It is clear that there is no real proof of subduction indicators.

The diagrams are not conclusive and do not indicate a single tectonic setting. They indicate that the felsic rocks of the Hooggenoeg Formation may have indeed been formed in subduction zones (in volcanic arcs). However, Hamilton (1998) states that intermediate and felsic rocks are also widespread in severely extensional settings and in some continental rift-shoulder regions; similarities between Archaean and modern rocks may reflect similar conditions of melting and equilibration, but not necessarily similar tectonic settings. The tectonic setting of the (ultra-) mafic rocks remains even more uncertain. Discrimination diagrams are not conclusive and the spider diagram patterns are not comparable to those from known tectonic settings. Possibly, isotopic Sr-Nd-Pb studies may shed more light on the possible sources of the mafic rocks.

5.5 COMPARISON OF THE FELSIC ROCKS OF THE HOOGGENOEG FORMATION WITH INTERMEDIATE AND FELSIC FORMATIONS OF THE WARRAWOONA GROUP, PILBARA CRATON, WESTERN AUSTRALIA

5.5.1 Vaalbara

Cheney (1996) stated that the western part of the Kaapvaal Craton and the Pilbara Province of Western Australia, must have once been part of the same continent, termed "Vaalbara". Similarities in terms of sedimentological characteristics between the two cratons (Cheney, 1996; Lowe, 1982) indicate a shared depositional and tectonic history from 2.7 to 2.1 Ga: Vaalbara possibly existed from >3.1 Ga to ≤1.5 Ga. Zegers *et al.* (1998) concluded from new structural, geochronological and palaeomagnetic data that Vaalbara existed at least as far back as 3.1 Ga and possibly further back to 3.6 Ga. The most remarkable correlation is the timing of pre-amalgamation felsic volcanism in the submarine sequences of both cratons (3.45 and 3.47 Ga), which predate the compressional phase between 3.3 and 3.1 Ga. Nelson *et al.* (1999) argued the existence of Vaalbara during the period from 3650 to 2200 Ma by stating that significant differences exist in the chronologies of magmatic events within the granite-greenstone crusts of the Pilbara and Kaapvaal Cratons, and that a number of magmatic events were identified in only one of the two cratons. Granite-greenstone crust formation within both cratons was episodic, with major episodes of ca 10-100 Myr of volcanism on (and granitic intrusion into) pre-existing granite-greenstone crust, separated by periods of magmatic quiescence and deposition of clastic and chemical sediments.

5.5.2 The Warrawoona Group and the Duffer and Panorama Formations

Figure 43 is a comparison between the position and stratigraphic sequence of the Archaean Kaapvaal and Pilbara Cratons and shows that the Onverwacht Group of the BGB is contemporaneous with the Warrawoona Group of the Pilbara (Zegers *et al.*, 1998; Thorpe *et al.*, 1992). The Warrawoona Group is also known for containing a range of shallow-water sedimentary and volcanic facies including carbonate sedimentary rocks, possibly stromatolites, and sulphate evaporites, as well as characteristic submarine volcanic greenstone-belt assemblages (Barley, 1997). The Duffer Formation makes up the bulk of the sequence of early Archaean felsic (and intermediate) volcanic and volcaniclastic rocks and chert present in the upper half of the Warrawoona Group (stratigraphic sequences by Hickman (1983, p.58) and DiMarco and Lowe (1989b); figure 44). It consists of up to 5 km of metamorphosed calc-alkaline dacitic to rhyolitic volcaniclastic breccia and lava, and lesser amounts of tuffaceous rocks and mafic lava. Post-Duffer felsic volcanism was marked by explosive pyroclastic activity and the widespread deposition of ash in surrounding shallow-water and subaerial systems, represented by the thinner, sandy Panorama Formation. The Panorama Formation comprises of silicified sandstone, tuff and volcaniclastic siltstone, silicified siltstone containing possible relict detrital clay, and altered felsic flow units (Cullers *et al.*, 1993).

Considerable debate has existed regarding the stratigraphic position of the Panorama Formation and its possible relation to the Duffer formation (for discussion and references see e.g. Nijman *et al.*, 1999). However, U-Pb age determinations of the felsic rocks of the Warrawoona Group were reported by Thorpe *et al.* (1992) to be 3471 ± 5 and 3465 ± 3 Ma for felsic volcanic and schistose rocks from the Duffer Formation and 3458 ± 1.9 Ma for a felsic lava from the Panorama Formation, similar to Hooggenoeg Formation ages (compare with figure 3). Unless the Duffer Formation was deposited over a period of 10 Myr, a Panorama-

Duffer correlation is not likely. Cullers *et al.* (1993) also suggested a polygenetic origin for felsic magmas of the Warrawoona Group, based on geochemical evidence that suggest that the Panorama felsic rocks were formed by direct melting of an eclogite residue without subsequent crystallization of feldspar, while the silicic volcanic rocks of the Duffer Formation are believed to have been produced by fractional crystallization of basaltic parents. This is evident from high $(La/Lu)_N$ ratios and the lack of negative Eu anomalies in the first, and negative Eu anomalies and lower $(La/Lu)_N$ ratios in the second case.

5.5.3 The Coppin Gap greenstone belt, Eastern Pilbara, Western Australia

The Coppin Gap greenstone belt, in the Eastern Pilbara (figure 45), is composed of an east-west striking asymmetric synclinorium between the Muccan and Mount Edgar batholiths. The vertical to overturned northern limb is intensely sheared, folded and tectonically reduced; the southern limb however, in which thick successions of the Duffer and Panorama Formations are located, is relatively undisturbed and irregularly intruded by the Mount Edgar batholith (Nijman *et al.*, 1999). Nijman *et al.* (1999) stated that a similar setting to the BGB existed in the Coppin Gap greenstone belt, involving detachment shear zones in the underlying Warrawoona basalts and ultramafic rocks and listric normal growth faulting, in places accompanied by synsedimentary, explosive intrusion of black chert veins, mega-brecciation and back tilt of fault blocks. They attributed this to either regional tensile stress or local caldera collapse, or both mechanisms acting simultaneously.

Due to its excellent preservation of the Warrawoona Group and its many similarities to the BGB, the (intermediate and) felsic Duffer and Panorama Formations of the Coppin Gap greenstone belt are a prime choice for comparison with the upper Hooggenoeg Formation of the BGB and to test the possible existence of Vaalbara ~3450 Ma (Zegers *et al.*, 1998; Nijman and de Wit, 1999). Data on the Duffer and Panorama Formations have been gathered and analysed within the framework of the EEB project (van der Meer, 2002, Unpubl.). Again, due to severe silicification (DiMarco and Lowe, 1989a) and alteration, comparisons were only attempted using evidence from petrography and REE (which are presumed immobile during alteration processes) trends.

The petrography of the Duffer Formation rhyodacite from the Coppin Gap greenstone belt was found to be fine-grained, but still relatively unaltered, with 1 cm sized phenocrysts of plagioclase and sanidine, smaller hexagonal quartz phenocrysts, and altered clinopyroxene phenocrysts with rims of microquartz. The Duffer Formation andesites are altered, with microquartz forming wavy patterns around phenocrysts of clinopyroxene and ghost structures of hornblende. The rocks contain a minor amount of plagioclase. Panorama Formation rhyolites are very similar to the silicified felsic Hooggenoeg Formation, with 4 mm sized clear quartz grains. Altered hornblende and plagioclase were only distinguishable due to ghost structures with diffuse grain boundaries and corroded/embayed phenocryst outlines (DiMarco and Lowe, 1989a; van der Meer, 2002, Unpubl.; Louzada, 2002, Unpubl.).

5.5.4 Geochemical comparisons between the (intermediate and) felsic units from the Barberton and Coppin Gap greenstone belts

Figure 46a shows that the Duffer intermediate and felsic rocks have higher ΣREE (the felsic rocks higher than the intermediate rocks) and are relatively less depleted in HREE than the rocks of the Hooggenoeg Formation. Also the significant negative Eu anomalies mentioned before are clearly visible in the felsic Duffer rocks. Two of the three REE patterns of the

Panorama felsic rocks in figure 46b however, resemble the differentiation trends of the Hooggenoeg felsic rocks very much and have ΣREE values slightly higher than those of the shallow intrusive rocks of the **intrusive group**. Van der Meer (2002, Unpubl.) also concluded that the felsic Duffer and felsic Panorama rocks do not have the same origin, and that the Panorama rocks originate form a melt without plagioclase as a residual phase. She stated that the Panorama rocks are a surface expression of felsic plutonic activity (also confirmed by DiMarco and Lowe, 1989b) and more resemble the Mt Edgar batholith and other granitic apophyses of the batholith into the Coppin Gap greenstone belt, just as the felsic **intrusive group** of the Hooggenoeg Formation is likely a high level equivalent of the nearby Stolzburg trondhjemitic pluton.

Both petrographic (including the pervasive silicification observed) and REE data show obvious similarities between the felsic Panorama Formation and the felsic rocks of the Hooggenoeg Formation. A more detailed geochemical and isotopic investigation is needed to confirm a possible equivalence of magma evolution in both parts of Vaalbara.

Chapter 6 – Conclusions

The following conclusions can be drawn from this geochemical study on the upper Hooggenoeg Formation of the Barberton Greenstone Belt:

- The felsic rocks of the upper Hooggenoeg Formation underlying the Buck Ridge Chert complex of the Barberton Greenstone Belt, consist of silicified and chloritized medium-grained interlocking intrusive rocks; finer grained shallow intrusive rocks with >50 % matrix; matrix-dominated, quartz (and plagioclase) rich porphyries; consolidated ashes or tuffs; and massive and flow banded lavas. Field relations between the groups were insufficiently exposed to indicate a genetic relationship between intrusive units, lava flows and vertical veins. Qualitative analysis of incompatible and immobile elemental data was undertaken and has shown that, although there are many similarities between the groups, there are two subdivisions to be made for the Hooggenoeg felsic rocks: an **intrusive group** which consists of interlocking and shallow intrusive rocks and a **porphyritic group** which consists of quartz porphyries. This distinction was made on the basis of differences in Sr, Zr, Hf, Ta, Nb, and K_2O/Ba, Rb/Sr and Ba/Sr ratios (and was not contradicted by the major elemental compositions, despite the pervasive alteration). It is possible that the two groups are related by the crystallization of accessory phases.

- Incompatible element data on the trondhjemitic Stolzburg Pluton from this study comply with that of other known Stolzburg samples and the are similar to that of the **intrusive group** of the felsic part of the Hooggenoeg Formation. The felsic rocks of the Hooggenoeg Formation are possibly indeed high level equivalents of the surrounding TTG terrain. Melting of amphibolite or quartz eclogite has been suggested as an origin for these high-Al_2O_3 suite magmas.

- The geochemical signatures of the different chert samples presented in this study (both sedimentary and from massive veins) are remarkable with extremely low major elemental concentrations (due to the extreme silicification) and extreme variability in trace elements. The process of sediments by the massive vertical veins was not substantiated by REE data.

- Despite geochronological indications that the pyroxene/amphibole porphyries are contemporaneous with the Kaap Valley Tonalite, a genetic relationship between the two rock types was not supported by REE patterns.

- No evidence was found to indicate that the tholeiitic (ultra-) mafic basalts of the Hooggenoeg Formation were a possible parent for the felsic groups.

- Trace elemental data suggests that subduction processes may have been responsible for the generation of the felsic part of the Hooggenoeg Formation, but the tectonic setting of the (ultra-) mafic part of the upper part of the Hooggenoeg Formation remains uncertain.

- Preliminary comparisons of the felsic rocks of the Hooggenoeg Formation and the (intermediate and) felsic rocks of the Duffer and Panorama Formations of the Coppin Gap greenstone belt (Pilbara Craton, Western Australia), based on geological setting, petrography, and REE data, suggest a possible genetic relation between the Panorama

Formation and the Hooggenoeg Formation. If true, this would suggest that Vaalbara did exist at the time of deposition of both formations (~3450 Ma).

Acknowledgements

I thank Dr. Manfred van Bergen for his supervision of this MSc project and revisions of this report. I thank Dr. Wout Nijman for introducing me to the Archaean geology of both the Barberton greenstone belt, and the Coppin Gap greenstone belt. I also heartily thank Prof. Maarten de Wit who arranged my two-month stay at the Department of Geological Sciences at the University of Cape Town, where I preformed my geochemical analyses supervised by Prof. Anton le Roex, Prof. David Reid and Mr. Andreas Spath. Finally, I would like to thank Sjoukje de Vries for the extreme fun we had during fieldwork (on both cratons).
This research was made possible by generous contributions from the Molengraaff Fonds (Delft), the Trajectum Fonds (Utrecht) and the Schürmann Fonds (Leiden).

References

Anhaeusser, C.R. and Robb, L.J. (1983). Chemical analyses of granitoid rocks from the Barberton Mountain Land. in C.R. Anhaeusser Ed., Contributions to the Geology of the Barberton Mountain Land, *Special Publication of the Geological Society of South Africa* **9**, 189-219.

Anhaeusser, C.R., Robb, L.J. and Viljoen, M.J. (1983). Notes on the provisional map of the Barberton greenstone belt and surrounding granitic terrane, Eastern Transvaal and Swaziland (1:250000 colour map) in C.R. Anhaeusser Ed., Contributions to the Geology of the Barberton Mountain Land, *Special Publication of the Geological Society of South Africa* **9**, 189-219.

Armstrong, R.A., Compston, W., de Wit, M.J., and Williams, I.S. (1990). The stratigraphy of the 3.5-3.2 Ga Barberton Greenstone Belt revisited: A single zircon ion microprobe study. *Earth and Planetary Science Letters* **101**, 90-106.

Barker, F. (1979). Trondhjemite: definition, environment and hypotheses of origin (1-12) *in* Developments in Petrology **6**: Trondhjemites, dacites, and related rocks. Barker, F. Amsterdam, Elsevier, 659 p.

Barker, F. and Arth, J.G. (1976). Generation of trondhjemitic-tonalitic liquids and Archean bimodal trondhjemite-basalt suites. *Geology* **4**, 596-600.

Barley, M.E. (1993). Volcanic, sedimentary and tectonostratigraphic environments of the ~3.46 Ga Warrawoona Megasequence: a review. *Precambrian Research* **60**, 47-67.

Barley, M.E. (1997). The Pilbara Craton (657-664) *in* de Wit, M.J. and Ashwal, L.D. (Eds), Greenstone Belts. Oxford, Clarendon Press, 809 p.

Brandl, G. and de Wit, M.J. (1997). The Kaapvaal Craton (581-607) *in* de Wit, M.J. and Ashwal, L.D. (Eds), Greenstone Belts. Oxford, Clarendon Press, 809 p.

Byerly, G.R., Kröner, A., Lowe, D.R., Todt, W., and Walsh, M.M. (1996). Prolonged magmatism and time constraints for sediment deposition in the early Archean Barberton greenstone belt: evidence from the Upper Onverwacht and Fig Tree groups. *Precambrian Research* **78**, 125-138.

Cas, R.A.F. and Wright, J.W. (1987). Volcanic Successions: Modern and Ancient: a Geological Approach to Processes, Products and Successions. London, Allen & Unwin (Publishers) Ltd, 487 p.

Cheney, E.S. (1996). Sequence stratigraphy and plate tectonic significance of the Transvaal succession of southern Africa and its equivalent in Western Australia. *Precambrian Research* **79**, 3-24.

Cloete, M. (1999). Aspects of volcanism and metamorphism of the Onverwacht Group lavas in the south-western portion of the Barberton greenstone belt. Memoir of the Geological Survey of South Africa **84**, Pretoria, Council for Geoscience, 232 p.

Condie, K.C. and Hunter, D.R. (1976). Trace element geochemistry of Archaean granitic rocks from Barberton region, south Africa. *Earth and Planetary Science Letters* **29**, 389-400.

Cullers, R.L., DiMarco, M.J., Lowe, D.R., and Stone, J. (1993). Geochemistry of a silicified, felsic volcaniclastic suite from the early Archaean Panorama Formation, Pilbara Block, Western Australia: an evaluation of depositional and post-depositional processes with special emphasis on the rare-earth elements. *Precambrian Research* **60**, 99-116.

de Ronde, C.E.J., Channer, D.M.deR., Faure, K., Bray, C.J., and Spooner, E.T.C. (1997). Fluid chemistry of Archean seafloor hydrothermal vents: Implications for the composition of circa 3.2 Ga seawater. *Geochimica et Cosmochimica Acta* **61**, 4025-4042.

de Ronde, C.E.J., Kamo, S., Davis, D.W., de Wit, M.J., and Spooner, E.T.C. (1991). Field geochemical and U-Pb isotopic constraints from hypabyssal felsic intrusions within the Barberton greenstone Belt, South Africa: Implications for tectonics and the timing of gold mineralization. *Precambrian Research* **49**, 261-280.

de Ronde, C.E.J., de Wit, M.J., Spooner, E.T.C. (1994). Early Archean (>3.2 Ga) Fe-oxide-rich, hydrothermal discharge vents in the Barberton greenstone belt, South Africa. *Geological Society of America Bulletin* **106**, 86-104.

de Ronde, C.E.J. and de Wit, M.J. (1994). Tectonic history of the Barberton greenstone belt, South Africa: 490 million years of Archean crustal evolution. *Tectonics* **13**, 983-1005.

de Vries, S.T. (July 1999). Sedimentology, deformation and felsic volcanism of the Early Archaean Buck Ridge Chert complex, Upper Onverwacht Group, Barberton Greenstone Belt, South Africa. *Unpublished MSc thesis*, 50 p. excl figures.

de Wit, M.J. (1983). Notes on a preliminary 1:25000 geological map of the southern part of the Barberton greenstone belt. in C.R. Anhaeusser Ed., Contributions to the Geology of the Barberton Mountain Land, *Special Publication of the Geological Society of South Africa* **9**, 185-187.

de Wit, M.J. (1998). On Archaean granites, greenstones, cratons and tectonics: does the evidence demand a verdict? *Precambrian Research* **91**, 181-226.

de Wit, M.J., Armstrong, R., Hart, R., and Wilson, A.H. (1987). Felsic igneous rocks within the 3.3-3.5 Ga Barberton Greenstone Belt: High crustal level equivalents of the surrounding tonalite-trondhjemite terrain, emplaced during thrusting. *Tectonics* **6**, 529-549.

de Wit, M.J., Roering, C., Hart, R.J., Armstrong, R.A., de Ronde, C.E.J., Green, R.W.E., Tredoux, M., Peberdy, E., and Hart, R.A. (1992). Formation of an Archaean continent. *Nature* **357**, 553-562.

DiMarco, M.J. and Lowe, D.R. (1989a). Petrography and provenance of silcified early Archaean volcaniclastic sandstones, eastern Pilbara Block, Western Australia. *Sedimentology* **36**, 821-836.

DiMarco, M.J. and Lowe, D.R. (1989b). Stratigraphy and Sedimentology of an Early Archean Felsic Volcanic Sequence, Eastern Pilbara Block, Western Australia, with Special Reference to the Duffer Formation and Implications for Crustal Evolution. *Precambrian Research* **44**, 147-169.

Drummond, M.S., and Defant, M.J. (1990). A model for trondhjemite-tonalite-dacite genesis and crustal growth via slab melting: Archean to modern comparisons. *Journal of Geophysical Research* **95 B13**, 21503-21521.

Fisher, R.V. and Schmincke, H.-U. (1984). Pyroclastic Rocks. Berlin, Springer-Verlag, 472 p.

Green, T.H. (1980). Island arc and continent building magmatism – a review of petrogenetic models based on experimental petrology and geochemistry. *Tectonophysics* **68**, 367-385.

Hamilton, W.B. (1998). Archean magmatism and deformation were not products of plate tectonics. *Precambrian Research* **91**, 143-179.

Hickman, A.H. (1983). The geology of the Pilbara Block and its environs. *Bulletin – Geological Society of Western Australia* **127**, 268 p.

Holcomb, R. (September 13, 2001). GEOrient 8.0: Stereographic projections and rose diagram plots for Windows 95/98/NT. Department of Earth Sciences, University of Queensland, Australia.

Houtzager, O. (June 2001). The 3.4 Ga-old Buck Ridge Chert complex of the Barberton Greenstone Belt: A comparison of tectono-sedimentary models. *Unpublished MSc thesis*, 45 p. + figures.

Hunter, D.R. and Stowe, C.W. (1997). A Historical Review of the Origin, Composition, and Setting of Archaean Greenstone Belts (Pre-1980) (5-29) *in* de Wit, M.J. and Ashwal, L.D. (Eds), Greenstone Belts. Oxford, Clarendon Press, 809 p.

Irvine, T.N. and Baragar, W.R.A. (1971). A guide to the chemical classification of the common volcanic rocks. *Canadian Journal of Earth Sciences* **8**, 523-548.

Kamo, S.L. and Davis, D.W. (1994). Reassessment of Archean crustal development in the Barberton Mountain Land, South Africa, based on U-Pb dating. *Tectonics* **13**, 167-192.

Kröner, A. and Compston, W. (1988). Ion-Microprobe ages of zircons from early Archaean granite pebbles and greywacke, Barberton Greenstone Belt, Southern Africa. *Precambrian Research* **38**, 367-380.

Kröner, A., Hegner, E., Wendt, J.I., and Byerly, G.R. (1996). The oldest part of the Barberton granitoid-greenstone terrain, South Africa: evidence for crust formation between 3.5 and 3.7 Ga. *Precambrian Research* **78**, 105-124.

Kröner, A. and Layer, P.W. (1992). Crust formation and plate motion in the Early Archean. *Science* **256**, 1405-1411.

Kröner, A. and Todt, W. (1988). Single zircon dating constraining the maximum age of the Barberton Greenstone Belt, Southern Africa. *Journal of Geophysical Research* **93**(B12), 15329-15337.

Krüner, A., Byerley, G.R. and Lowe, D.R. (1991). Chronology of early Archaean granite-greenstone evolution in the Barberton Mountain Land, South Africa, based on precise dating by single zircon evaporation. *Earth and Planetary Science Letters* **103**, 41-54.

Lachance, G.R. and Claisse, F. (1995). Quantitative x-ray fluorescence analysis: theory and application. Chichester, Wiley, 402 p.

Lagabrielle, Y., Goslin, J., Martin, H., Thirot, J-L., and Auzende, J-M. (1997). Multiple active spreading centres in the hot North Fiji Basin (Southwest Pacific): a possible model for Archaean seafloor spreading? *Earth and Planetary Science Letters* **149**, 1-13.

Le Bas, M.J., Le Maitre, R.W., Strekeisen, A., and Zanettin, B. (1986). A chemical classification of volcanic rocks based on the total alkali-silica diagram. *Journal of Petrology* **27**, 745-750.

Louzada, K.L. (July 2002). The Coppin Gap greenstone belt at Kittys Gap, Eastern Pilbara, Western Australia: third year lithological mapping-exercise field report, *Unpublished thesis*, 27 p. excl. figures and appendices.

Lowe, D.R. (1982). Comparative sedimentology of the principal volcanic sequences of Archean greenstone belts in South Africa, Western Australia and Canada: Implications for crustal evolution. *Precambrian Research* **17**, 1-29.

Lowe, D.R. (1999). Geologic evolution of the Barberton Greenstone Belt and vicinity. *Special Paper Geological Society of America* **329**, 287-312.

Lowe, D.R. and Byerly, G.R. (1999). Stratigraphy of the west-central part of the Barberton Greenstone Belt, South Africa. *Special Paper Geological Society of America* **329**, 1-36.

Lowe, D.R., Byerly, G.R., Ransom, B.L. and Nocita, B.W. (1985). Stratigraphic and sedimentological evidence bearing on structural repetition in Early Archean rocks of the Barberton Greenstone Belt, South Africa. *Precambrian Research* **27**, 165-186.

Lowe, D.R., Byerly, G.R. and Heubeck, Ch. (1999). Structural divisions and development of the west-central part of the Barberton Greenstone Belt. *Special Paper Geological Society of America* **329**, 37-82.

MacKenzie, W.S., Donaldson, C.H. and Guilford, C. (1982). Atlas of igneous rocks and their textures. Essex, Longman Group Ltd, 148 p.

Martin, H. (1986). Effect of steeper Archean geothermal gradient on geochemistry of subduction-zone magmas. *Geology* **14**, 753-756.

Martin, H. (1993). The mechanisms of petrogenesis of the Archaean continental crust – comparison with modern processes. *Lithos* **30**, 373-388.

Martin, H. (1999). Adaktitic magmas: modern analogues of Archaean granitoids. *Lithos* **46**, 411-429.

Martin, H. and Moyen, J.-F. (2002). Secular changes in tonalite-trondhjemite-granodiorite composition as markers of the progressive cooling of Earth. *Geology* **30**, p.319-322.

Nakamura, N. (1974). Determination of REE, Ba, Fe, Mg, Na and K in carbonaceous and ordinary chondrites. *Geochimica et Cosmochimica Acta* **38**, 757-775.

Nelson, D.R., Trendall, A.F. and Altermann, W. (1999). Chronological correlations between the Pilbara and Kaapvaal cratons. *Precambrian Research* **97**, 165-189.

Nijman, W. and de Wit, M.J. (November, 1999). Earth's earliest sedimentary basins; an integrated approach to Early Archean basin dynamics (a project proposal). 14 p.

Nijman, W., Willigers, B.J.A. and Krikke, A. (1999). Tensile and compressive growth structures: relationships beteen sedimentation, deformation and granite intrusion in the Archaean Coppin Gap greenstone belt, Eastern Pilbara, Western Australia. *Precambrian Research* **95**, 277-302.

Robb, L.J. and Anhaeusser, C.R. (1983). Chemical and Petrogenetic Characteristics of Archaean Tonalite-Trondhjemite Gneiss Plutons in the Barberton Mountain Land. in C.R. Anhaeusser Ed., Contributions to the Geology of the Barberton Mountain Land, *Special Publication of the Geological Society of South Africa* **9**, 103-116.

Parman, S.W., Grove, T.L., and Dann, J.C. (2001). The production of Barberton komatiites in an Archean subduction zone. *Geophysical Research Letters* **28**, 2513-2516.

Pearce, J.A. and Cann, J.R. (1973). Tectonic setting of basic volcanic rocks determined using trace element analysis. *Earth and Planetary Science Letters* **19**, 290-300.

Pearce, J.A. Harris, N.B.W. and Tindle, A.G. (1984). Trace Element Discrimination Diagrams for the Tectonic Interpretation of Granitic Rocks. *Journal of Petrology* **25**, 956-983.

Philpotts, A.R. (1990). Principles of Igneous and Metamorphic Petrology. Englewood Cliffs, Prentice Hall, 498 p.

Potts, P.J. (1987). A Handbook of Silicate Rock Analysis. New York, Blackie &Son Ltd, 622 p.

Smithies, R.H. (2000). The Archaean tonaltie-trondhjemite-granodiorite (TTG) series is not an analogue of Cenozoic adakite. *Earth and Planetary Science Letters* **182**, 115-125.

South African Committee for Stratigraphy (SACS). (1980). Barberton Sequence (p. 29-44) *in* Kent, L.E., Stratigraphy of South Africa, Part I, Handbook Geological Survey South Africa vol. **8**, 690 p.

Surveys and Land Information, South Africa. (1984). 1: 50000 Topographical map 2530DD Nelshoogte.

Sylvester, P.J. (2001). Archaean magmatic record and crustal evolution. 4th International Archaean Symposium, extended abstracts. Perth, AGSO – Geoscience Australia, 25-27.

Thompson, R.N., Morrison, M.A., Hendry, G.L., and Parry, S.J. (1984). An assessment of the relative roles of a crust and mantle in magma genesis: an elemental approach. *Philosophical Transactions of the Royal Society of London* **A310**, 549-590.

Thorpe, R.I., Hickman, A.H., Davis, D.W., Mortensen, J.K., and Trendall, A.F. (1992). U-Pb zircon geochronology of Archaean felsic units in the Marble Bar region, Pilbara Craton, Western Australia. *Precambrian Research* **56**, 169-189.

van der Meer, J. (June 2002). Magmatic evolution in the Archean: new evidence from the ~3.5 Ga old Duffer Formation, East Pilbara craton, Western Australia. *Unpublished thesis*, 34 p. excl appendices.

van Niekerk, C. B. and Burger, A. J. (1969). A note on the minimum age of the acid lava of the Onverwacht Series of the Swaziland System. *Transactions of the Geological Society of South Africa* **72**, 9-21.

Viljoen, M.J. and Viljoen, R.P. (1969a). The geochemical evolution of the granitic rocks of the Barberton region. *Special Publication Geological Society of South Africa (Upper mantle project)* **2**, 189-219.

Viljoen, R.P. and Viljoen, M.J. (1969b). The geological and geochemical significance of the upper formations of the Onverwacht Group. *Special Publication Geological Society of South Africa (Upper mantle project)* **2**, 113-164.

Vlaar, N.J., van Keken, P.E. and van den Berg, A.P. Cooling of the Earth in the Archaean: Consequences of pressure release melting in a hotter mantle. *Earth and Planetary Science Letters* **121**, 1-18.

Walraven, F. and Hartzer, F.J. (1986). 1:250,000 Geological Series, sheet 2530 Barberton, Geological Survey of the Republic of South Africa, (+ explanation, 1989).

Westall, F., de Wit, M.J., Dann, J., van der Gaast, S., de Ronde, C.E.J., and Gerneke, D. (2001). Early Archean fossil bacteria and biofilms in hydrothermally-influenced sediments from the Barberton greenstone belt, South Africa. *Precambrian Research* **106**, 93-116.

Willis, J.P. (November 1999) Information Circular: Instrumental parameters and data quality for routine major and trace element determinations by WDXRFS. Department of Geological Sciences, University of Cape Town.

Wilson, M. (1989). Igneous Petrogenesis. London, Unwin Hyman Ltd, 466 p.

Wolf, M.B. and Wyllie, P.J. (1991). Dehydration-Melting of Solid Amphibolite at 10 kbar: Textural Development, Liquid Interconnectivity and Applications to the Segregation of Magmas. *Mineralogy and Petrology* **44**, 151-179.

Wood, D.A., Joron, J-L. and Treuil, M. (1979). A re-appraisal of the use of trace elements to classify and discriminate between magma series erupted in different tectonic settings. *Earth and Planetary Science Letters* **45**, 326-336.

Zegers, T.E., de Wit, M.J., Dann, J. and White, S.E. (1998). Vaalbara, Earth's oldest assembled continent? A combined structural, geochronological, and palaeomagnetic test. *Terra Nova* **10**, 250-259.

Figure 1: Map of the Kaapvaal Craton with the Barberton greenstone belt indicated (from Brandl and de Wit, 1997) (a) and map of the Barberton greenstone belt with the Onverwacht bend indicated (b).

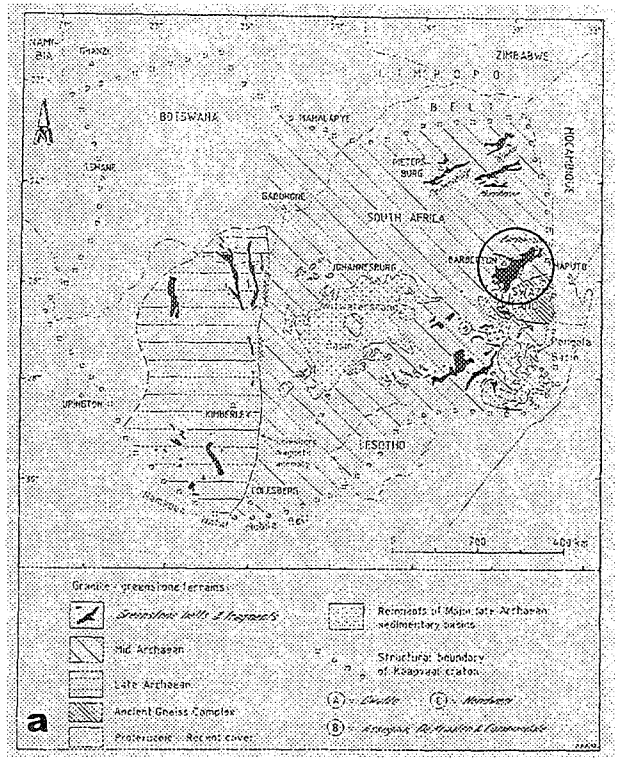

Figure 2: Stratigraphic subdivision of the Swaziland Supergroup, from Brandl and de Wit (1997).

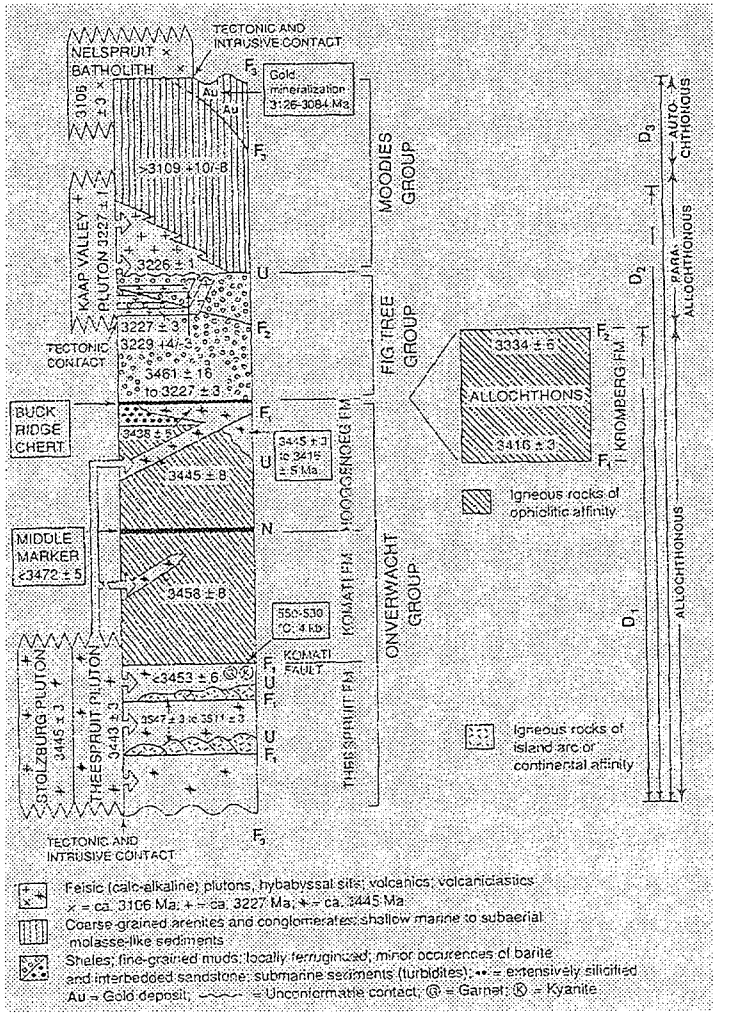

Figure 3: Diagram showing geochronological data on the Barberton greenstone belt. ThF = Theespruit Formation, KF = Komati Formation, HF = Hooggenoeg Formation, KrF =Kromberg Formation, MF = Mendon Formation, FTG = Fig Tree Group, D = Doornhoek, St = Stolzburg, Th = Theespruit, KV = Kaap Valley, Dal = Dalmein, Pl = Pluton, Bath = Batholith, AGC = Acient Gneiss complex.

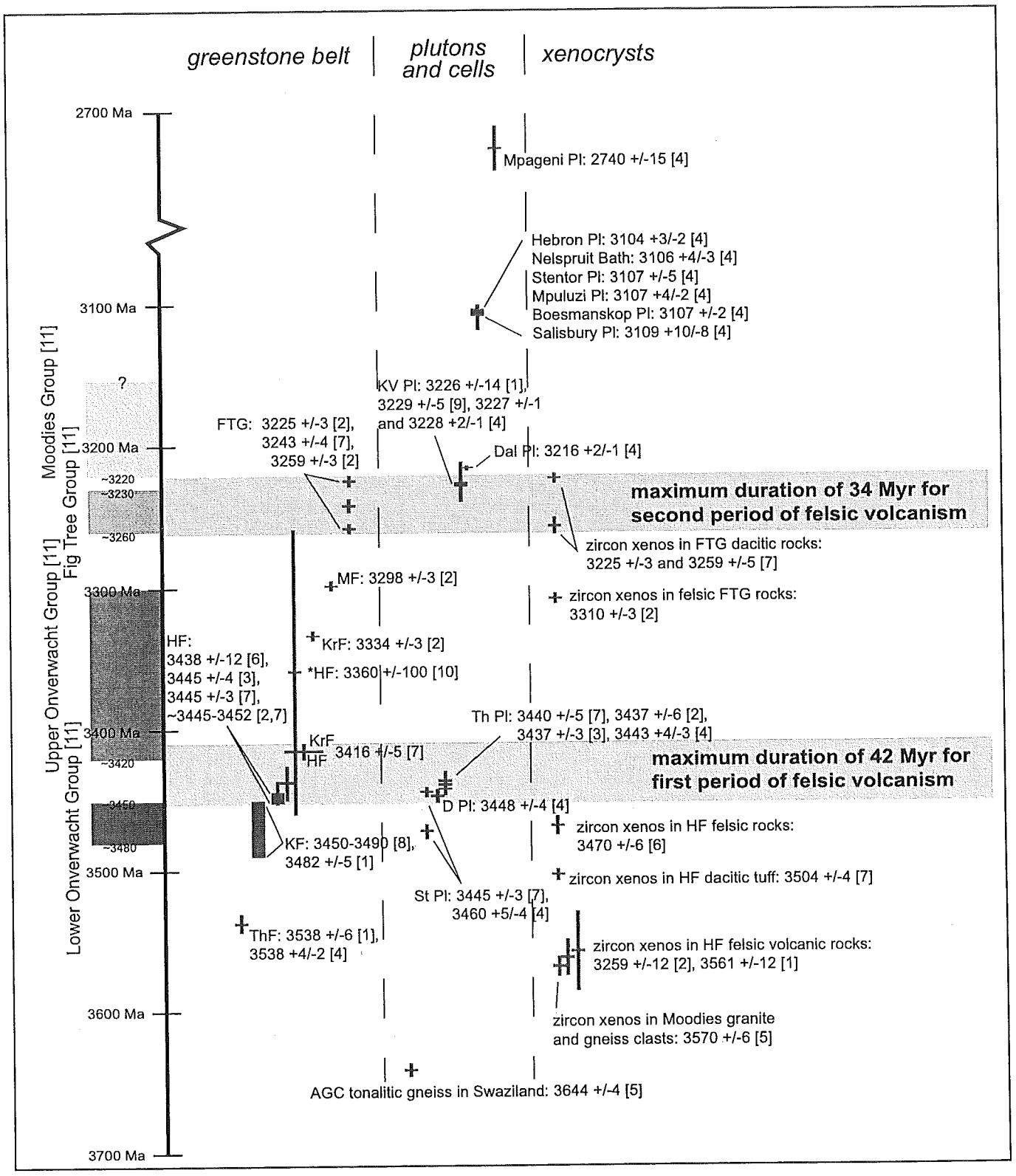

References: [1] Armstrong et al., 1990; [2] Byerly et al., 1996; [3] de Wit et al., 1987; [4] Kamo and Davis, 1994; [5] Kröner and Compston, 1988; [6] Kröner and Todt, 1988; [7] Krüner et al., 1991; [8] Lopez-Martinez, 1984 (ref. in Armstrong et al., 1990); [9] Tegtmeyer et al., 1987 (ref. in Armstrong et al., 1990); [10] van Niekerk and Burger, 1969; [11] Kröner et al., 1996.

Figure 4: Aerial photographs showing part of the Barberton greenstone belt in the Buck Ridge area, on the western limb of the Onverwacht anticline.

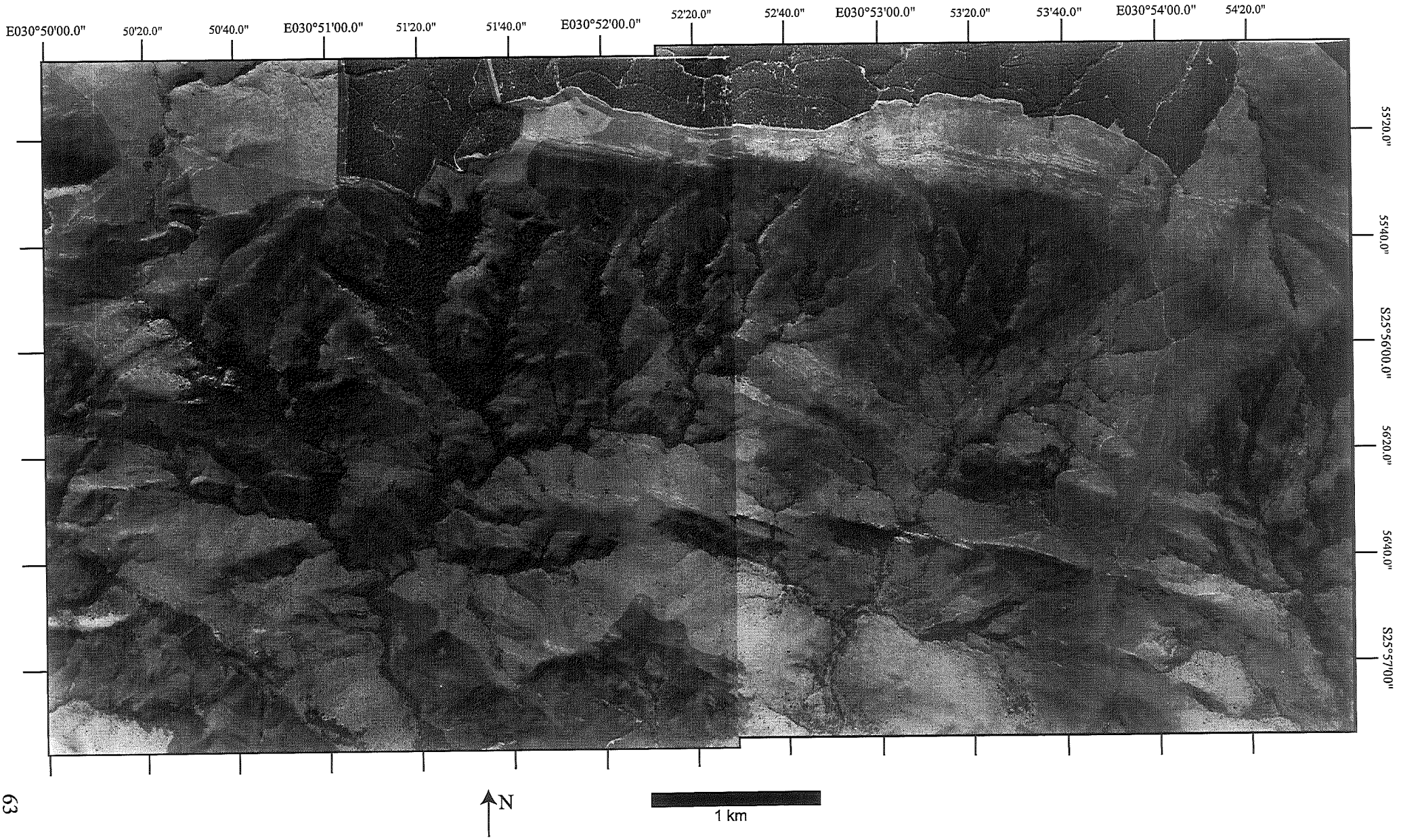

Figure 5a: Aerial photographs showing the locations of the two key areas and the locations of sampling and mapping. For legend see figure 7. The location density in the dashed box is too high to indicate all locations. The reader is referred to figures 5b and 9a of key area I. See Appendix B for sample and orientation tables.

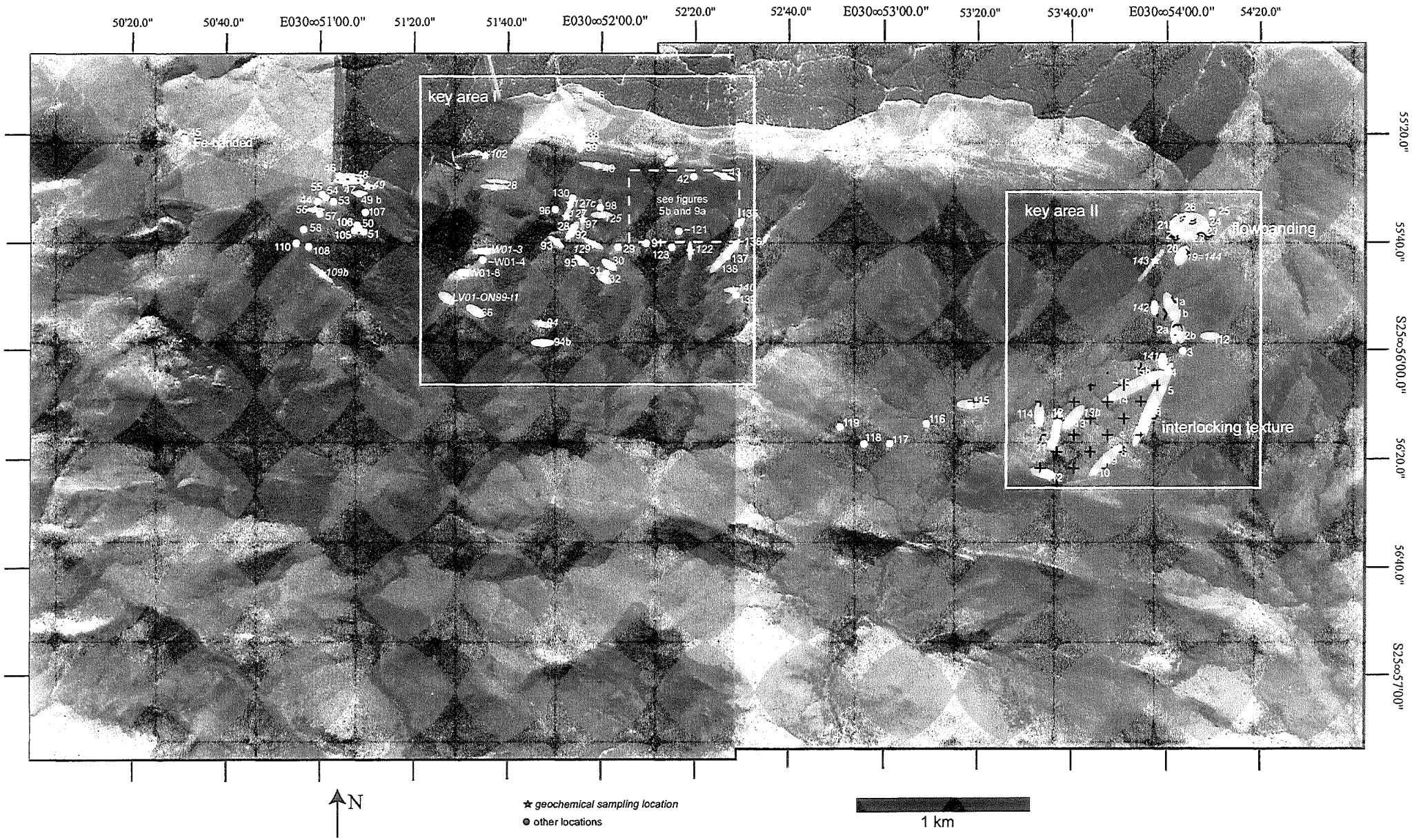

Figure 5b: Aerial photograph showing locations of mapping and sampling in key aera I. See Appendix B for sample and orientation tables.

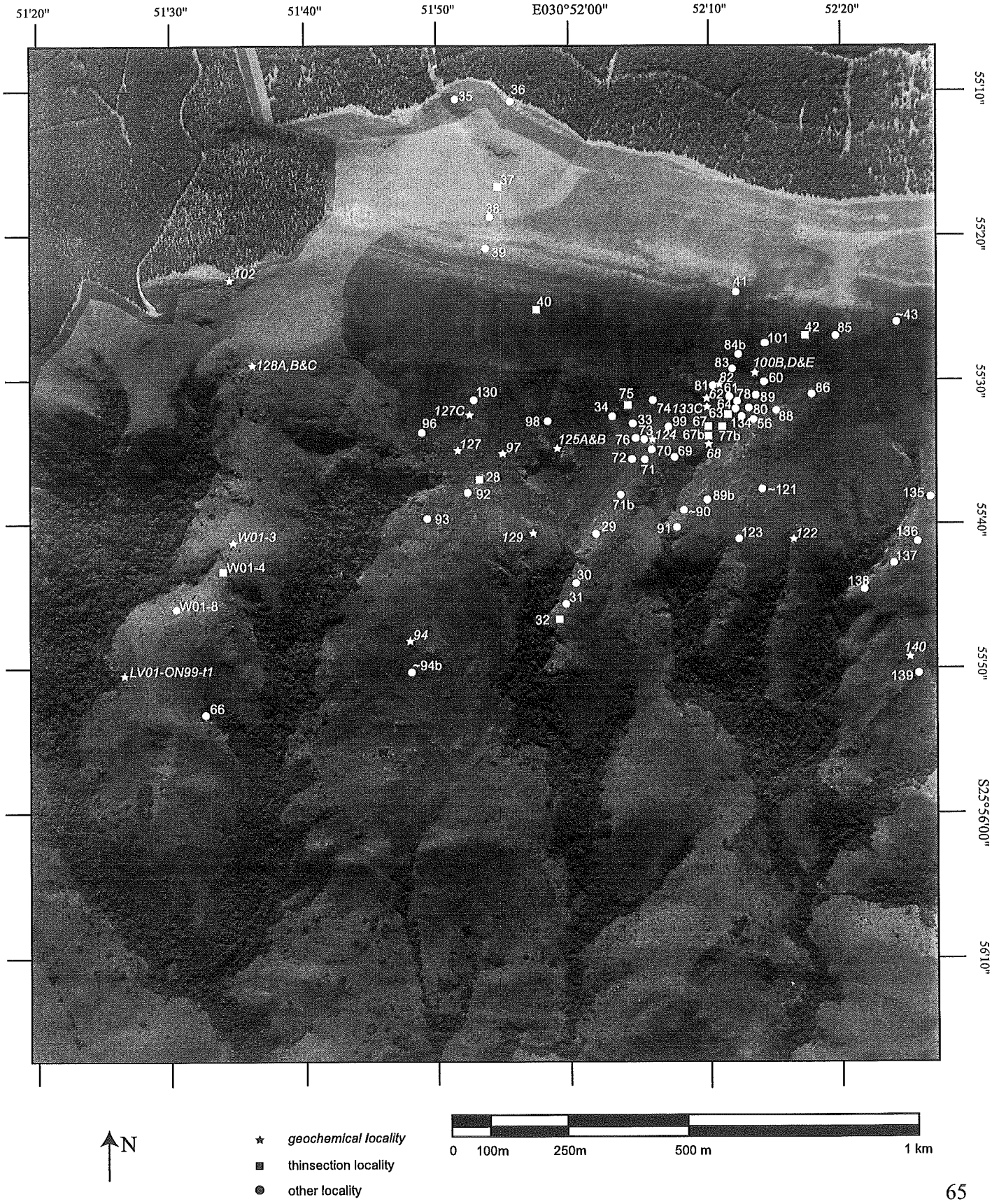

Figure 7: Geological map of key area I.

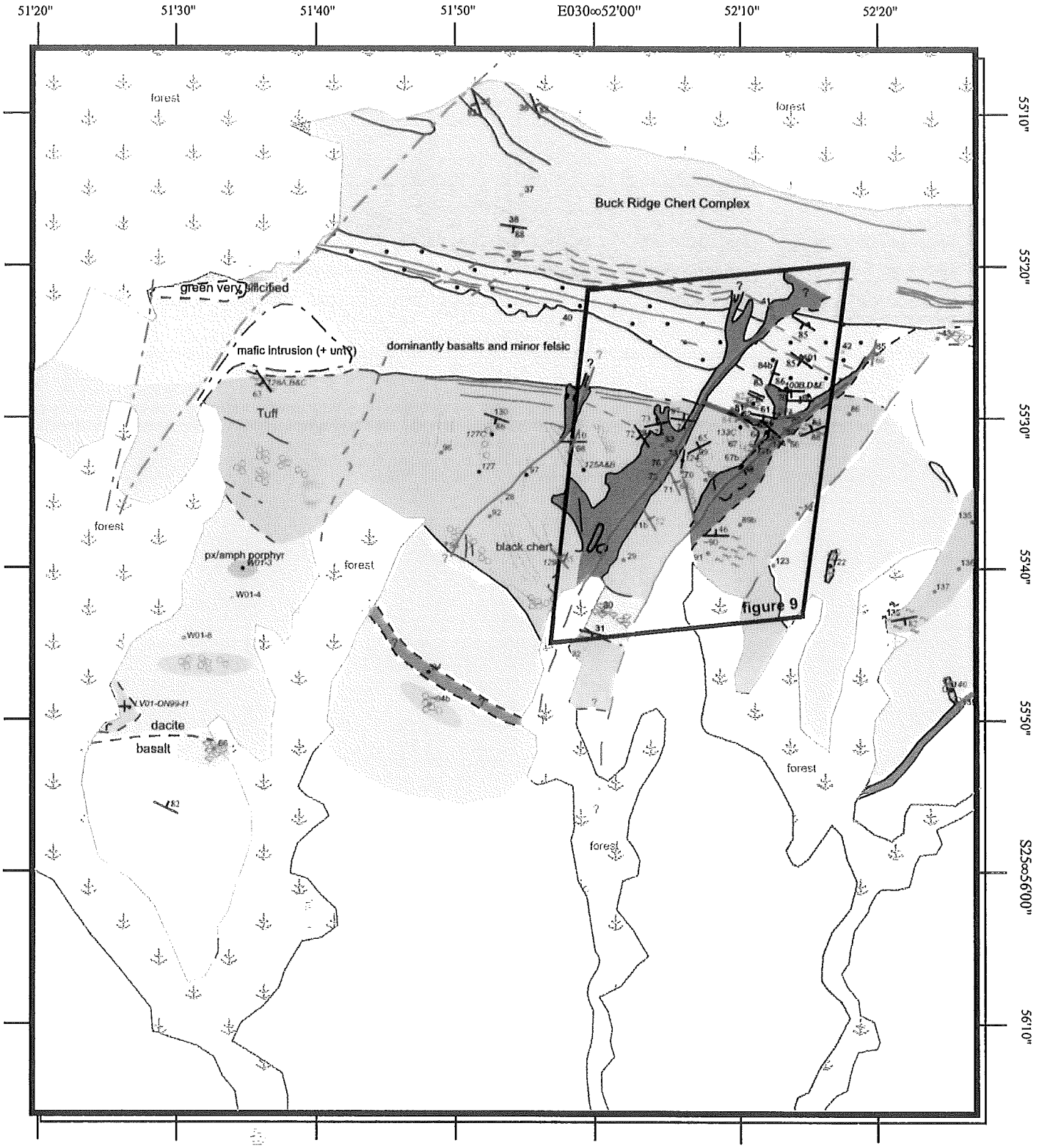

MAP LEGEND

symbols

- bedding indicating dip
- fracture indicating dip
- *geochemical locality*

Thinsection and other localities can be found on figure #.

- rock unit boundary
- inferred rock unit boundary
- fault
- inferred fault

0 100m 250m 500 m 1 km

N W E S

colors

felsic
- flowbanded
- porphyritic
- interlocking

basalt
- silicified
- pillow

- ultramafic intrusion
- sedimentary chert
- chert vein
- felsic vein
- px/amph porphyr
- units 2, 3 and 4 of the BRCC after de Vries, 1999, Unpubl.

Karin L. Louzada January 2003

Figure 5c: Geological map of part of the Barberton Mountain Land indicating the field area and locations of sampling of the Stolzburg Pluton. Modified after Walraven and Hartzer, 1986.

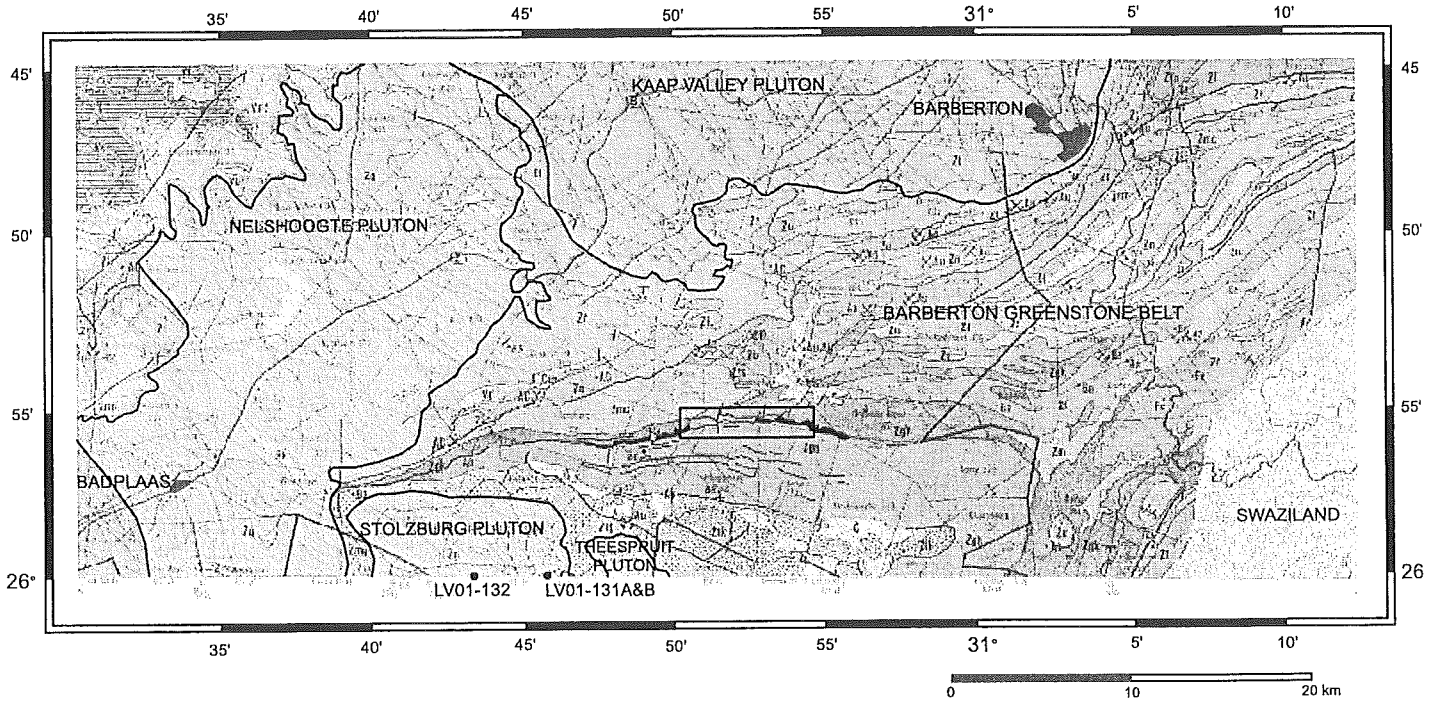

Figure 6: Boxdiagram showing steps undertaken for reduction and preparation of samples for whole rock geochemical analyses at UCT, South Africa

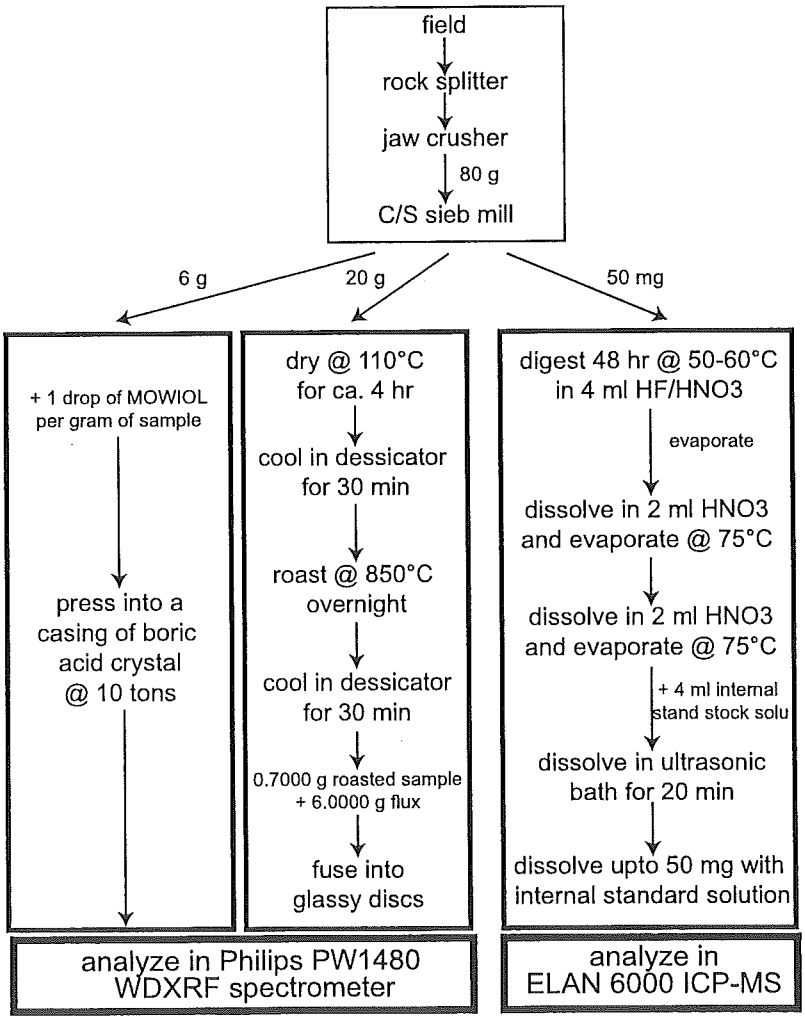

Figure 8: Stereographic projections of flow banded rocks in the felsic unit in area I (a), upper vertical chert veins (b), sedimentary cherts in mafic unit (and upper part of felsic unit) in area I (c), fractures parallel to chert veins at LV01-129 and wide felsic vein at LV01-70 (d), remaining fractures and faults (e), and faults at LV01-77b and LV01-98 (f).

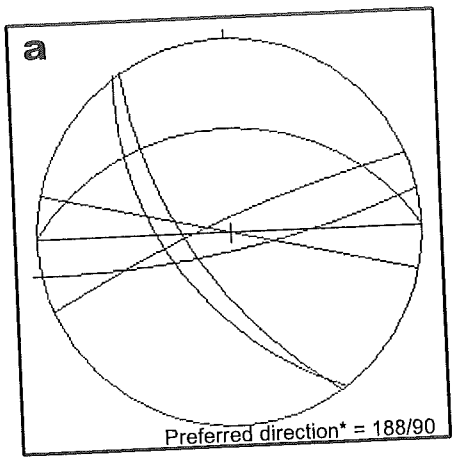

Flow banded rocks of the felsic unit in area

locality	dipdirection/dip
LV01-128a	169/82
LV01-138	235/63
LV01-90	000/46
LV01-60	180/90
LV01-62(?) hostrock	013/90
LV01-87	338/84
LV01-34	237/72

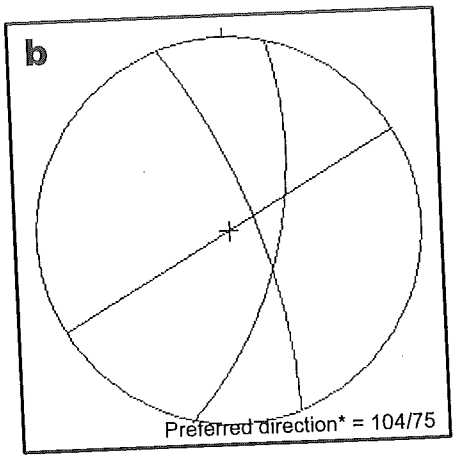

Veinsplot

locality	dipdirection/dip
LV01-96	070/78
LV01-97	103/68
LV01-127/97	150/90

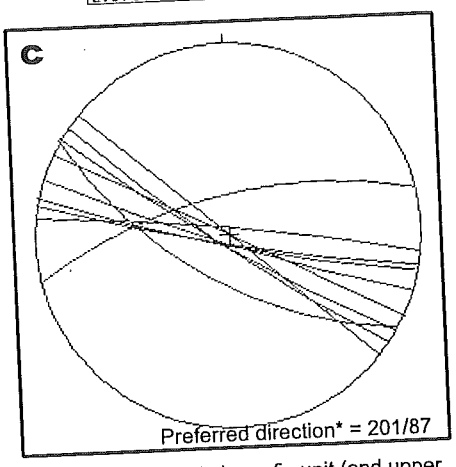

Sedimentary cherts in mafic unit (and upper part felsic unit) in area I

locality	dipdirection/dip
LV01-61	191/86
LV01-62	027/89
LV01-63	221/88
LV01-74	007/87
LV01-75	348/73
LV01-78	193/85
LV01-128b	211/70
LV01-130	199/86
LV01-101	216/85
LV01-101 to the N	212/85

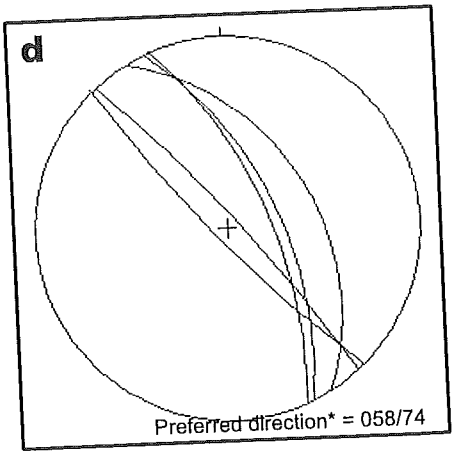

Fractures and veins

locality	dipdirection/dip
LV01-62	227/84
LV01-71	066/68
LV01-71b	060/52
LV01-74	068/72
LV01-129	049/85

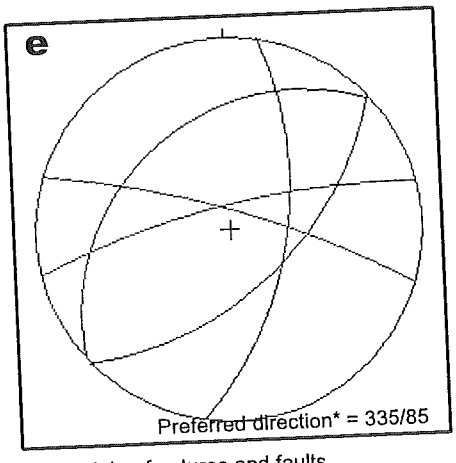

Remaining fractures and faults

locality	dipdirection/dip
LV01-77b	320/42
LV01-85	100/66
LV01-89	348/80
LV01-98	138/64
LV01-81	018/82

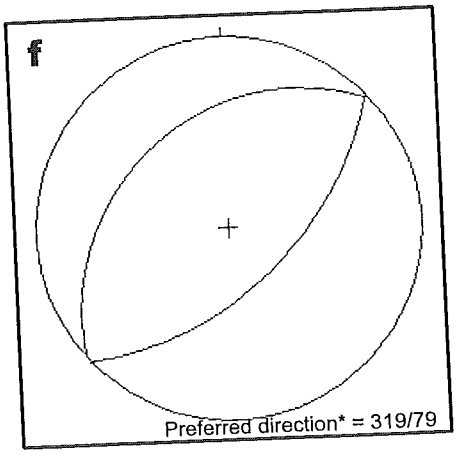

Fractures and faults 2

locality	dipdirection/dip
LV01-77b	320/42
LV01-98	138/64

* Output from GEOrient 8.0

Figure 9: Detail photograph of felsic (orange), chert (grey) and mafic (green) veins in area I. For legend see figure 7.

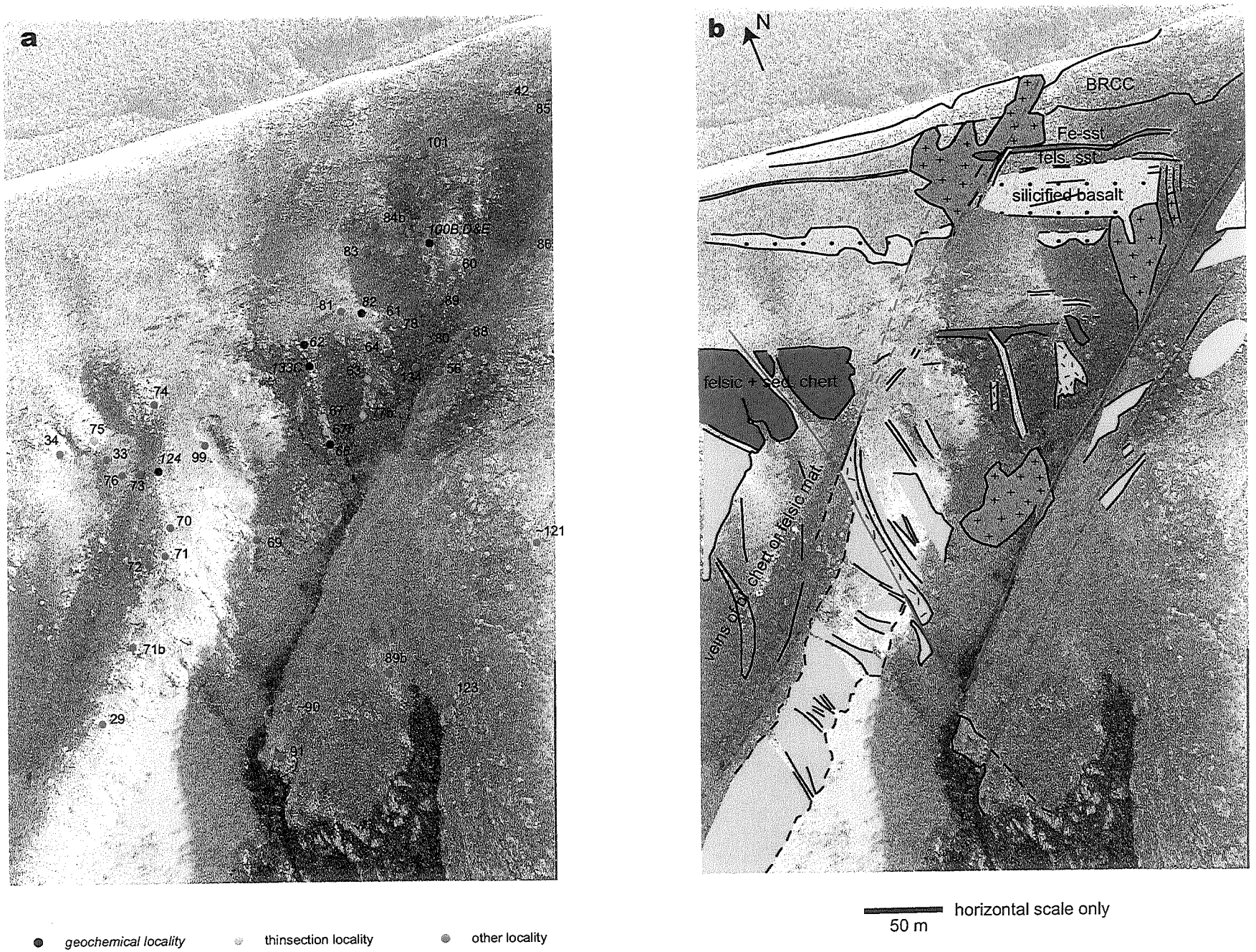

Figure 10: Millimetre sized chert veins in felsic rock observed at LV01-59 (S25∞55'37.7"

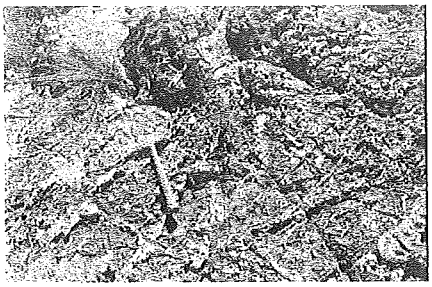

Figure 11: Photomicrographs of shallow intrusive felsic rocks from area I at LV01-ON99-t1 in ppl (a) and xpl (b).

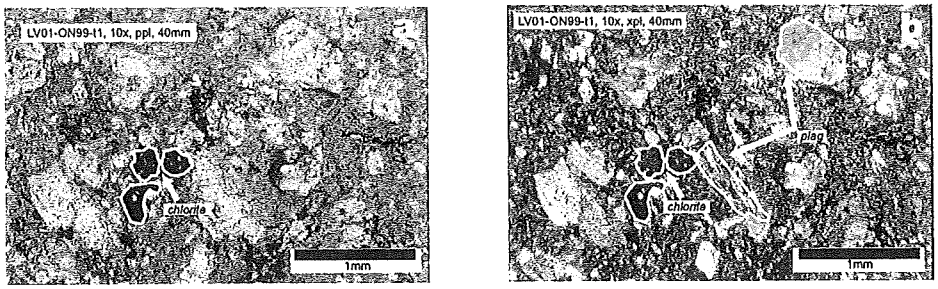

Figure 12: Photomicrographs of consolidated ash or tuff from area I at LV01-109b in ppl (a) and xpl (b).

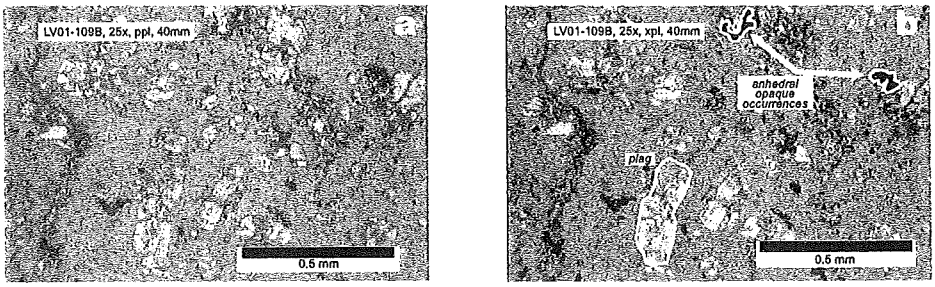

Figure 13: Photomicrographs of interlocking felsic rock from area II at LV01-11 in ppl (a), xpl (b) and a detail (c).

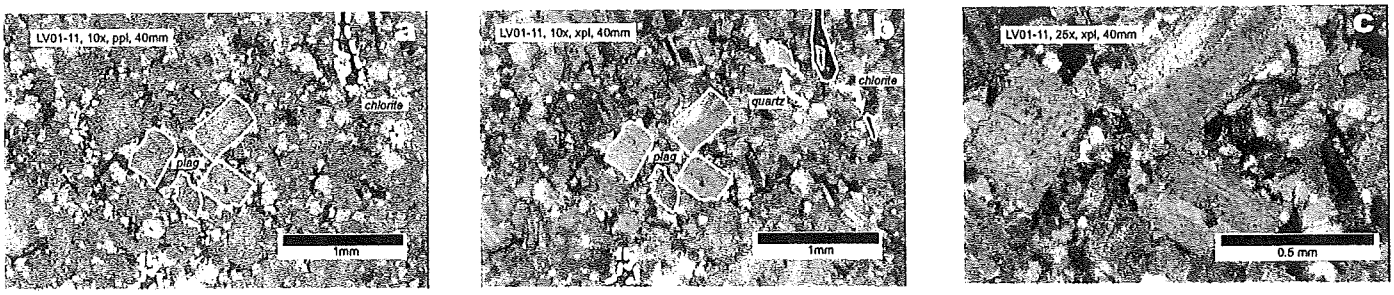

Figure 14: Photomicrographs of quartz porphyry from area I at LV01-122 in ppl (a) and xpl (b).

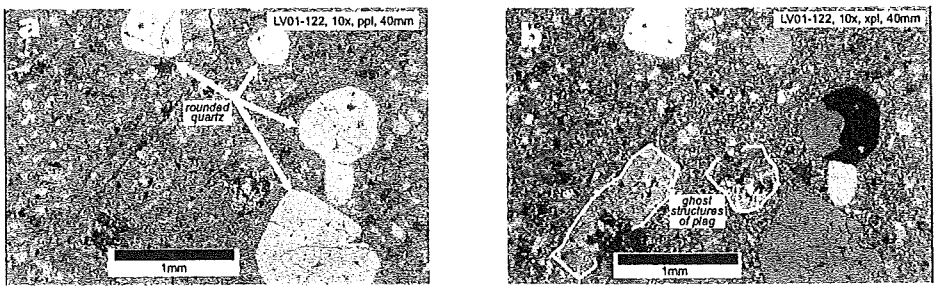

Figure 15: Photomicrographs from top of felsic vein from area I at LV01-127c in ppl (a) and xpl (b).

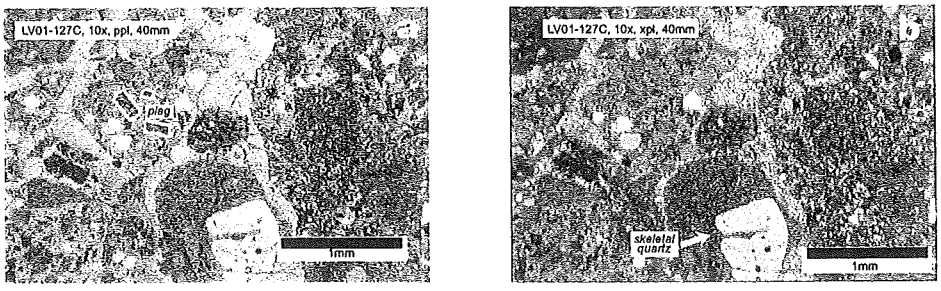

Figure 16: Photomicrographs of flow banded felsic rock from area I at LV01-128a in ppl (a) and a detail (b).

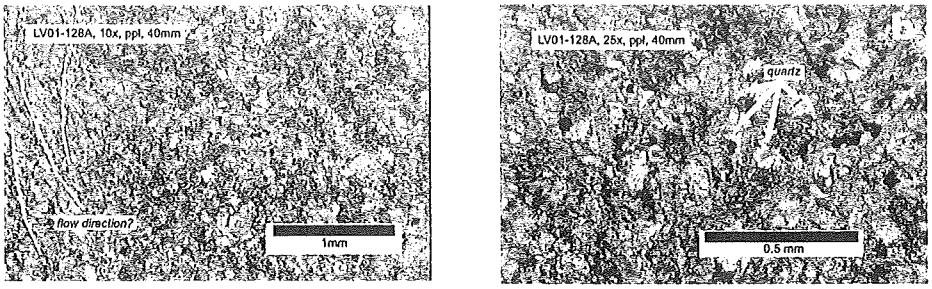

Figure 17: Photomicrographs of flow banded felsic rock from area II at LV01-23 in ppl (a) and xpl (b).

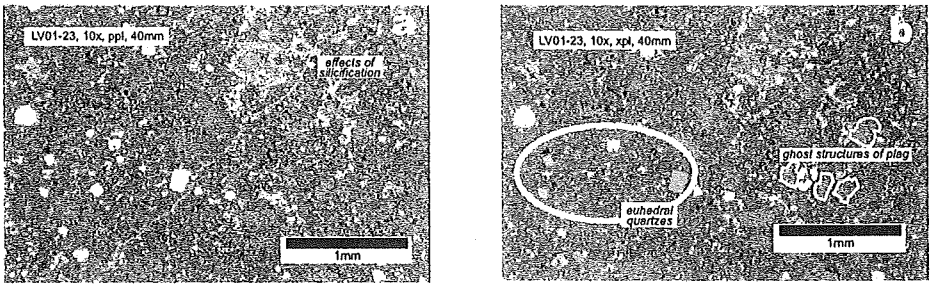

Figure 18: Photomicrographs of the Stolzburg Pluton at LV01-131a in ppl (a), xpl (b) and a detail (c).

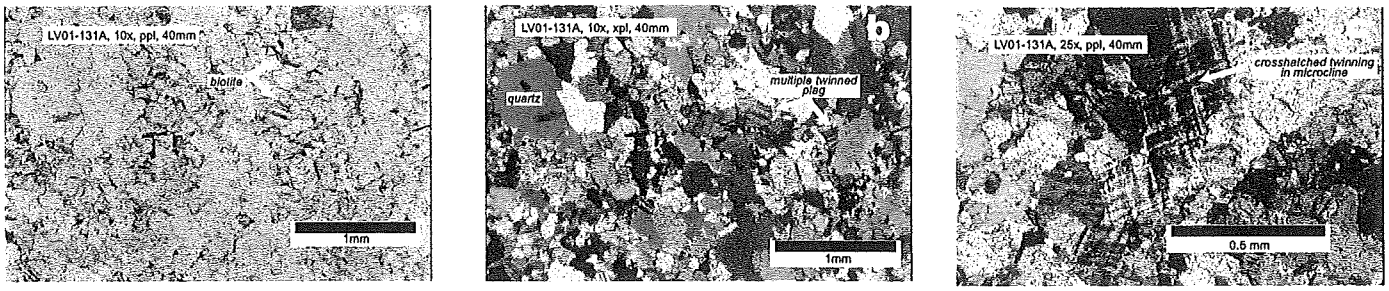

Figure 19: Photomicrograph of a fine-grained mafic rock at LV01-56.

Figure 20: Photomicrographs of silcified basalts at LV01-47 (a) and LV01-100b (b).

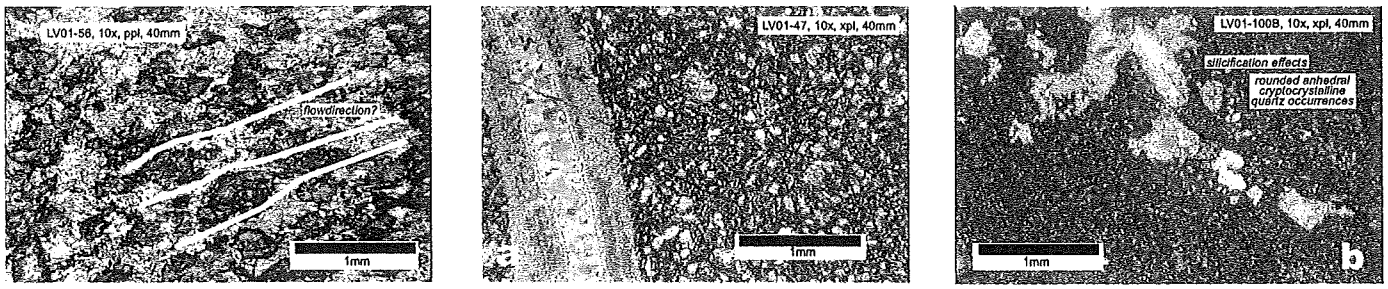

Figure 21: Photomicrograph of sedimentary chert at LV01-128b.

Figure 22: Photomicrograph of vertical black chert vein at LV01-133c.

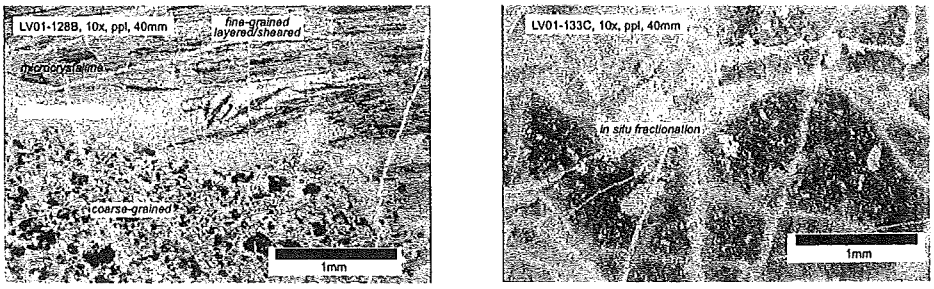

Figure 23: Photomicrographs of pyroxene/amphibole porphyries at W01-3 (a) and SV01-46 (b).

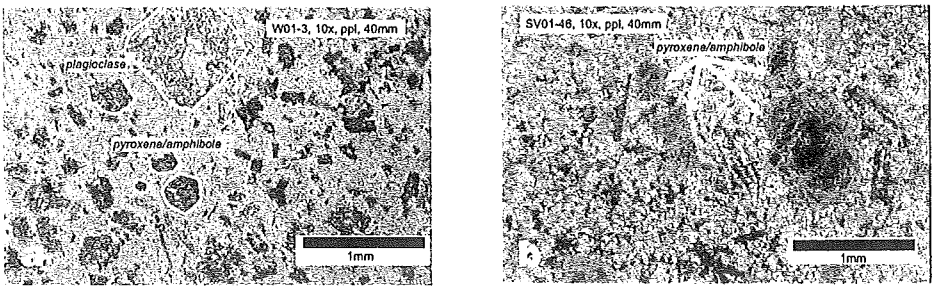

Figure 24: Harker diagrams of SiO2 (wt%) versus H2O- (a), LOI (b), TiO2 (c), Al2O3 (d), Fe2O3 (e), MnO (f), MgO (g), CaO (h), Na2O (i), K2O (j), P2O5 (k), NiO (l) and Cr2O5 (m) (wt%).

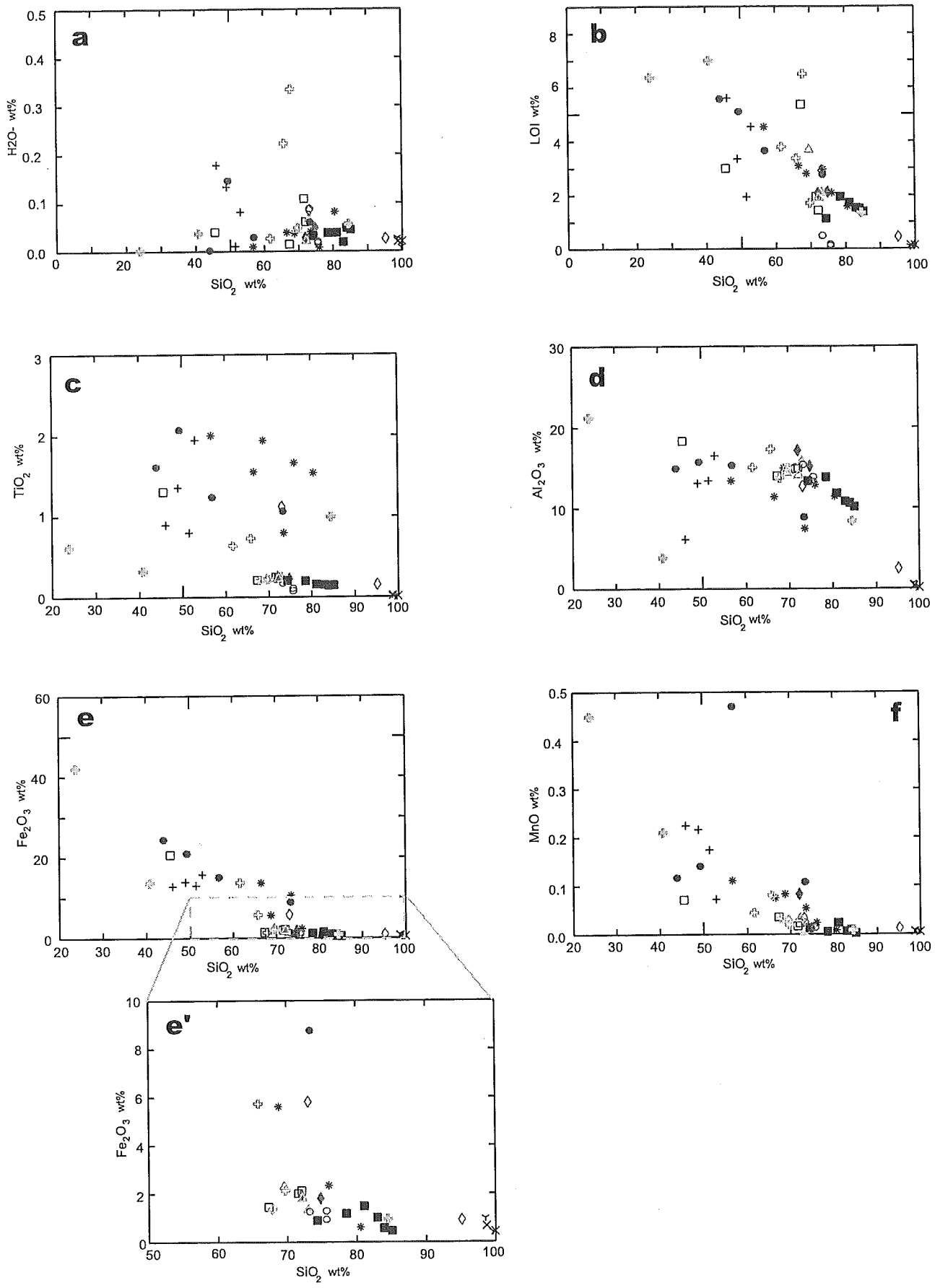

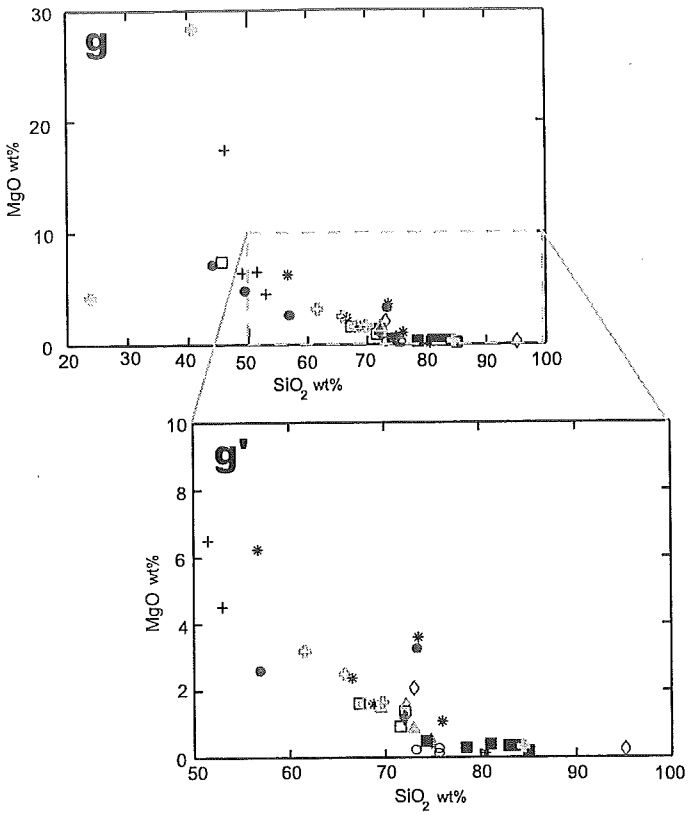

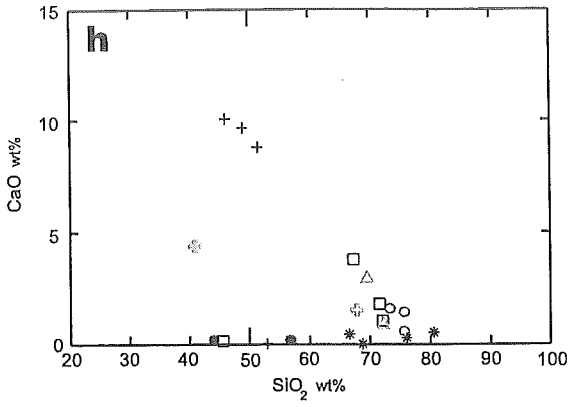

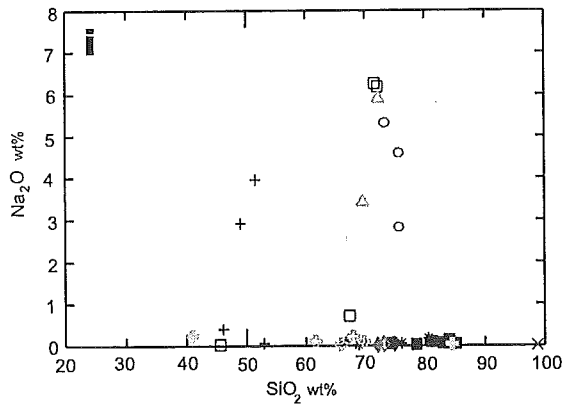

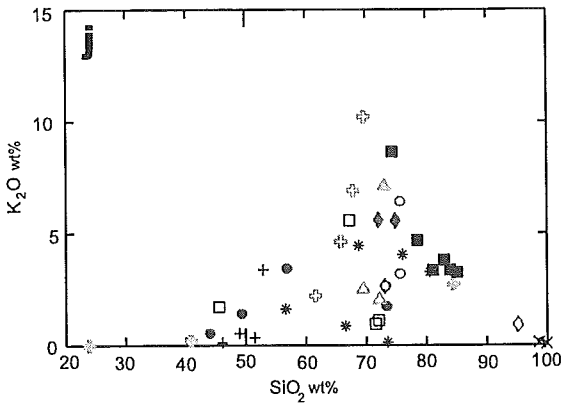

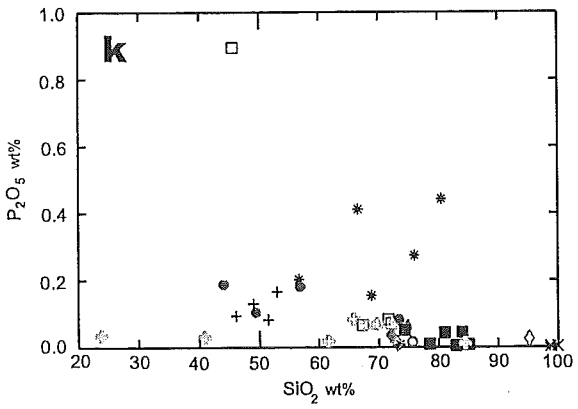

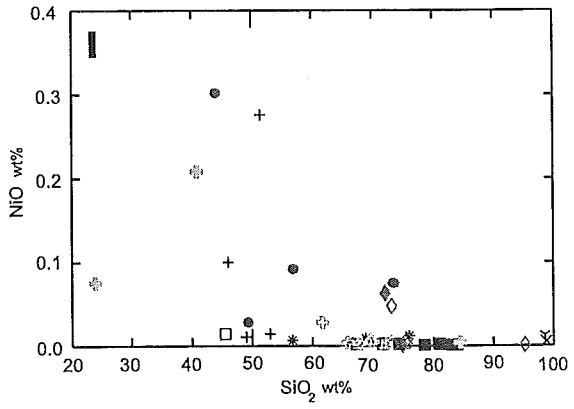

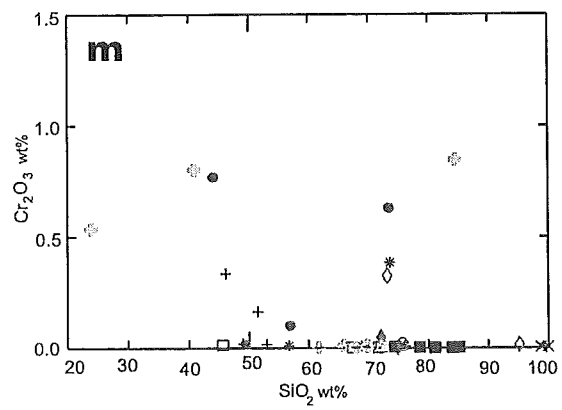

Legend of symbols

- △ Shallow intrusives from area I
- △ Consolidated ash or tuff from area I
- □ Interlocking felsic rocks from area II
- ■ Quartz porphyries from area I
- ◇ Felsic lavas from area I
- ◆ Felsic lavas from area II
- ○ Stolzburg Pluton
- ● Fine-grained basalts
- \+ Coarse-grained dolerites
- ✱ Silicified basalts
- × Sedimentary cherts
- Y Massive cherts
- ✣ Pyroxene/amphibole porphyriess
- ✣ Others

Figure 25: Total Alkali Silica (TAS) diagram, after le Bas et al. (1986) and Irvine and Baraber (1971). Sample SV01-39 is not included in this graph, SiO2 < 25 wt% For meaning of symbols see legend of figure 24.

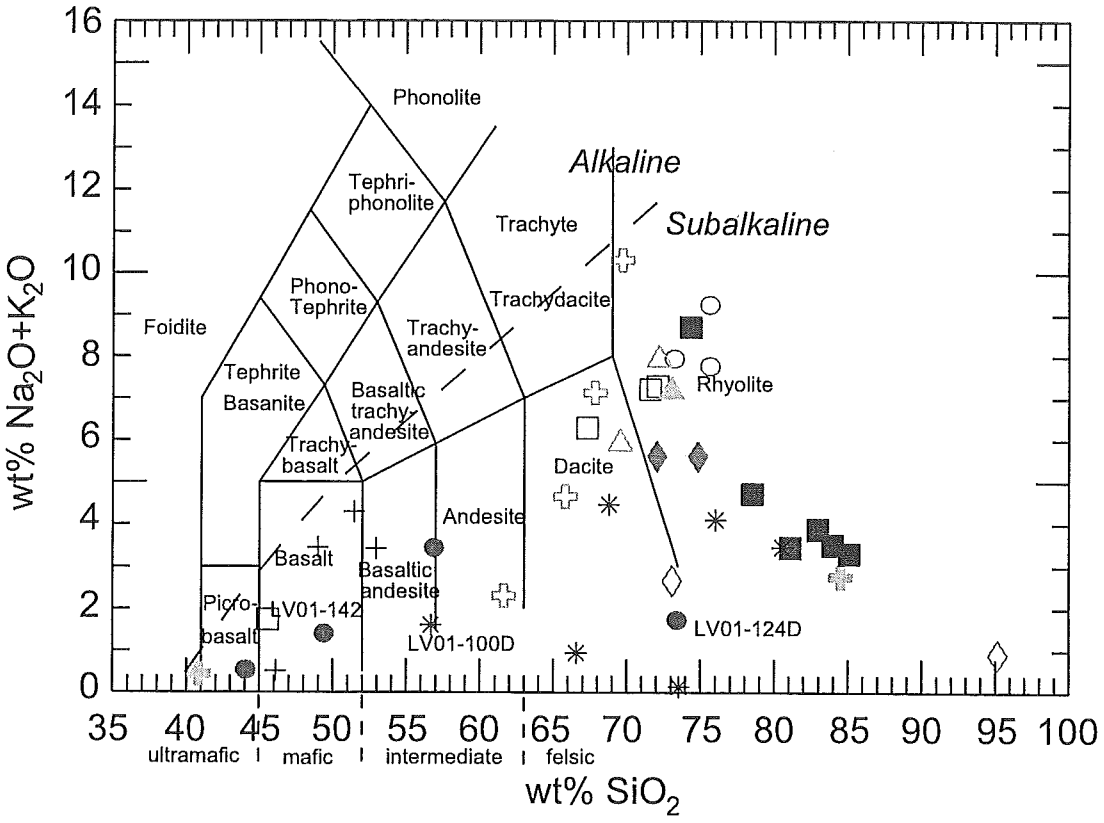

Figure 26: Classification of subalkaline rocks into tholeiitic and calc-alkaline series based on the major elemental characteristics (Alkali-FeO*-MgO) of the rocks. After Irvine and Baragar (1971). For meaning of symbols seee legend of figure 24.

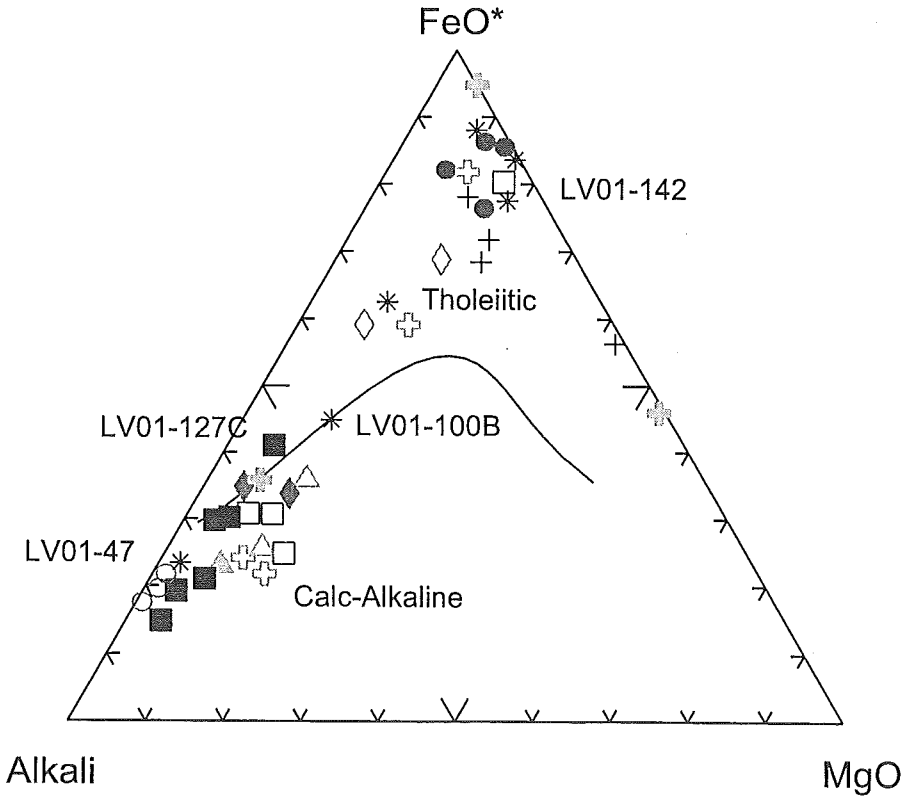

Figure 27: SiO2 (wt%) versus V (a), Cr (b), Mn (c), Co (d), Ni (e), Cu (f), Zn (g), and Ga (h) (ppm); Y (ppm) versus Zr (i), Nb (j) and Mo (k) (ppm); Hf (ppm) versus Ta (ppm) (l); SiO2 (wt%) versus Pb (m), Th (n), and U (o) (ppm); Sr (ppm) versus Rb (p), Cs (q) and Ba (r) (ppm). For meaning of symbols see legend of figure 24.

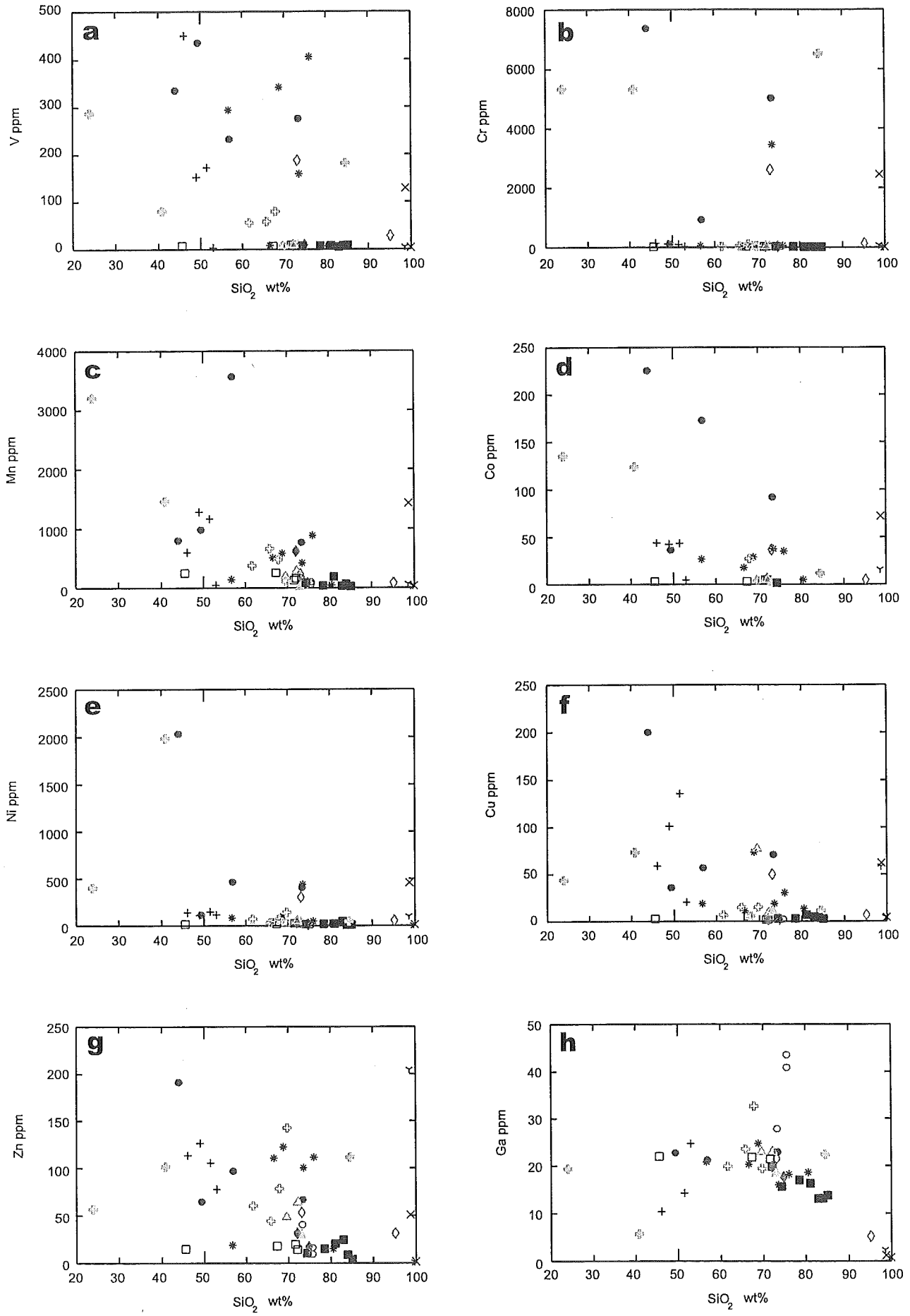

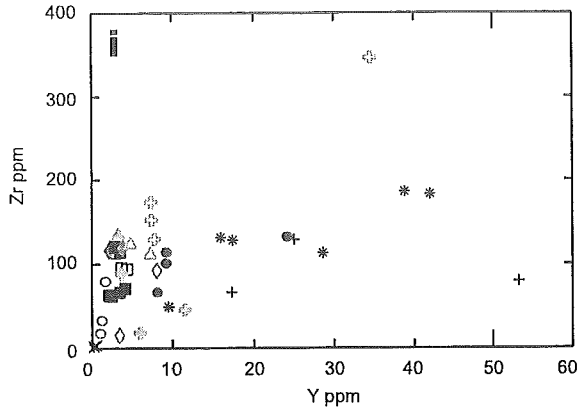
i
Zr ppm
Y ppm

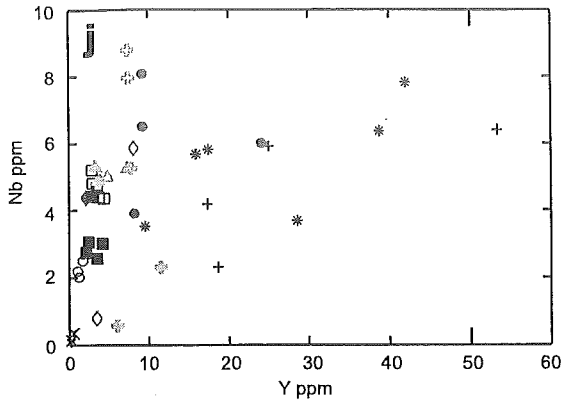
j
Nb ppm
Y ppm

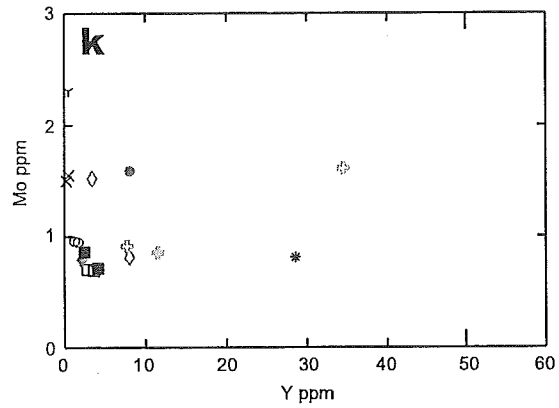
k
Mo ppm
Y ppm

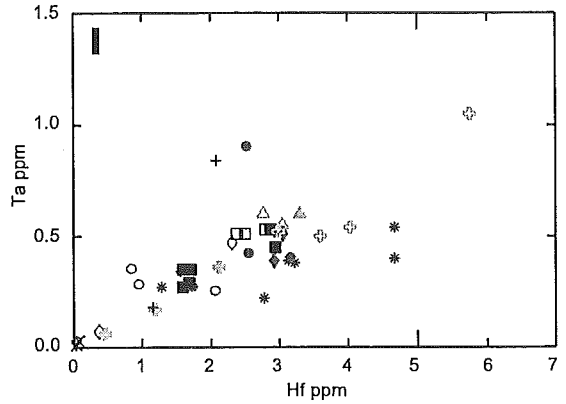
l
Ta ppm
Hf ppm

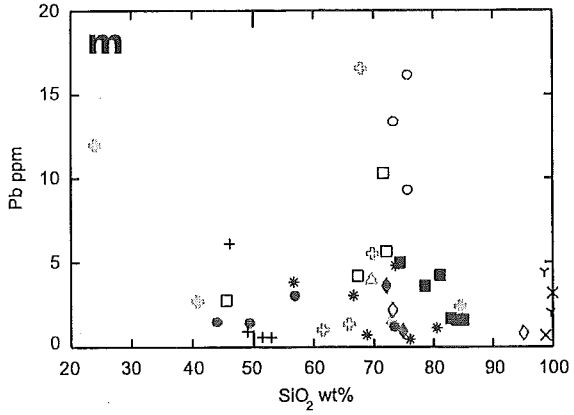
m
Pb ppm
SiO2 wt%

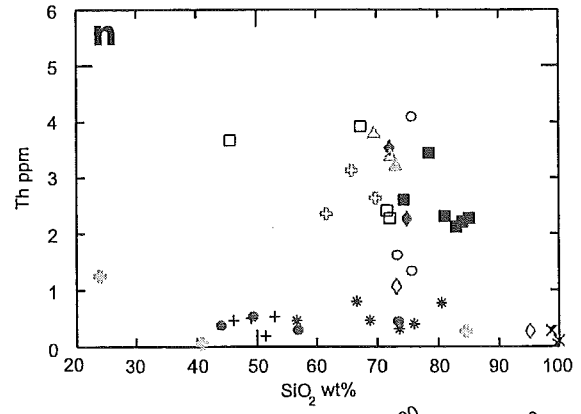
n
Th ppm
SiO2 wt%

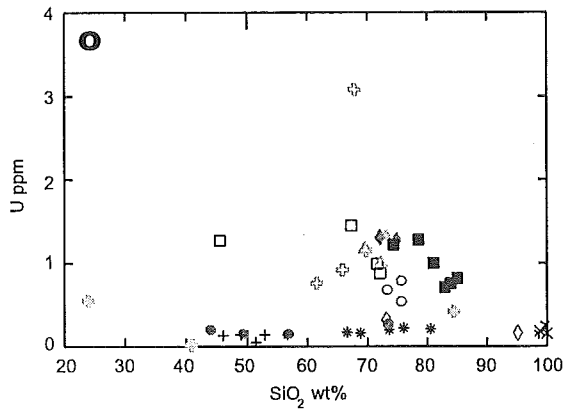
o
U ppm
SiO2 wt%

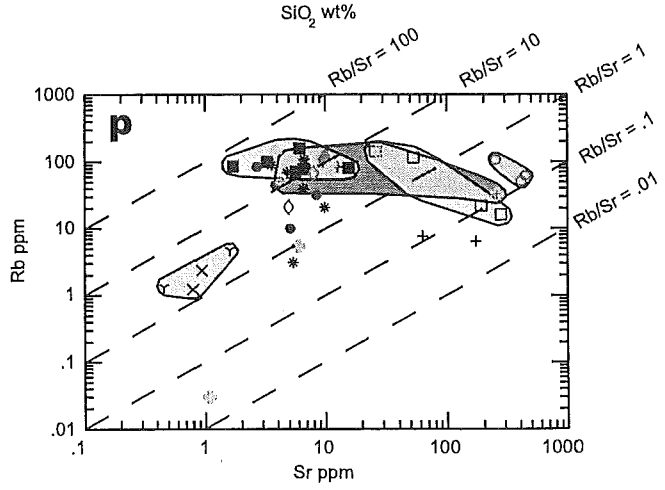
p
Rb/Sr = 100
Rb/Sr = 10
Rb/Sr = 1
Rb/Sr = .1
Rb/Sr = .01
Rb ppm
Sr ppm

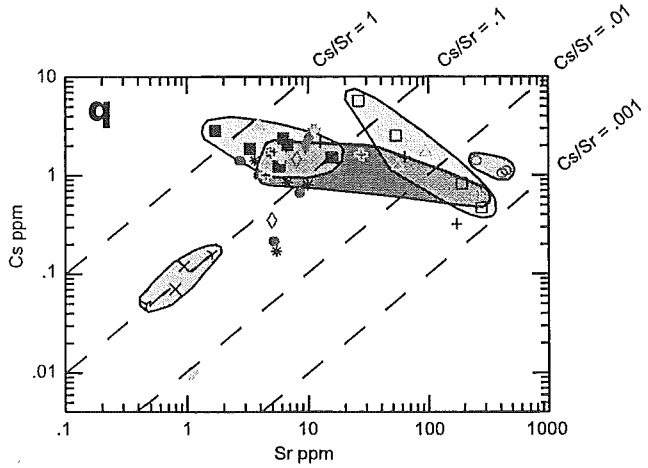
q
Cs/Sr = 1
Cs/Sr = .1
Cs/Sr = .01
Cs/Sr = .001
Cs ppm
Sr ppm

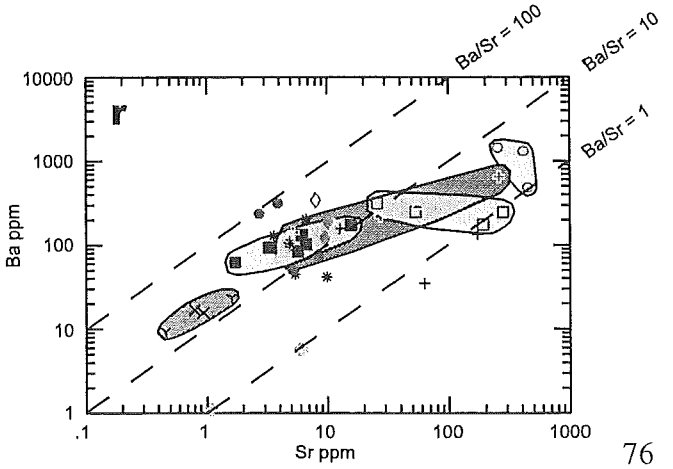
r
Ba/Sr = 100
Ba/Sr = 10
Ba/Sr = 1
Ba ppm
Sr ppm

Figure 28: Chondrite normalized REE diagrams for shallow intrusives and consolidated ash or tuff from area I (a), interlocking felsic rocks from area II(b), quartz porphyries from area I (c), felsic lavas from areas I and II (d), Stolzburg Pluton (e), (ultra-) mafic rocks (f), silicified basalts (g), sedimentary and massive cherts (h), pyroxene/amphibole porphyries (I) and others (j). After Nakamura, 1974. For meaning of symbols see legend of figure 24.

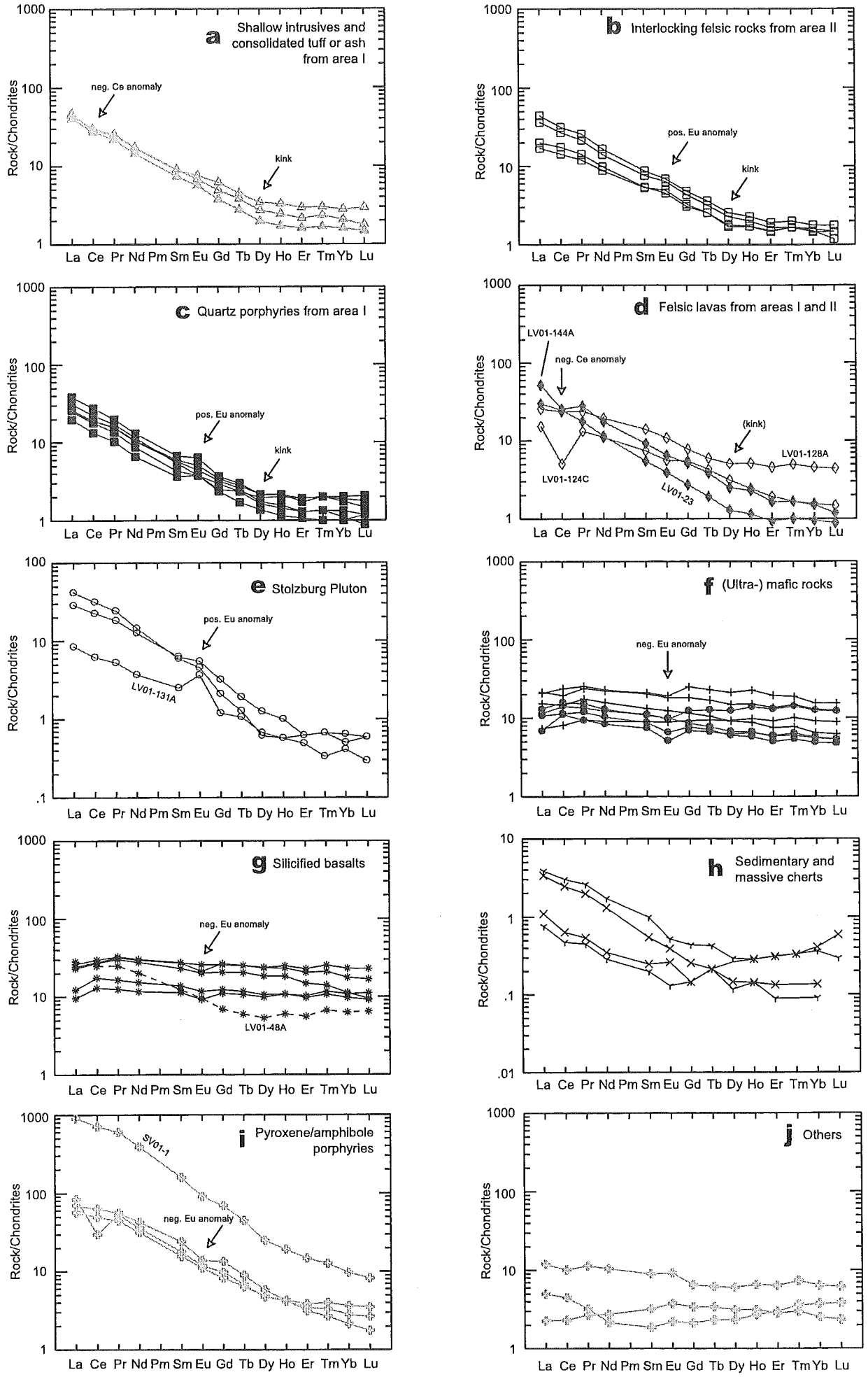

Figure 29: Spider diagrams normalized to Primordial Mantle for shallow intrusives and consolidated ash or tuff from area I (a), interlocking felsic rocks from area II(b), quartz porphyries from area I (c), felsic lavas from areas I and II (d), Stolzburg Pluton (e), (ultra-) mafic rocks (f), silicified basalts (g), sedimentary and massive cherts (h), pyroxene/amphibole porphyries (I) and others (j). After Wood et al., 1979. For meaning of symbols see legend of figure 24.

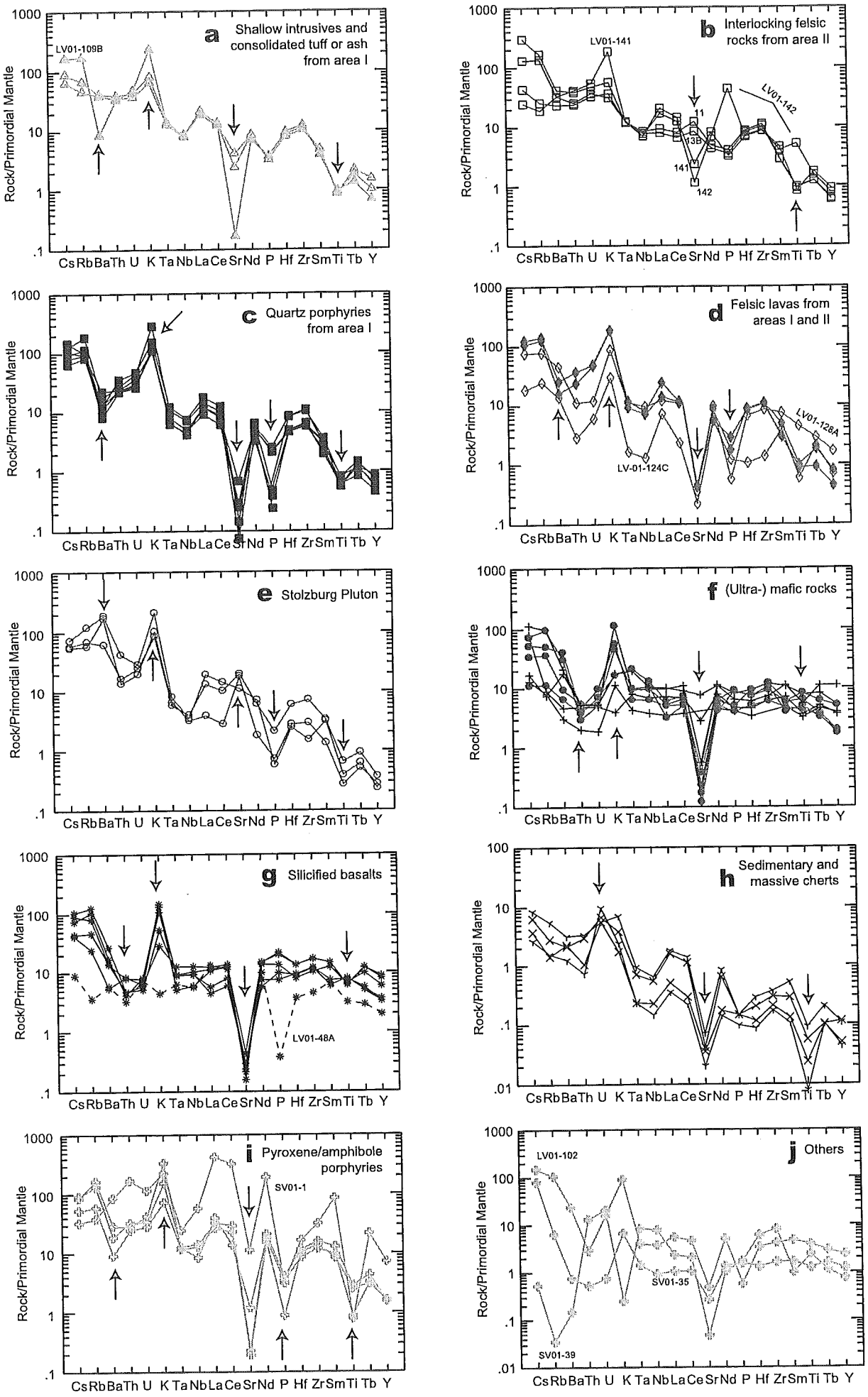

Figure 30: Table showing summary of results from mapping, and petrographic and geochemical analyses.

groups		outcrop characteristics	petrography	SiO2	major element characteristics		trace element characteristics		REEs	spider diagram	exceptions
intermediate and felsic groups	*shallow intrusives from area I*	massive outcrops without woolsack weathering	>50% matrix, plag and quartz phenos	70-75 wt%	low in TiO2, Fe2O3, MnO, MgO, P2O5, NiO, and Cr2O3; Al2O3: 10-18 wt%	CaO: 1-4 wt%; Na2O: 3.5-6 wt%; K2O: 2 wt%	low in V, Cr, Mn, Co, Ni, Cu, and Mo; Ga: ~21 ppm; Y: 2-10 ppm; Zr: 60-130 ppm; Nb: 2.5-3.5 ppm; Pb: 1-10 ppm; Th: 0.5-4 ppm; U: 0.5-1.5 ppm	Sr: 50-100 ppm	decreasing trend from La to Dy; flat trend Dy to Lu; slight neg Ce anomaly	pos K, neg Sr, P and Ti anomalies relative to Primordial Mantle	LV01-140 rich in Cu ~75 ppm; LV01-ON99-t1 Pb: ~70 ppm
	consolidated ash or tuff from area I	glassy, fractured massive outcrop	~80% matrix, plag larger than quartz phenos +/- black anhedral mineral	~75 wt%		low in CaO and Na2O; K2O: ~7 wt%		low in Sr	decreasing trend from La to Dy; flat trend Dy to Lu; slight neg Ce anomaly, slight pos Eu anomalies	neg Ba anomalies, pos K anomalies, neg Sr and P anomalies, neg Ti anomalies relative to Primordial Mantle	
	interlocking felsic rocks from area II	smooth rounded outcrops	<20% matrix, plag > quartz +/- chlorite	(45-) 65-75 wt%		CaO: 0-4.5 wt%; Na2O: 0-6.5 wt%; K2O: 0.5-2 (-6) wt%		low in Zn; Sr: 25-275 ppm	decreasing trend from La to Dy; flat trend Dy to Lu; some small pos Eu anomalies		LV01-142: positive P and Ti anomalies; increase in Sr, decrease in Rb and Cs from LV01-142, LV01-141, LV01-13B, and LV01-11; slight pos Sr anomalies in LV01-11 and LV01-13B
	quartz porphyries from area I	often long thin outcrops oriented perpendicular to the bedding	upto 90-95% matrix, quartz + plag	75-85 wt%		linear Al2O3 trend; depleted in Fe2O3 and MgO relative to other felsic groups; low in CaO and Na2O; K2O: 3-5 (-8.5) wt%		low in Zn; Ga: 12-18 ppm; low in Sr; Zr: 60-80 ppm; Nb: 2.5-3.5 ppm	decreasing trend from La to Dy; flat trend Dy to Lu; significant pos Eu anomalies		
	felsic lavas from both areas	flow banded bedding parallel flow units	flow banding not visible on microscopic scale (silicified), matrix dominated with often euhedral quartz and plag phenos	75-95 wt%		low in CaO and Na2O; K2O: 0.5-2.5 wt% for area I and ~6 wt% for area II		low in Sr	decreasing trend from La to Dy; flat trend Dy to Lu; two strong neg Ce anomalies, neg Eu anomalies		LV01-128A high in Cu: ~50 ppm, high in MgO, FeO and TiO2; LV01-124C is extremely enriched in SiO2
Stolzburg Pluton		large smooth low relief outcrops	interlocking quartz, plagioclase (albite), microcline and biotite grains +/- chlorite	75 wt%	similar to felsic groups	Al2O3: 13-17 wt%; CaO: 0.5-2 wt%; Na2O: 4.5-5.5 wt%; K2O: 2.5-3 wt%	similar to felsic groups	Ga: 25-45 ppm; Rb: 50-100 ppm; Sr: 250-450 ppm; Cs: 1-2 ppm; Ba: 500-1100 ppm; Y: ~1 ppm; Zr: ~10-80 ppm; Nb: 2-2.5 ppm	similar to felsic groups, but less enriched in HREE; pos Eu anomly	similar to felsic groups, but lower and with pos Ba and Sr anomalies	LV01-131B: K2O: ~6.5 wt% and low in Na2O: ~2.8 wt% (later intrusion into the Stolzburg Pluton)
mafic groups	*(ultra-) mafic rocks*	(thin) bedding parallel outcrops; coarse grained doleritic verticle intrusions along faults	fine- and course-grained rocks	45-55 wt%	variable TiO2, Al2O3, Fe2O3, K2O, P2O5, NiO, and Cr2O3		variable trace element compositions	Rb: 6-90 ppm; Sr: 2.5-150 ppm; Cs: 0.2-2 ppm; Ba: 30-200 ppm; Pb similar to felsic groups	flat trends; neg Eu anomalies	"flat"trends; low in Th and U; strong pos K anomalies; strong neg Sr anomalies	coarse grained doleritic intrusions richest in MnO, MgO, CaO (9-10 wt%) and Na2O (3-4 wt%)
	silicified basalt	"bedding parallel" unit of	fine- to medium grained matrix dominated rocks with secondary anhedral quartz occurrences and a high content of chlorite	50-70 wt%	variable TiO2, Al2O3, Fe2O3, MnO, MgO; low NiO and Cr2O3; low CaO and Na2O; K2O: 0-4.5 wt%; P2O5: 0-0.42 wt%		similar to mafic groups	Ga: 15-25 ppm; Rb: 2-100 ppm; Sr: 3.5-10 ppm; Cs: 0.15-2 ppm; Ba: 40-200 ppm; Zr: 50-200 ppm; Hf: 1.25-4.75 ppm; Ta similar to felsic groups	flat trends; neg Eu anomalies	strong pos K anomalies; strong neg Sr anomalies	LV01-48A: abnormal REE (decrease LREE and MREE) and spider (neg Rb, K and P anomalies) trends; LV01-48A rich in Cr and NI; LV01-100D: MgO: ~6.5 wt%
cherts	*sedimentary cherts*	fine grained banded rocks with small scale sedimentary structures	fine grained samples consisting completely of microquartz	~100 wt%	very low or undetectable for all major elements		very low or undetectable for all trace elements	Pb: 0-5 ppm	inconsequent REE trends	more consequent trends; positive U and K anomalies; negative Sr, P and Ti anomalies	LV01-62 and LV01-133C have very similar trends
	massive cherts	glassy dark fine grained rocks from long outcrops perpendicular to bedding	fine grained samples consisting completely of microquartz	~100 wt%							LV01-62 rich in V, Cr, Mn, Co, Ni, Cu, and Zn
pyroxene/amphibole porphyries		bedding parallel intrusions in the BRCC	matrix dominated rocks containing phenocrysts of plagioclase, and brown hexagonal pyroxene/amphibole grains	60-70 wt%	similar to felsic groups (quartz porphyries)	low in NaO; low in CaO; K2O: 2-10.5 wt%; P2O5: ~0.1 wt%	similar to felsic groups	V: 10-80 ppm; Mn: 100-700 ppm; Zr: 140-180 (-350) ppm; Nb: 5-9 ppm; Y: ~8 ppm; Rb: 20-110 ppm; Sr: 4-120 ppm; Cs: 0.6-2 ppm; Ba: 60-150 ppm; Hf: 3-4 (-5.75) ppm; Ta: 0.5 ppm	similar to felsic groups; not all show kink at Dy; neg Eu anomalies	similar to felsic groups	SV01-1 is extremely enriched in most elements

Figure 31: Sm(rock)/Sm(chondrite) versus Yb(rock)/Yb(chrondrite) after Nakamura (1974). For meaning of symbols see legend of figure 24.

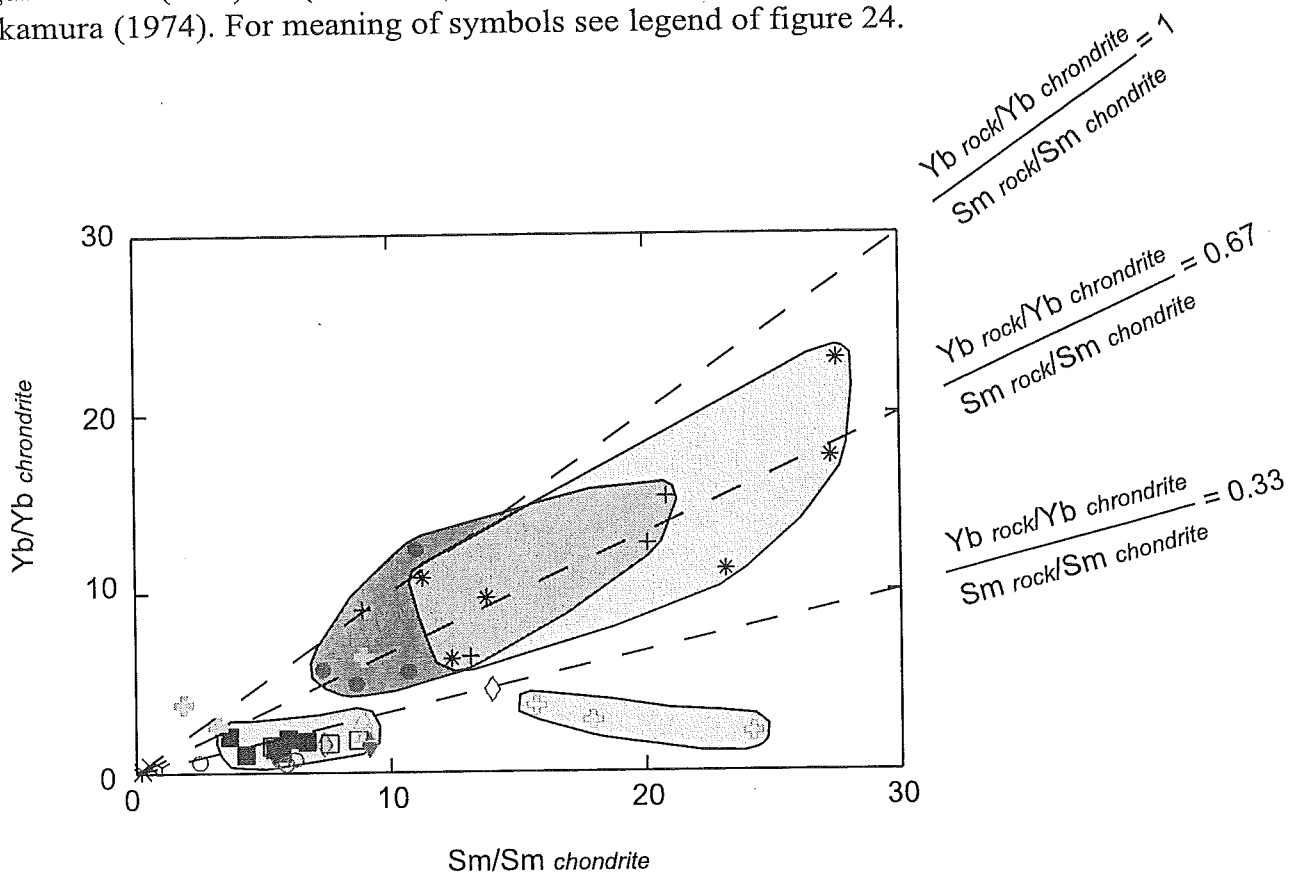

Figure 32: Schematic diagram showing the possible distribution of the felsic intrusives, shallow intrusives, quartz porphyries and lavas of the Hooggenoeg Formation and their most significant chemical differences.

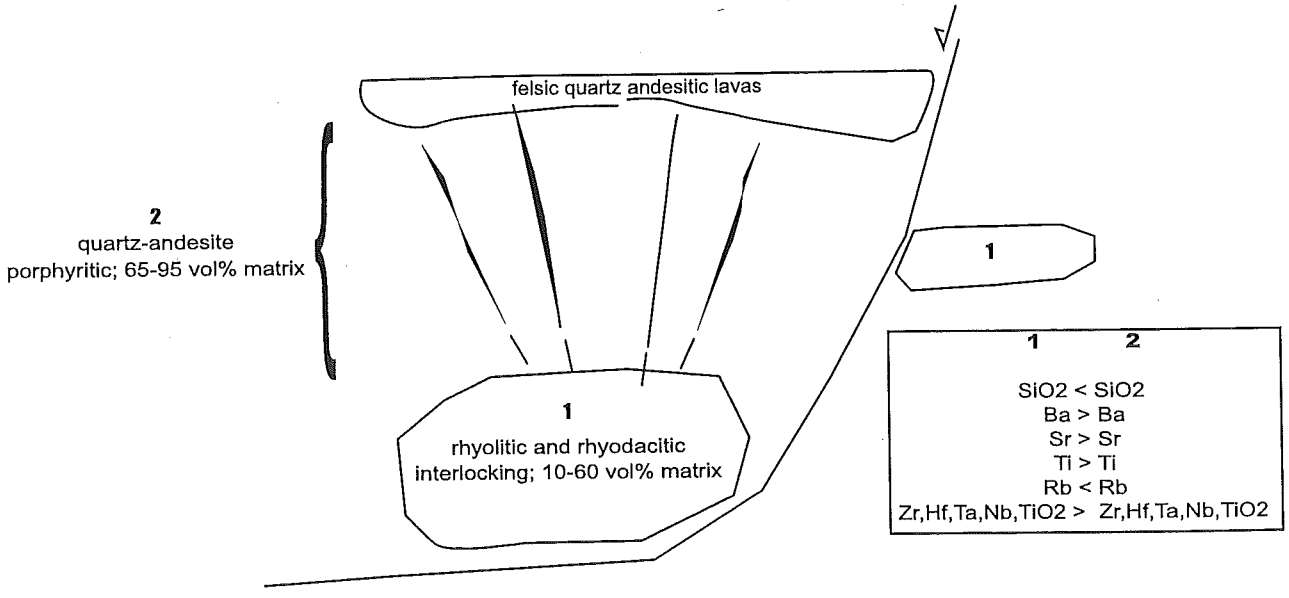

Figure 33: Plots showing SiO2 (wt%) versus TiO2 (a), Rb (b), Sr (c), Ba (d), Zr (e), Nb (f), Hf (g), and La (h) (ppm) for the felsic groups of the Hooggenoeg Formation and the Stolzburg Pluton.

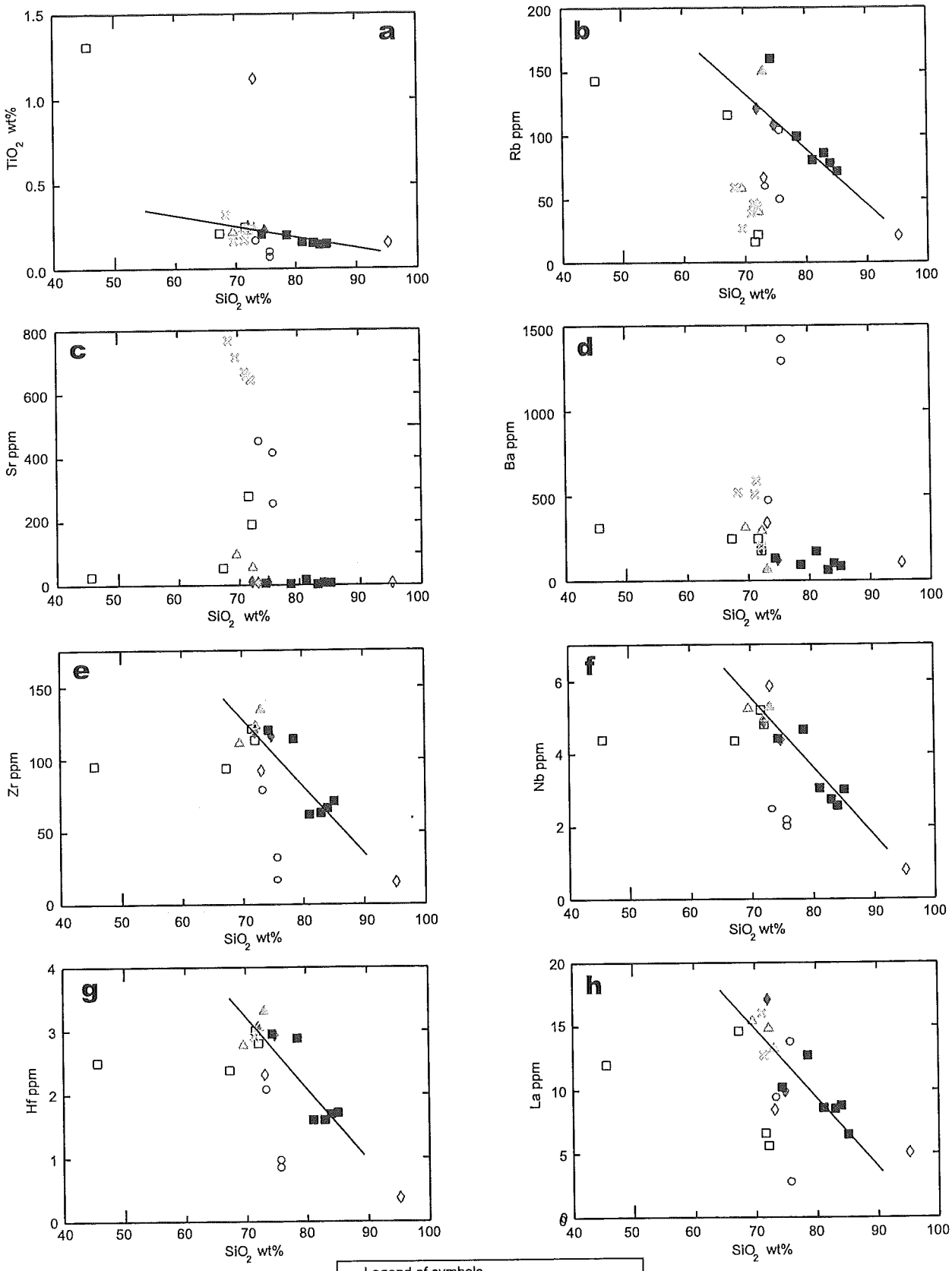

Figure 34: REE trends of the representative samples of the felsic groups: LV01-11, LV01-13b, LV01-23, LV01-144a, LV01-125b, LV01-127, LV01-127c, LV01-129, LV01-ON99-t1. After Nakamura (1974). For the meaning of symbols see legends of figures 24 or 33.

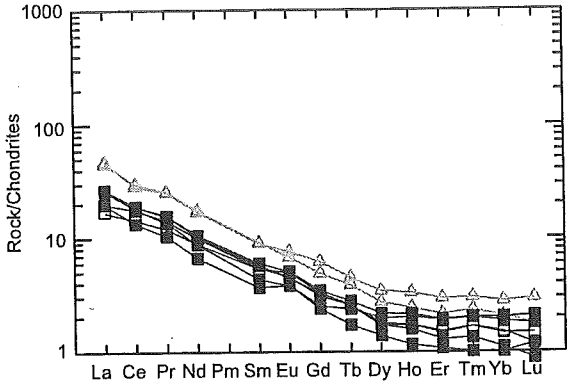

Figure 35: Plots of Nd (ppm) versus Sm (ppm) (a); Hf (ppm) versus Ta (ppm) (b); U (ppm) versus Th (ppm) (c); K2O (wt%) versus Ba (ppm) (d); K/Rb versus Ba/Sr (e) and Rb/Sr (f); and Sr (ppm) versus Eu/Eu* (g) for the felsic groups of the Hooggenoeg Formation and the Stolzburg Pluton. For the meaning of symbols see the legend of figure 33.

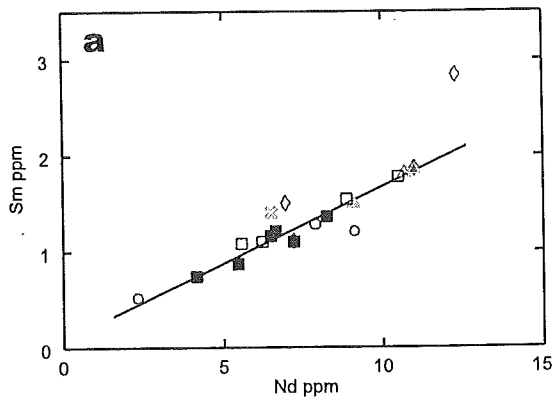

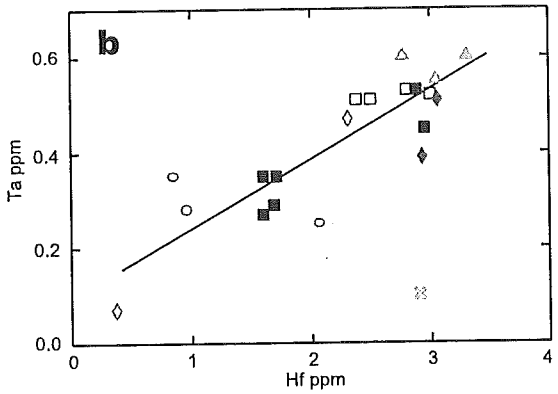

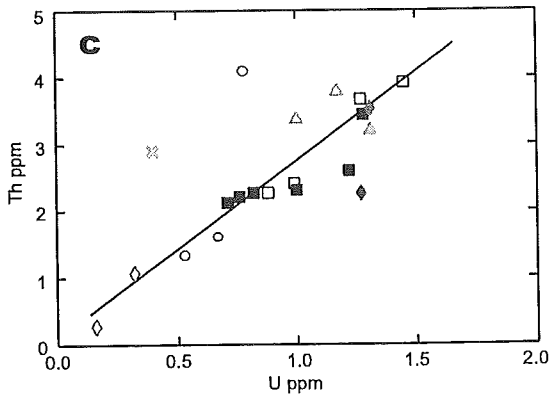

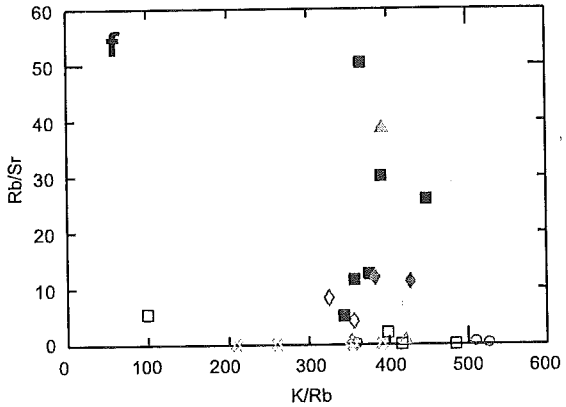

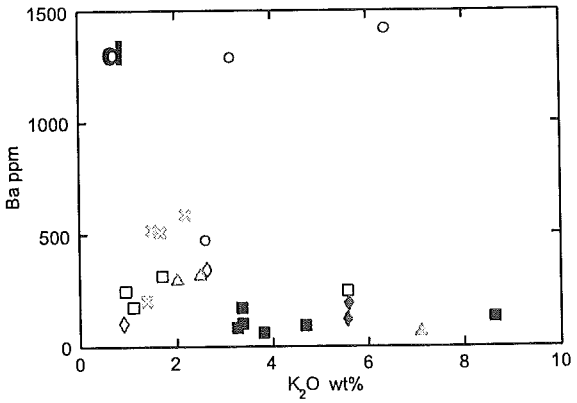

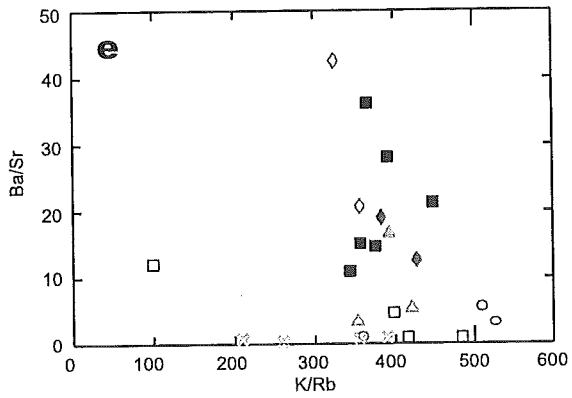

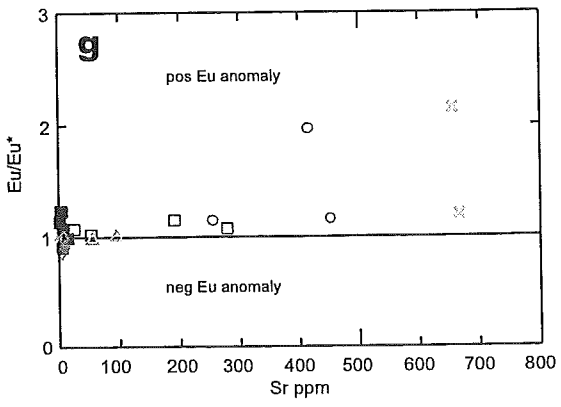

Figure 36: REE trends of Stolzbrug Pluton data from this study and from Condie and Hunter (1976) and de Ronde et al. (1991) (a) and of all Stolzburg Pluton data and the felsic intrusive group of the Hooggenoeg Formation (b), after Nakamura, 1974. For the meaning of symbols see legends of figure 33.

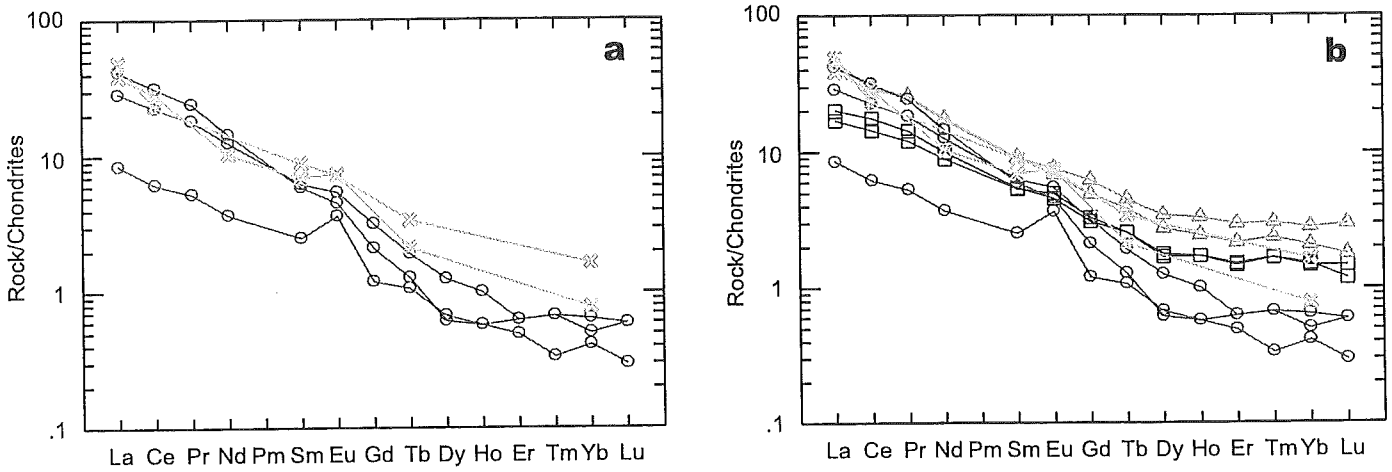

Figure 37: YbN versus LaN/YbN (after Nakamura, 1974) diagram showing the fields of Archaean TTG and post-Archaean TTG as defined by Martin (1993). For the meaning of symbols see the legend of figure 33.

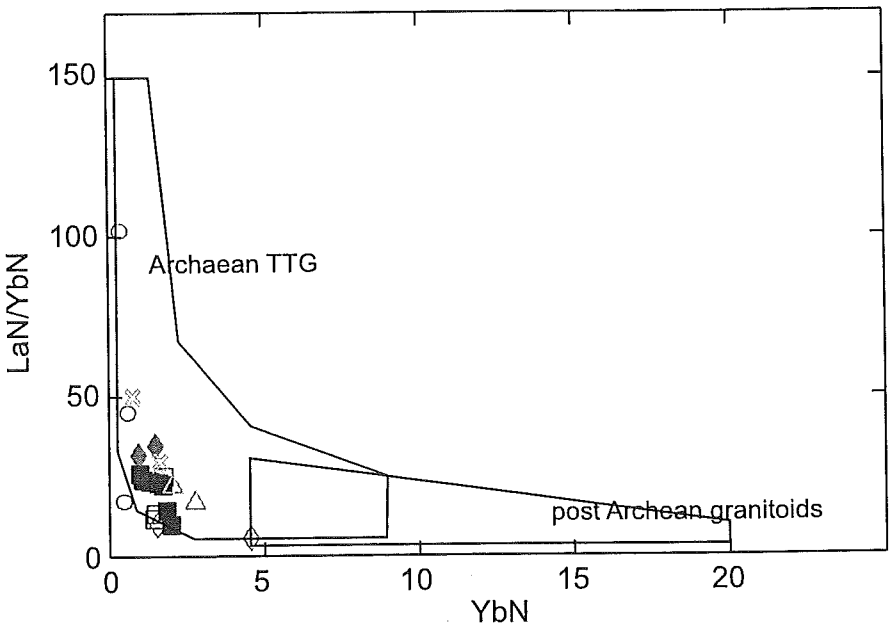

Figure 38: Schematic diagram showing the different possible origins for low-Al2O3 and high-Al2O3 trondhjemitic magmas, from Barker and Arth (1976).

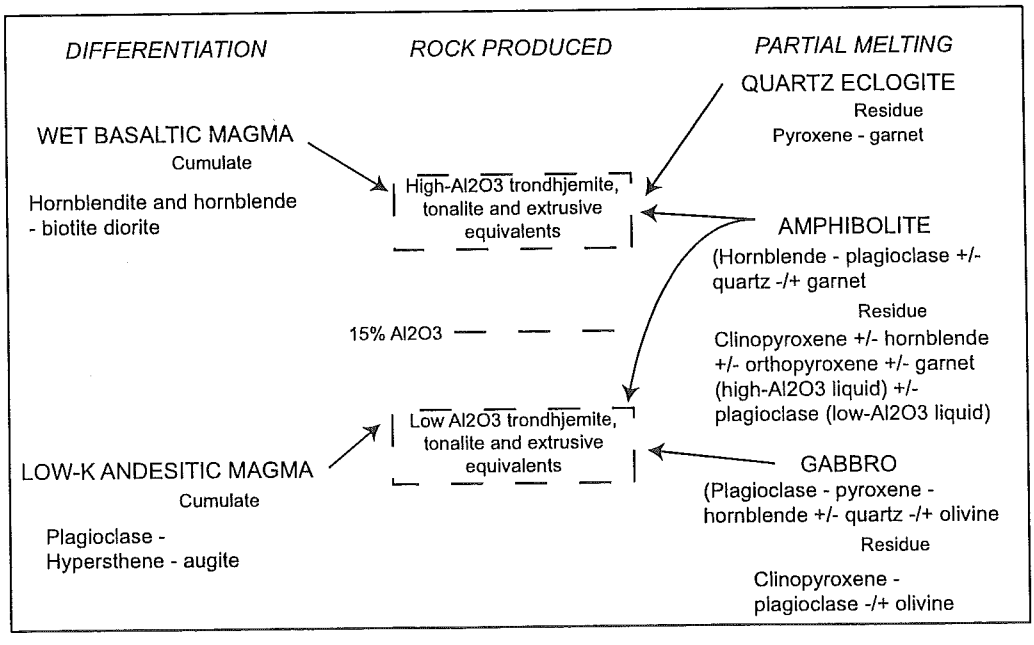

Figure 39: REE diagram of the pyroxene/amphibole porphyries and the Kaap Valley Tonalite from Robb and Anhaeusser (1983), Condie and Hunter (1976) and de Ronde et al. (1991), after Nakamura (1974).

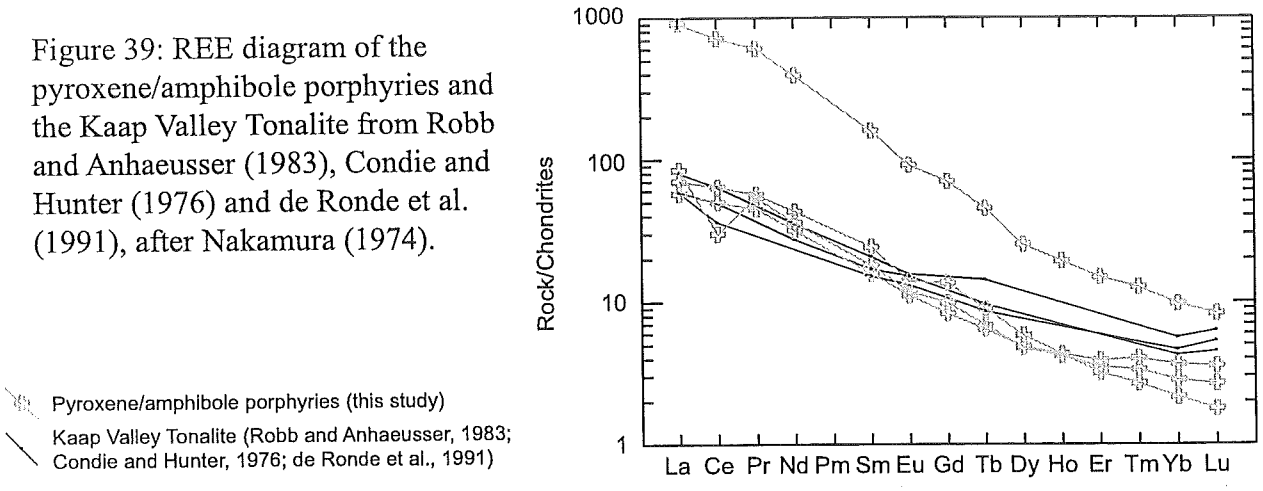

Figure 40: Classification of magma series and there associated specific tectonic settings. After Irvine and Baragar (1971) and Wilson (1989, p.11).

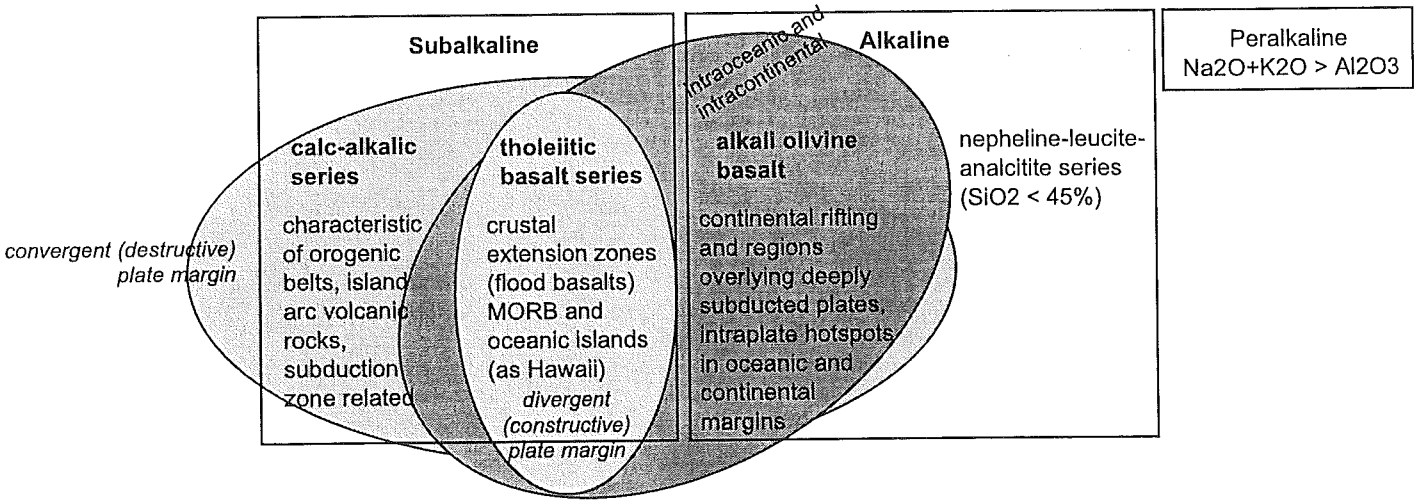

Figure 41a: Y (ppm) versus Nb (ppm) granitic classification diagram showing all felsic Hooggenoeg Froamttaion, Stolzburg and pyroxene/amphibole porphyry data. After Pearce et al. (1984). For meaning of symbols see legend of figure 33.

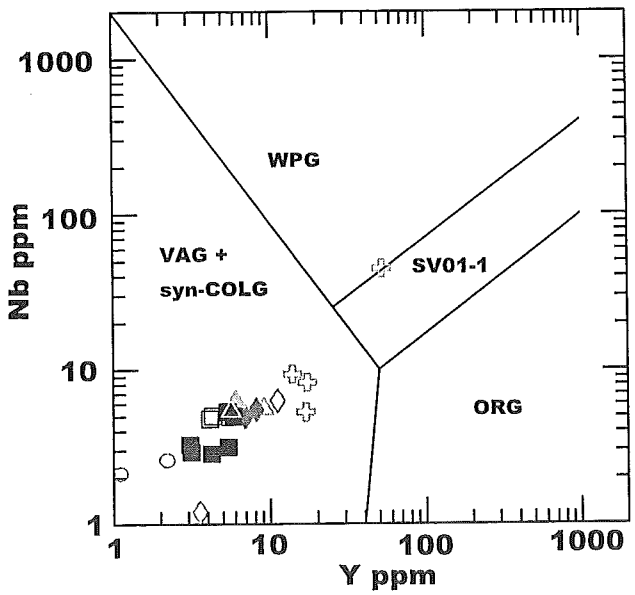

Figure 41b: Zr-Ti/100-Y*3 classification scheme for basic volcanic rocks shwoing all (ultra-) mafic and silicified basaltic samples. After Pearce and Cann (1973).

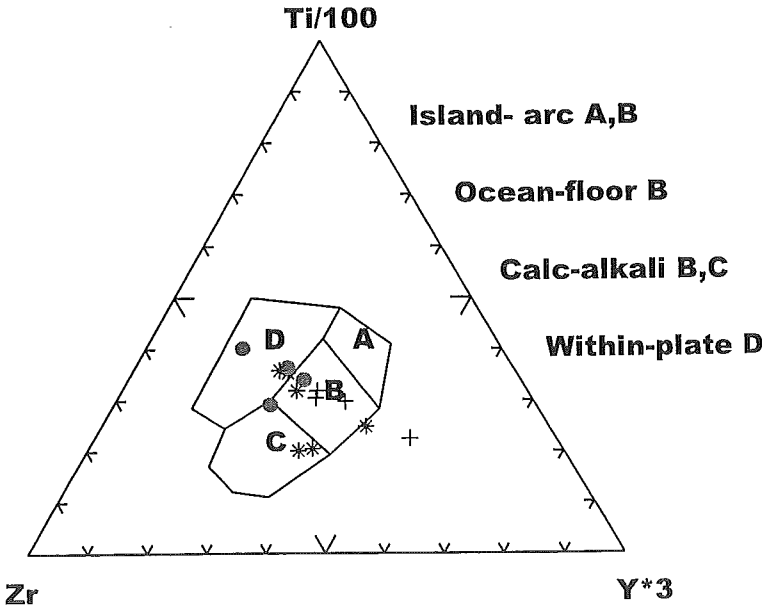

Figure 41c: Th-Hf-Ta diagram with the fields of magma compositions erupted in different tectonic environments outlined, showing all felsic, (ultra-) mafic, silicified basaltic rocks and pyroxene/amphibole porphyries from the Hooggenoeg Formation, and all Stolzburg Pluton data. A: N-type MORB, B: E-type MORB, C: within plate basalt, D: magma series at destructive plate margin. After Wood et al. (1979).

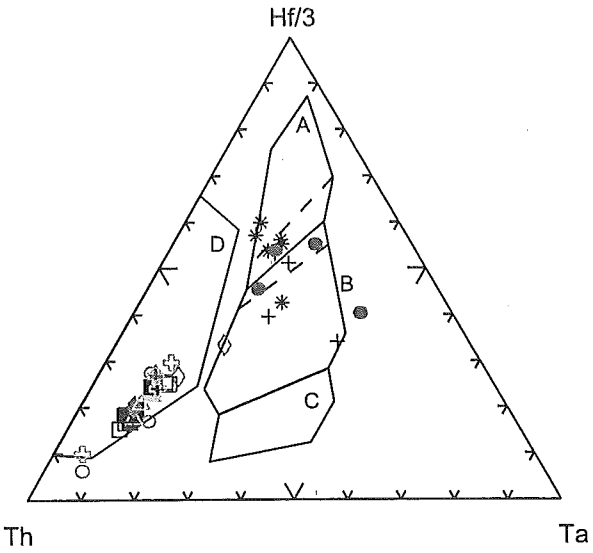

Figure 42: Spider diagram patterns for (ultra-) mafic and silicified basaltic rocks of the Hooggenoeg Formation (a) and for mid-ocean ridge (MORB), oceanic-island (OIB) and island-arc basalts (from Wilson, 1989, p.20) (b), after Thompson et al. (1984).

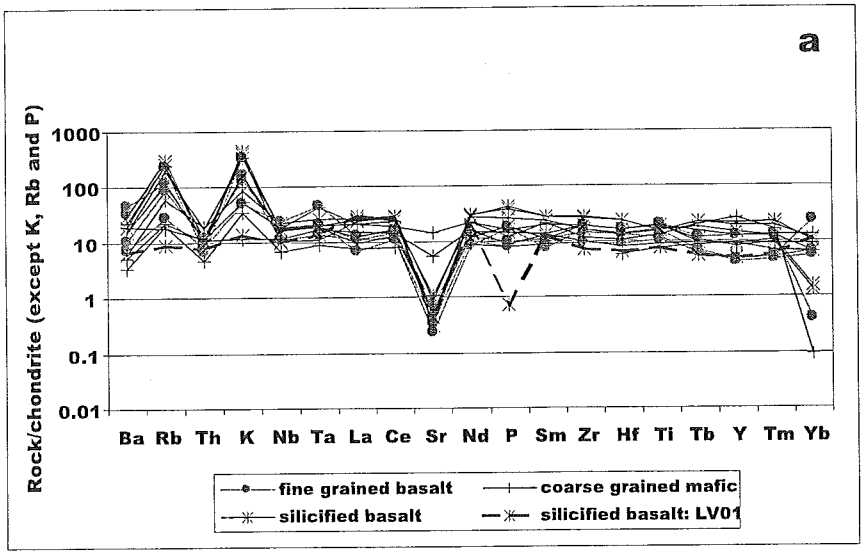

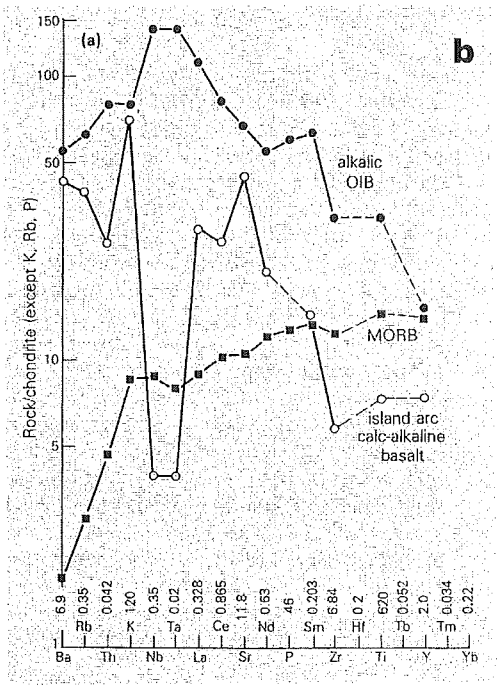

Figure 43: Comparison between the position and stratigraphic sequence of the Archaean of the Kaapvaal and Pilbara Cratons (from Zegers et al., 1998).

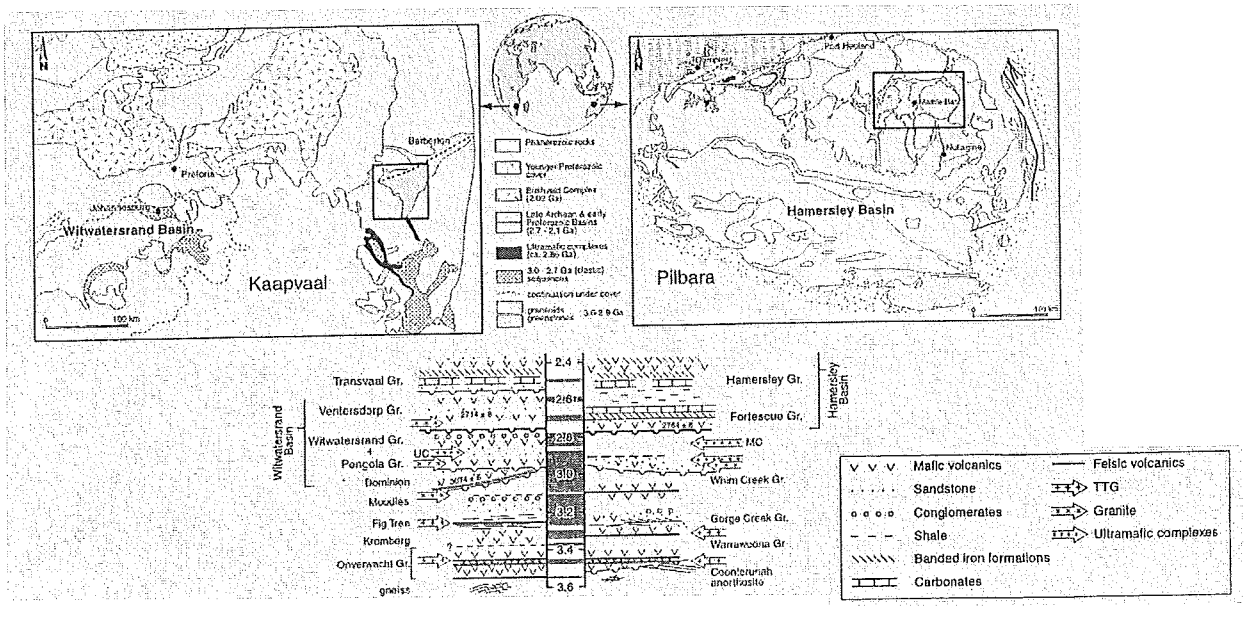

Figure 44: Stratigraphic schemes for the Warrawoona Group / Megasequence (from Barley, 1993). After Hickman (1983) (a) and after DiMarco and Lowe (1989b) (b). The two differ in the positions of the Panorama and Duffer Formations.

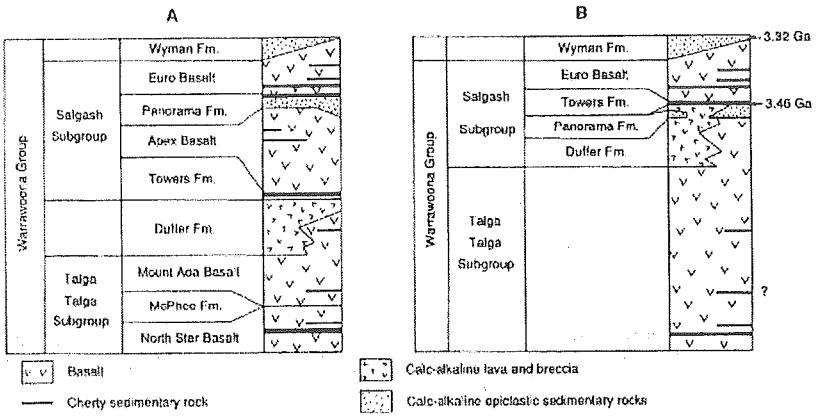

Figure 45: The Eastern Pilbara and the Coppin Gap greenstone belt highlighted

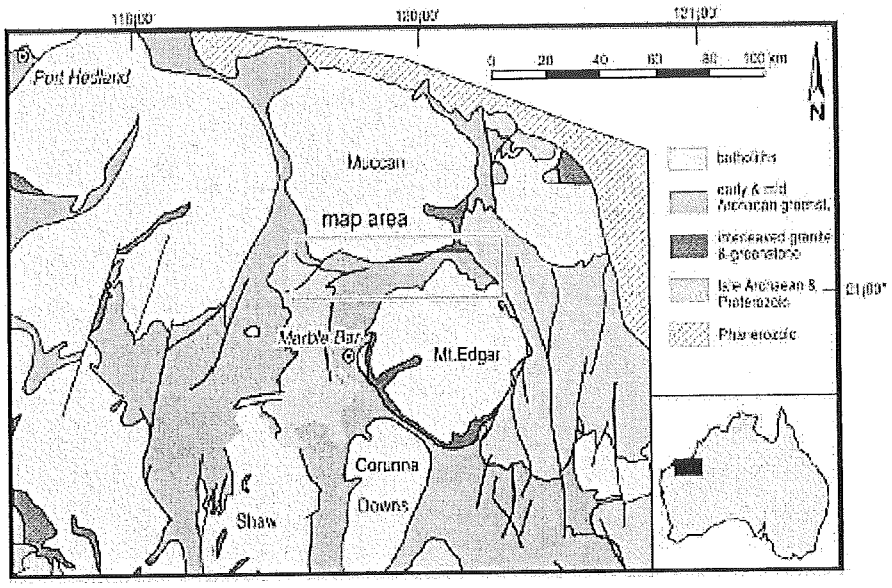

Figure 46: REE diagrams of the felsic intrusive and porphyritic groups of the Hooggenoeg Formation, and the intermediate and felsic Duffer Formation (a) and the felsic Panorama Formation (b) rocks, after van der Meer (2002, Unpubl.) and Nakamura (1974).

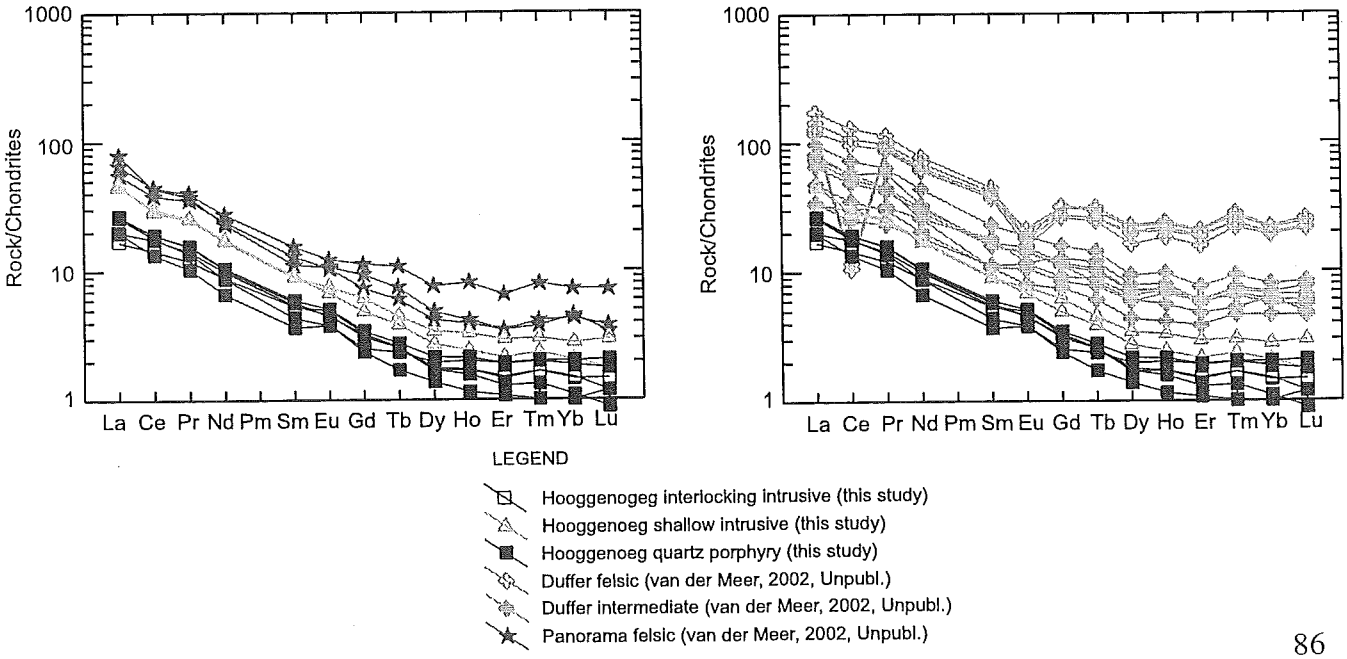

Appendix B: Tables

Appendix B
Table 1: List of measured orientations

locality	GPS coordinates	rocktype	bedding	fracture/fault plane	other predominant directions
LV01-16		quartz and plagioclase rich porphyritic felsic rock			108/45, 062/84
LV01-16b		quartz and plagioclase rich porphyritic felsic rock			307/66, 151/78, 067/74, 008/70
LV01-17		diaclased felsic volcanic porphyritic rock			291/46, 251/40?, 216/35 (diaclases?)
LV01-FIB		flowbanded (wavy, platy) felsic volcanic rock	248/69		187/20 (diaclase)
LV01-19		flowbanded porphyritic rock	236/50		330/08 (diaclase)
LV01-22		flowbanded(?) felsic rock	052/68 (flowbanding?), 040/80 (crossbedding?)		
LV01-27		flowbanded felsic rock	063/74	288/57, 025/90	
LV01-31		chert bed	193/70		
LV01-34		felsic silicified rock?			237/72
LV01-35		cm thick banding in chert bed	251/82		
LV01-36		black and white banded chert with imbricated slabs	068/88		
ON99-29A	S25°55'10.8", E030°51'55.1"	iron breccia	174/?		
LV01-37		ultramafic intrusion rich in pyroxenes			270 (strike outcrop)
LV01-38		banded iron stone	138/88		
to the east of LV01-41		folded banded iron formations			095/90 (axialplane)
LV01-47	S25°55'29.1", E030°51'01.8"	cherts (on eastern side of valley)	354/64		
		banded chert	003/69		
LV01-57	S25°55'34.4", E030°50'58.2"	thin felsic unit			070 (strike outcrop)
LV01-59	S25°55'32.7", E030°52'14.0"	quartz rich felsic rock	210/88?		306/74 (orientation parallel to thick black chert veins)
LV01-60		thinly, wavy, closely spaced flowbanded felsic rock	180/90		
LV01-61		banded chert	191/86		
LV01-62		black chert running bedding parallel	027/89	227/84	
		hostrock	013/90		
LV01-63		angular and rounded fragments of heterogeneous composition, possible sediment	221/88(?)		
ON99-101		thinly laminated chert	025/62		
LV01-68	S25°55'32.7", E030°52'10.2"	heavy, coarse grained intrusion	040/80?		059 (orientation outcrop)
to the west over the creek			327/50?		
LV01-71	S25°55'34.5", E030°52'06.1"	fractures in felsic rock parallel to black chert veins		066/68	
LV01-71b		patchy outcrop of felsic rock		060/52 (vein/fracture surfaces)	
LV01-72	S25°55'34.7", E030°52'03.6"	massive, smooth, coarse grained, dark and heavy, intrusive rock			261/68 (contact intrusive with host rock?)
LV01-74		thin, finely banded chert interval in silicified, quartz rich felsic unit	007/87	068/72	

Appendix B
Table 1: List of measured orientations

locality	GPS coordinates	rocktype	bedding	fracture/fault plane	other predominant directions
LV01-75		banded chert with small scale ripples	348/73		
LV01-77b		massive, veined by black chert, quartz rich rock		320/42	
LV01-78		banded black and white chert	193/85		
LV01-81		fine grained basaltic rock		018/82	
LV01-84b		banded chert	108/86		
LV01-85		dark, heavy, fractured rock		100/66(?)	
LV01-87	S25°55'31.6", E030°52'16.3"	possibly flow banded felsic rock	338/84		
LV01-89		vein/fractures in felsic rock		348/80	
LV01-90		very veined, flow banded (with thick spacings) felsic rock	000/46		
LV01-96		vertical, 5 metre wide, black chert vein			070/76
LV01-97		vertical, 3 metre wide, black chert vein			103/68
LV01-98		black chert, massive black chert vein, and black chert and white quartz	327/76	138/64, 005/10(?)	295/90
LV01-99		quartz porphyry veins			332/65, 010 (strike quartz porphyry vein or pipe)
LV01-100	S25°55'28.5", E030°52'13.5"	silicified dolerite and basalt with many secondary quartz grains in it			181/70?
LV01-101		thin banded chert	216/85 (overkipt)		
a few metres to the north		banded chert overlying Fe-sst	212/85		
LV01-103		black chert vein			029/76
LV01-104	S25°55'39.4", E030°51'03.5"	broken and brecciated by black chert veins, volcanic rocks	038/72?		
LV01-105		broken and brecciated by black chert veins, volcanic rocks	038/86		
LV01-106		conglomerates or breccia	022/90		
LV01-108	S25°55'40.6", E030°50'56.5"	thinly flow banding in coarse grained dark fresh rock	040/80-85, 056/74		
LV01-109(b)	S25°55'46.5", E030°50'59.5"	quartz and plagioclase rich porphyritic felsic rock		039/82	
LV01-119		simple shear in komatiite and sedimentary chert			324/50 (orientation tension gash), 020/50 (PDZ)
LV01-120	S25°56'12.5", E030°52'49.2"	sheared and altered rock with spinifex texture			045/68 (shearing direction?)
LV01-124a	S25°55'32.0", E030°52'06.2"	contact between sediment and basalt(?)	025/90		
LV01-126=97	S25°55'33.7", E030°51'55.0"	black chert vein			150/90
LV01-128(a)	S25°55'28.1", E030°51'34.6"	flowbanded felsic rock	235/63		
LV01-128(b)		banded chert	211/70		
LV01-129	S25°55'39.2", E030°51'54.6"	black chert veins a few cms thick in a felsic rock			049/85
LV01-130	S25°55'29.8", E030°51'46.7"	grey laminated chert beds	199/86		
LV01-138		flowbanded(?) quartz and plagioclase rich, felsic rock	169/82		

Appendix B
Table 2: List of samples taken

locality	GPS coordinates	rocktype	thin sect.	petro. descr.	geochem. analyses	drawer
LV01-1A		medium- to coarse-grained grey-green glassy rock	N		N	kl5
LV01-2A		columnar jointed basalt	Y		N	kl5
LV01-3		quartz rich, glassy felsic rock	N		N	kl5
LV01-4A		quartz and feldspar (lath-shaped phenos) rich felsic rock	N		N	kl5
LV01-7		fractured, soft quartz and plagioclase rich felsic rock	N		N	kl5
LV01-8		interlocking felsic rock with greenish appearance, and less dark minerals	N		N	kl5
LV01-9		interlocking felsic rock, in the strike of "tonalite"outcrop 140 of Houtzager and de Vries	N		N	kl5
LV01-10		more and more intrusive characteristics (grainsize and interlocking texture)	N		N	kl5
LV01-11	S25°56'16.8", E030°53'37.5"	fresh, light grey, interlocking felsic rock rich in quartz, plagioclase and pyroxene(?)	Y (pol.)	p.19	Y	kl5, kl12
LV01-12		similar to LV01-11, but less darker minerals	N		N	kl5
LV01-13A		medium- to coarse-grained massive outcrop of felsic rock, veinlets filled with green material (chlorite?)	N		N	kl5
LV01-13B	S25°56'11.0", E030°53'43.5"	finer grained interlocking felsic rock than LV01-11, also with less black or opaque minerals	Y (pol.)	p.19	Y	kl5
LV01-14		coarse-grained felsic rock with green glassy groundmatrix	N		N	kl5
LV01-15		weathered quartz rich rock	N		N	kl5
LV01-16		rounded quartz grains and weathered (red-brown) grains in a fine matrix	N		N	kl5
LV01-16B		similar to LV01-16, but with larger quartz grains and more red-brown weathered grains	N		N	kl5
LV01-16C		similar to LV01-16B, but with a slightly darker grey fresh colour	N		N	kl5
LV01-17		diaclased felsic volcanic porphyritic rock	Y		N	kl5
LV01-21A		black chert vein, with angular 1 cm sized pieces of host (white felsic rock turned yellow) rock	Y		N	kl5
LV01-22		flowbanded(?) felsic rock	N		N	kl5
LV01-23	S25°55'33.6", E030°54'07.1"	columnar jointed, massive, felsic lava with euhedral quartz grains	Y (pol.)	p.21	Y	kl5
LV01-24		angular fragments of felsic lava in similar matrix - agglomerate or top/bottom of other felsic flow	Y		N	kl5
LV01-25B		black chert	N		N	kl5
LV01-27		fine-grained flowbanded felsic rock	N		N	kl5
LV01-27B		yellow euhedral quartz grains in light felsic rock	N		N	kl5
LV01-27C		light grey, felsic, fine-grained rock	Y		N	kl5
LV01-27C'		silicified fine grained felsic rock	N		N	kl5
LV01-28A		silicified felsic rock with white and yellow laths	Y		N	kl5
LV01-28B		similar to LV01-28B but silicified and broken-up by black and white quartz veins	Y		N	kl5
LV01-29A		abundant large (up to 3 mm) quartz grains and weathered out holes (plagioclase, 1 mm)	N		N	kl5
LV01-29B		abundant large (up to 3 mm) quartz grains and weathered out holes (plagioclase, 1 mm)	N		N	kl5
LV01-30		heavy, dark, fine-grained pillow basalts	N		N	kl5
LV01-31		(sedimentary) chert bed	N		N	kl5
LV01-31B		large euhedral quartz in flowbanded(?) felsic rock	N		N	kl5

Appendix B
Table 2: List of samples taken

locality	GPS coordinates	rocktype	thin sect.	petro. descr.	geochem. analyses	drawer
LV01-32		felsic rock riddled with many chert veins on cm scale	Y		N	kl5
LV01-33		felsic, silicified, veined rock	N		N	kl6
LV01-37		dunitic ultramafic intrusion rich in pyroxenes	Y		N	kl6
LV01-37A		wherlitic ultramafic intrusion	N		N	kl6
LV01-39A		banded black chert with grains visible in the not so glassy parts, layers are 1.5-2 cm thick	N		N	kl6
LV01-39B		banded black chert with fine sedimentary structures indicating a top to the north	N		N	kl6
LV01-39C		black massive glassy chert	N		N	kl6
LV01-40A		quartz rich felsic rock	Y		N	kl6
LV01-40B		greenish angular fragments in felsic quartz rich rock	N		N	kl6
LV01-42		few large quartz grains and many plagioclase laths in massive outcrop in otherwise black and white banded chert outcrop	Y		N	kl6
LV01-43		silicified basalt with rounded and elongated quartz occurrences	N		N	kl6
LV01-45		opzoeken boekje sjoukje	N		N	kl6
LV01-46A		breccia (but not tectonic) with rounded, finer and coarser grained clasts	N		N	kl6
LV01-46B		similar to LV01-46A, but with shards of broken material and infillings of quartz or chert surrounding the fragments	N		N	kl6
LV01-47	S25°55'29.1", E030°51'01.8"	silicified basalt with quartz occurrences	Y (pol.)	p.23	Y	kl6
LV01-48A	S25°55'28.5", E030°51'01.3"	silicified basalt with quartz occurrences	Y (pol.)	p.24	Y	kl6
LV01-49	S25°55'29.3", E030°51'09.3"	silicified basalt with quartz occurrences	Y (pol.)	p.23	Y	kl6
LV01-54		green, mafic intrusion with yellow and dark laths and an interlocking texture	N		N	kl6
LV01-56	S25°55'33.6", E030°50'58.3"	mafic plagioclase rock with a fine-grained matrix	Y (pol.)	p.22	Y	kl7
LV01-57	S25°55'34.4", E030°50'58.2"	thin felsic unit	N		N	kl6
LV01-58B		felsic rock	N		N	kl6
LV01-59A	S25°55'32.7", E030°52'14.0"	quartz rich felsic rock??	Y		N	kl7
LV01-59B		no quartz grains visible in felsic rock	N		N	kl6
LV01-60		thinly, wavy, closely spaced flowbanded felsic rock	N		N	kl6
LV01-62	S25°55'29.7", E030°52'09.8"	black chert running bedding parallel	Y (pol.)	p.24	Y	kl6, kl7
LV01-63A		large euhedral quartz grains in felsic rock with small angular and rounded fragments of heterogeneous composition	Y		N	kl7
LV01-63B		similar to LV01-63A, but with smaller rounded quartz grains	N		N	kl6
LV01-66		elliptical, very weathered, red/brown basalt pillows	N		N	kl7
LV01-67		very weathered, blue/green fine-grained veined rock with large euhedral quartz(?) phenocrysts	Y		N	kl7
LV01-67B		very silicified fine-grained pink/yellow rock with a sugary texture, mode is uncertain	Y		N	kl7

Appendix B
Table 2: List of samples taken

locality	GPS coordinates	rocktype	thin sect.	petro. descr.	geochem. analyses	drawer
LV01-68 and to the west over the creek	S25°55'32.7", E030°52'10.2"	heavy, coarse grained intrusion	Y (pol.)	p.23	Y	kl7
LV01-69		large, euhedral quartz grains in felsic rock	Y		N	kl7
LV01-72	S25°55'34.7", E030°52'03.6"	massive, smooth, coarse grained, dark and heavy, mafic intrusive rock	N		N	kl7
LV01-73		mafic intrusion	N		N	kl7
LV01-75		banded chert with small scale ripples	Y		N	kl7
LV01-76		fine-grained mafic intrusion	N		N	kl7
LV01-77B		massive, veined by black chert, quartz rich rock	Y		N	kl7
LV01-79		very fine-grained, green rock with heterogeneous colouring	N		N	kl7
LV01-80		loose rocks of dark, heavy, medium-grained mafic composition	N		N	kl8
LV01-82	S25°55'28.4", E030°52'11.0"	medium-grained, dark and heavy, mafic intrusion	Y (pol.)	p.23	Y	kl7
LV01-83		veined by white quartz massive outcrop of basaltic or sedimentary material	N		N	kl7
LV01-84B		small needle shaped laths and quartz grains in a patchy outcrop of silicified material				kl8
LV01-88		possibly sediment (?) in a smooth outcrop oriented 040	N		N	kl7
LV01-89		vein/fractures in felsic rock	Y		N	kl8
LV01-93B		light grey-greenish felsic rock with quartz and plagioclase grains of similar sizes	N		N	kl7
LV01-94	S25°55'46.9", E030°51'48.4"	coarse-grained mafic intrusion with large pyroxene phenocrysts	Y (pol.)	p.23	Y	kl8, kl12
LV01-94B		fine-grained mafic material	N		N	kl8
LV01-97	S25°55'33.7", E030°51'55.0"	vertical, 3 metre wide, fine-grained, black chert vein	Y (pol.)	p.25	Y	kl8
LV01-100A	S25°55'28.5", E030°52'13.5"	silicified dolerite and basalt with many secondary quartz grains in it	N		N	kl7
LV01-100B	S25°55'28.5", E030°52'13.5"	silicified basalt	Y (pol.)	p.24	Y	kl8
LV01-100D	S25°55'28.5", E030°52'13.5"	silicified basalt	Y (pol.)	p.24	Y	kl7, kl8
LV01-100E	S25°55'28.5", E030°52'13.5"	silicified basalt	Y (pol.)	p.24	Y	kl9
LV01-102	S25°23'45.7", E029°01'20.0"	green silicified rock in Buck Ridge Chert Complex	Y (pol.)	p.26	Y	kl8
LV01-104	S25°55'39.4", E030°51'03.5"	broken and brecciated by black chert veins, felsic volcanic rock	N		N	kl7
LV01-107		dark green and heavy rock with angular fragments of 0.5 cm of lighter coloured material, and without interlocking texture	N		N	kl9
LV01-108A	S25°55'40.6", E030°50'56.5"	thinly flowbanded coarse-grained dark rock	N		N	kl8
LV01-108B	S25°55'40.6", E030°50'56.5"	dark green and purple colours in rock similar to LV01-108B	N		N	kl8
LV01-109A		felsic rock with irregularly shaped quartz grains	N		N	kl8
LV01-109B	S25°55'46.5", E030°50'59.5"	possible interlocking texture in felsic rock with green, glassy appearance	Y (pol.)	p.19	Y	kl8
LV01-110		loose blocks of heterogeneous dark, green rock	N		N	kl8

Appendix B
Table 2: List of samples taken

locality	GPS coordinates	rocktype	thin sect.	petro. descr.	geochem. analyses	drawer
LV01-111A		rhyolitic felsic phenocrytic rock	N		N	kl8
LV01-111B		small rounded white-red grains in a more mafic rock than LV01-111A	N		N	kl8
LV01-112		interlocking texture in felsic rock rich in plagioclase, but with less dark grains than e.g. LV01-113	Y		N	kl9
LV01-113	S25°56'14.5", S25°56'14.5"	interlocking texture in felsic rock rich in plagioclase	Y (pol.)		Zr	kl9
LV01-114		interlocking texture in felsic rock rich in plagioclase	N		N	kl8, kl9
LV01-115		yellow weathered felsic rock rich in plagioclase	Y		N	kl9
LV01-116		interlocking texture in felsic rock rich in plagioclase	Y		N	kl9
LV01-117		felsic rock with more matrix than LV01-113 - LV01-116	Y		N	kl8
LV01-120	S25°56'12.5", E030°52'49.2"	sheared and altered rock with spinifex texture	N		N	kl9
LV01-122	S25°55'38.7", E030°52'17.0"	euhedral quatz grains in a porphyritic felsic rock	Y (pol.)	p.20	Y	kl9
LV01-124A	S25°55'32.0", E030°52'06.2"	basalt?	Y (pol.)	p.22	Y	k9, kl10
LV01-124B	S25°55'32.0", E030°52'06.2"	sediment	Y		N	kl10
LV01-124C	S25°55'32.0", E030°52'06.2"	silicified felsic flowbanded rock	Y (pol.)	p.21	Y	kl8
LV01-124D	S25°55'32.0", E030°52'06.2"	dark, green and heavy (ultra-)mafic rock	Y (pol.)	p.22	Y	kl10
LV01-125A	S25°55'32.6", E030°51'58.6"	quartz rich porphyritic felsic rock	Y (pol.)	p.20	Y	kl10
LV01-125B	S25°55'32.6", E030°51'58.6"	quartz rich porphyritic felsic rock	Y (pol.)	p.20	Y	kl9
LV01-126=97						
LV01-127	S25°55'32.0", E030°51'45.8"	quartz porphyritic felsic rock from vertical felsic vein	Y (pol.)	p.20	Y	kl9
LV01-127B		quartz porphyritic felsic rock from vertical felsic vein	Y		N	kl10
LV01-127C	S25°55'30.5", E030°51'46.3"	quartz porphyritic felsic rock from top of vertical felsic vein at LV01-127	Y (pol.)	p.20	Y	kl9
LV01-128	S25°55'28.1", E030°51'34.6"		N		N	kl8
LV01-128A	S25°55'28.1", E030°51'34.6"	flowbanded felsic rock	Y (pol.)	p.21	Y	kl8
LV01-128B	S25°55'28.1", E030°51'34.6"	banded sedimentary chert	Y (pol.)	p.25	Y	kl10, kl9
LV01-128C	S25°55'28.1", E030°51'34.6"	interlocking, fine-grained, mafic intrusive (?) rock	Y (pol.)	p.22	Y	kl9
LV01-129	S25°55'39.2", E030°51'54.6"	black chert veins (few cm thick) in felsic porphyritic rock	Y (pol.)	p.20	Y	kl8
LV01-131A	S26°01'25.4", E030°45'43,0"	Stolzburg Pluton: gneissic trondhjemite coarser grained than the interlocking felsic rocks from the BGB	Y (pol.)	p.21	Y	kl10, shelf
LV01-131B	S26°01'25.4", E030°45'43,0"	white, coarse-grained vein into Stolzburg Pluton, with many large feldspars (upto 1.5 cm)	Y (pol.)	p.21	Y	shelf

Appendix B
Table 2: List of samples taken

locality	*GPS coordinates*	*rocktype*	*thin sect.*	*petro. descr.*	*geochem. analyses*	*drawer*
LV01-132	S26°00'29.0", E030°43'17.5"	Stolzburg Pluton: gneissic trondhjemite coarser grained than the interlocking felsic rocks from the BGB	Y (pol.)	p.21	Y	kl10, shelf
LV01-133C	S25°55'30.3", E030°52'10.0"	black massive chert from vertical chert vein terminating in bedding parallel massive chert at LV01-62	Y (pol.)	p.25	Y	kl10
LV01-134		medium- to coarse-grained dolerite with interlocking texture	Y (pol.)		N	kl10
LV01-136(B)		angular fragments of quartz-rich prophyritic felsic material in a fine matrix	Y		N	kl8
LV01-138		flowbanded(?) quartz and plagioclase rich, felsic rock	Y		N	kl8
LV01-140	S25°55'49.1", E030°52'25.5"	euhedral quartz and plagioclase grains and dark needle shaped laths in felsic interlocking rock	Y (pol.)	p.18	Y	kl10
LV01-141	S25°55'59.8", E030°54'00.6"	interlocking felsic rock	Y (pol.)	p.19	Y	kl10
LV01-142	S25°55'49.8", E030°53'58.3"	interlocking felsic rock	Y (pol.)	p.19	Y	kl10
LV01-143	S25°55'39.1", E030°53'57.9"	coarse grained dolerite with light plagioclase grains (1-1.5 mm) and dark minerals as well	Y (pol.)	p.22	Y	kl10
LV01-144A	S25°55'40.5", E030°54'02.6"	very weathered flow banded felsic lava	Y (pol.)	p.21	Y	kl10
LV01-144B	S25°55'40.5", E030°54'02.6"	very weathered flow banded felsic lava, more heterogeneous than LV01-144A, with regions rich and poor in phenocrysts	Y		N	kl10
LV01-ON99-t1	S25°55'49.5", E030°51'26.0"	felsic phenocryst rich rock with interlocking texture, but still matrix	Y (pol.)	p.19	Y	kl9, kl12
W01-3	S25°55'40.7", E030°51'34.4"	pyroxene/amphibole porphyry	Y (pol.)	p.25	Y	kl11
W01-4		loose, very red, weathered block from path	Y		N	kl11
SV01-1	S25°55'21.3", E030°52'46.1"	fine grained mafic rock	Y (pol.)	p.25	Y	kl12
SV01-3	S25°55'22.5", E030°53'02.0"	pyroxene/amphibole porphyry	Y (pol.)	p.26	Y	kl12
SV01-35	S25°55'45.3", E030°56'00.3"	coarse grained (upto 3mm) mafic rock, with amphiboles	Y (pol.)	p.26	Y	kl12, shelf
SV01-39	S25°55'47.7", E030°55'36.8"	very fine grained very green igneous rock	Y (pol.)	p.26	Y	kl12
SV01-46	S25°55'46.9", E030°55'46.5"	pyroxene/amphibole porphyry	Y (pol.)	p.26	Y	kl12

Appendix B
Table 3a: Results of the H2O- and LOI determinations

groups		sample	crucible (g)	crucible + sample (g)	weight sample (g)	weight (g) after drying @ 110 °C	loss during drying (g)	weight (g) after roasting @ 850 °C	loss during roasting (g)	H2O- (wt%)	LOI (wt%)
intermediate and felsic groups	shallow intrusives from area I	LV01-140	17.34317	19.34999	2.00682	19.34910	0.00089	19.27517	0.07393	0.04435	3.68394
		LV01-ON99-t1	12.05626	14.06653	2.01027	14.06611	0.00042	14.02795	0.03816	0.02089	1.89825
	consolidated ash or tuff from area I	LV01-109B	17.34325	19.34551	2.00226	19.34418	0.00133	19.30225	0.04193	0.06642	2.09413
	interlocking felsic rocks from area II	LV01-11	12.72465	14.71727	1.99262	14.71510	0.00217	14.67606	0.03904	0.10890	1.95923
		LV01-13B	12.83156	14.84576	2.01420	14.84453	0.00123	14.81556	0.02897	0.06107	1.43829
		LV01-141	19.46505	21.47246	2.00741	21.47216	0.00030	21.36477	0.10739	0.01494	5.34968
		LV01-142	15.54795	17.55257	2.00462	17.55176	0.00081	17.49175	0.06001	0.04041	2.99358
	quartz porphyries from area I	LV01-122	19.46504	21.47149	2.00645	21.47085	0.00064	21.44805	0.02280	0.03190	1.13634
		LV01-125A	10.68389	12.68177	1.99788	12.68101	0.00076	12.64193	0.03908	0.03804	1.95607
		LV01-125B	11.74286	13.74482	2.00196	13.74393	0.00089	13.71589	0.02804	0.04446	1.40063
		LV01-127	11.86793	13.86731	1.99938	13.86635	0.00096	13.83595	0.03040	0.04801	1.52047
		LV01-127C	10.86568	12.88766	2.02198	12.88688	0.00078	12.85195	0.03493	0.03858	1.72751
		LV01-129	12.72418	14.72774	2.00356	14.72736	0.00038	14.69644	0.03092	0.01897	1.54325
	felsic lavas from area I	LV01-124C	12.72884	14.72940	2.00056	14.72888	0.00052	14.71997	0.00891	0.02599	0.44538
		LV01-128A	10.86266	12.86792	2.00526	12.86621	0.00171	12.80773	0.05848	0.08528	2.91633
	felsic lavas from area II	LV01-23	12.72936	14.78074	2.05138	14.77973	0.00101	14.73612	0.04361	0.04924	2.12589
		LV01-144A	11.19051	13.19276	2.00225	13.19009	0.00267	13.12309	0.06700	0.13335	3.34624
Stolzburg Pluton		LV01-131A	12.85394	14.85698	2.00304	14.85659	0.00039	14.85372	0.00287	0.01947	0.14328
		LV01-131B	12.72869	14.73061	2.00192	14.73029	0.00032	14.72854	0.00175	0.01598	0.08742
		LV01-132	12.83124	14.83774	2.00650	14.83599	0.00175	14.82659	0.00940	0.08722	0.46848
mafic groups	(ultra-)mafic rocks	LV01-56	11.86796	13.79856	1.93060	13.79855	0.00001	13.69172	0.10683	0.00052	5.53351
		LV01-68	10.61119	12.63913	2.02794	12.63552	0.00361	12.52216	0.11336	0.17801	5.58991
		LV01-82	10.68401	12.66036	1.97635	12.65875	0.00161	12.56912	0.08963	0.08146	4.53513
		LV01-94	12.05640	14.10123	2.04483	14.10101	0.00022	14.06118	0.03983	0.01076	1.94784
		LV01-124A	12.85418	14.85841	2.00423	14.85785	0.00056	14.78505	0.07280	0.02794	3.63232
		LV01-124D	11.19064	13.20036	2.00972	13.19918	0.00118	13.14411	0.05507	0.05871	2.74018
		LV01-128C	12.05631	14.05630	1.99999	14.05341	0.00289	13.95212	0.10129	0.14450	5.06453
		LV01-143	11.74279	13.74944	2.00665	13.74888	0.00056	13.70726	0.04162	0.02791	2.07410
	silicified basalts	LV01-47	12.85439	14.85909	2.00470	14.85745	0.00164	14.82555	0.03190	0.08181	1.59126
		LV01-48A	11.19073	13.27436	2.08363	13.27352	0.00084	13.21173	0.06179	0.04031	2.96550
		LV01-49	10.86289	12.89072	2.02783	12.88993	0.00079	12.82735	0.06258	0.03896	3.08606
		LV01-100B	19.46554	21.42545	1.95991	21.42529	0.00016	21.38428	0.04101	0.00816	2.09244
		LV01-100D	15.54782	17.54499	1.99717	17.54480	0.00019	17.45434	0.09046	0.00951	4.52941
		LV01-100E	17.34366	19.33947	1.99581	19.33873	0.00074	19.28276	0.05597	0.03708	2.80438
cherts	sedimentary	LV01-62	11.74302	13.73695	1.99393	13.73656	0.00039	13.73411	0.00245	0.01956	0.12287
		LV01-128B	10.61106	12.61624	2.00518	12.61584	0.00040	12.61337	0.00247	0.01995	0.12318
	massive	LV01-97	10.86573	12.86129	1.99556	12.86113	0.00016	12.85961	0.00152	0.00802	0.07617
		LV01-133C	9.58590	11.58924	2.00334	11.58870	0.00054	11.58706	0.00164	0.02695	0.08186
pyroxene/amphibole porphyries		W01-3	12.72429	14.72846	2.00417	14.72750	0.00096	14.69330	0.03420	0.04790	1.70644
		SV01-1	10.86558	12.86656	2.00098	12.85988	0.00668	12.73019	0.12969	0.33384	6.48132
		SV01-3	10.61124	12.61198	2.00074	12.61145	0.00053	12.53559	0.07586	0.02649	3.79160
		SV01-46	12.83139	14.84167	2.01028	14.83720	0.00447	14.76955	0.06765	0.22236	3.36520
others		LV01-102	9.58614	11.57280	1.98666	11.57168	0.00112	11.54492	0.02676	0.05638	1.34698
		SV01-35	10.68393	12.69473	2.01080	12.69399	0.00074	12.55344	0.14055	0.03680	6.98976
		SV01-39	11.86785	13.87034	2.00249	13.87030	0.00004	13.74284	0.12746	0.00200	6.36508

Appendix B
Table 3b: Results of the XRF analyses

	shallow intrusives from area I		*consolidated ash or tuff from area I*	*interlocking felsic rocks from area II*				*quartz porphyries from area I*					
	LV01-140	LV01-ON99T1	LV01-109B	LV01-11	LV01-13B	LV01-141	LV01-142	LV01-122	LV01-125A	LV01-125B	LV01-127	LV01-127C	LV01-129
SiO2	69.543	72.207	73.038	71.590	72.091	67.295	73.479	74.354	78.535	85.093	83.983	81.086	82.974
TiO2	0.215	0.225	0.240	0.245	0.232	0.208	1.054	0.204	0.197	0.144	0.140	0.156	0.151
Al2O3	14.386	14.076	15.794	14.869	14.993	14.017	8.798	13.381	13.860	10.172	10.642	11.877	10.859
Fe2O3	2.292	1.805	1.331	2.008	2.128	1.448	8.740	0.889	1.176	0.463	0.571	1.483	1.014
MnO	0.029	0.031	0.002	0.017	0.023	0.035	0.106	0.013	0.005	0.002	0.009	0.024	0.006
MgO	1.473	1.560	0.851	0.921	1.369	1.618	3.237	0.494	0.284	0.187	0.345	0.393	0.345
CaO	2.918	0.873	<0.05	1.792	1.044	3.776	<0.01	<0.02	<0.08	<0.07	<0.04	<0.07	<0.07
Na2O	3.418	5.895	0.059	6.259	6.177	0.710	<0.02	0.059	0.029	0.049	0.138	0.098	0.069
K2O	2.486	2.018	7.100	0.945	1.102	5.567	1.692	8.638	4.684	3.253	3.366	3.350	3.804
P2O5	0.066	0.068	0.076	0.083	0.072	0.066	0.082	0.051	0.010	0.008	0.044	0.043	0.005
SO3	0.013	0.009	<0.007	<0.009	<0.004	0.131	0.022	<0.028	<0.02	<0.006	<0.003	<0.007	<0.002
NiO	0.006	0.001	0.004	0.002	0.003	0.002	0.074	0.002	0.001	<0.001	0.001	0.002	0.001
Cr2O3	0.009	0.003	0.003	0.002	0.006	0.002	0.625	0.005	0.003	0.003	0.001	0.001	<0.001
H2O-	0.044	0.021	0.066	0.109	0.061	0.015	0.059	0.032	0.038	0.044	0.048	0.039	0.019
LOI	3.684	1.898	2.094	1.959	1.438	5.350	2.740	1.136	1.956	1.401	1.520	1.728	1.543
Total	100.582	100.690	100.658	100.801	100.739	100.241	100.709	99.259	100.779	100.819	100.807	100.280	100.789
Mo	<0.65	<0.63	<0.65	0.7	<0.61	<0.66	0.69	<0.66	<0.63	0.71	<0.61	0.86	<0.62
Nb	5.59	5.4	6.25	5.4	4.97	4.8	5.03	5.33	4.99	3.15	2.85	3.26	2.92
Zr	124.63	133.07	154.34	128.68	126.59	112.96	118.3	121.67	121.94	77.05	73.82	81.27	78.17
Y	9.13	5.65	6.04	5.63	5.57	4.13	4.32	5.33	5.81	5.44	4.25	3.09	3.15
Sr	119.79	64.77	5.58	382.37	284.51	53.72	30.7	8.67	6.52	6.99	9.15	19.34	4.18
U	<1.43	1.55	<1.45	<1.35	<1.35	1.93	<1.48	<1.47	<1.38	<1.33	<1.34	1.87	1.52
Rb	68.3	41.32	169.45	21.04	26.89	115.63	151.48	166.87	102.75	71.88	79.68	82.69	88.45
Th	5.54	4.78	4.96	4.32	4.23	4.81	3.72	3.34	4.55	2.45	3.16	3.62	2.78
Pb	4.68	16.69	2.7	9.01	6.74	4.6	3.11	4.57	2.46	2.52	2.47	4.46	2.17
Zn	48.32	63.81	29.57	19.59	14.1	17.82	14.83	10.51	14.99	3.96	8.71	20.41	24.26
Cu	77.17	9.42	11.4	1.7	1.8	5.48	2.69	2.9	2.91	2.67	3.76	7.06	4.92
Ni	28.03	48.78	35.48	23.79	24.65	17.22	14.88	15.71	18.39	9.73	7.57	20.29	43.5
Co	3.75	4.58	2.04	4.44	4.81	2.81	2.98	1.38	<1.31	<1.22	<1.2	<1.36	<1.28
Mn	193.88	286.3	11.48	128.47	158.95	255.8	248.05	86.01	35.58	22.19	62.86	188.42	30.13
Cr	24.1	36.88	25.43	24.45	28.62	21.81	22.03	28.23	23.81	19.87	17.99	18.67	18.61
V	6.18	8.56	8.16	8.71	8.76	6.6	7.14	6.8	6.87	8.46	6.79	7.28	4.73

Concentrations of the major elements are given in wt%.
Concentrations of minor and trace elements are given in ppm.

Appendix B
Table 3b: Results of the XRF analyses

	felsic lavas from area I		*felsic lavas from area II*		*Stolzburg Pluton*			*(ultra-)mafic rocks*							
	LV01-124C	LV01-128A	LV01-23	LV01-144A	LV01-131A	LV01-131B	LV01-132	LV01-56	LV01-68	LV01-82	LV01-94	LV01-124A	LV01-124D	LV01-128C	LV01-143
SiO2	95.161	73.089	74.833	72.051	75.716	75.732	73.312	44.113	46.092	52.957	51.472	56.967	45.562	49.470	48.977
TiO2	0.150	1.120	0.225	0.250	0.068	0.097	0.164	1.605	0.895	1.946	0.798	1.234	1.309	2.064	1.359
Al2O3	2.488	12.720	15.203	17.144	13.817	13.236	15.325	14.865	6.136	16.511	13.444	15.265	18.331	15.656	13.111
Fe2O3	0.916	5.812	1.810	1.929	0.909	1.259	1.233	24.233	12.819	15.729	13.003	14.928	20.629	20.831	13.873
MnO	0.012	0.033	0.012	0.082	0.013	0.012	0.023	0.115	0.224	0.072	0.175	0.469	0.071	0.139	0.216
MgO	0.239	2.076	0.489	1.194	0.100	0.250	0.209	7.045	17.400	4.521	6.501	2.581	7.397	4.729	6.391
CaO	<0.03	<0.07	<0.05	<0.03	1.398	0.539	1.551	0.161	10.057	0.019	8.796	0.154	0.145	<0.08	9.654
Na2O	<0.02	0.039	0.039	0.020	4.573	2.807	5.300	<0.02	0.396	0.057	3.952	<0.02	0.029	<0.02	2.916
K2O	0.902	2.626	5.560	5.587	3.148	6.389	2.599	0.495	0.118	3.365	0.339	3.391	1.707	1.364	0.530
P2O5	0.025	0.012	0.059	0.036	0.015	0.012	0.044	0.185	0.094	0.166	0.082	0.178	0.895	0.102	0.130
SO3	<0.021	0.004	<0.008	0.002	0.005	0.023	<0.008	0.105	0.014	0.009	0.036	0.148	0.008	0.003	0.026
NiO	0.001	0.048	0.001	0.063	0.001	0.007	0.001	0.300	0.100	0.014	0.276	0.091	0.015	0.027	0.011
Cr2O3	0.014	0.325	0.001	0.048	0.002	0.021	<0.001	0.765	0.336	0.016	0.165	0.097	0.013	0.012	0.018
H2O-	0.026	0.085	0.049	0.028	0.019	0.016	0.087	0.001	0.178	0.081	0.011	0.028	0.040	0.145	0.133
LOI	0.445	2.916	2.126	2.074	0.143	0.087	0.468	5.534	5.590	4.535	1.948	3.632	2.994	5.065	3.346
Total	100.379	100.904	100.407	100.507	99.927	100.488	100.316	99.521	100.450	99.999	100.998	99.163	99.143	99.607	100.693
Mo	1.52	0.81	0.79	<0.65	0.95	<0.65	0.94	<0.91	<0.8	<0.81	<0.84	<0.85	1.58	<0.9	<0.87
Nb	1.19	6.31	4.95	5.52	2.08	2.21	2.55	7.17	4.07	5.69	2.11	5.94	4.18	5.77	5.71
Zr	16.94	102.54	119.6	140.81	43.05	18.97	94.9	100.8	63.62	128.65	50.59	113.8	68.71	132.89	87.75
Y	3.57	11.13	6.93	8.15	1.12	<0.92	2.22	23.15	19.63	40.27	20.75	22.79	8.78	36.48	64.26
Sr	5.24	11.3	19.32	18.43	454.78	293.71	550.31	5.51	59.54	16.92	151.1	4.26	4.23	14.54	192.35
U	<1.31	<1.57	<1.39	1.62	<1.42	1.62	<1.42	<2.09	<1.81	<1.84	<1.9	<1.93	<1.67	<2.05	<1.98
Rb	21.67	68.53	113.6	129.87	52.21	109.15	69.57	13.25	7.49	88.23	6.97	83.85	41.96	36.75	8.38
Th	<1.38	<1.64	4.13	4.9	<1.47	5.78	2.08	<2.2	<1.9	<1.94	<1.99	<2.03	<1.76	<2.15	<2.06
Pb	<1.77	2.5	2.22	5.22	10.08	17.67	14.28	<2.83	7.1	2.57	<2.56	<2.62	<2.27	<2.78	<2.65
Zn	31.06	53.19	16.97	31.38	15.39	8.78	39.82	190.67	113.27	77.77	105.57	96.3	66.14	63.96	126.28
Cu	6.82	50.08	2.21	1.93	1.88	1.39	2.45	199.49	58.95	20.52	135.75	56.46	70.31	35.28	101.2
Ni	52.35	303.2	13.18	28.34	3.23	1.55	3.11	2025.73	137.88	114.55	146.74	456.79	396.82	107.04	111.19
Co	4.77	36.62	<1.47	6.01	<1.25	<1.16	<1.4	224.61	43.82	4.46	43.29	172.05	91.16	35.71	42.43
Mn	79.41	230.19	79.25	620.54	88.4	54.98	157.76	789.87	600.45	46.32	1165.97	3556.74	756.95	972.66	1282.43
Cr	135.39	2613.88	25.76	27.45	11.87	6.47	12.21	7355.31	143.54	26.6	97.03	903.12	4994.41	89.98	114.2
V	27.6	187.14	8.76	8.27	<1.36	<1.3	3.22	333.26	450	3.02	172.18	230.98	274.06	433.69	151.84

Concentrations of the major elements are given in wt%.
Concentrations of minor and trace elements are given in ppm.

Appendix B
Table 3b: Results of the XRF analyses

	silicified basalts						*cherts*				*px/amph porphyries*				*others*		
							sedimentary		massive								
	LV01-47	LV01-48A	LV01-49	LV01-100B	LV01-100D	LV01-100E	LV01-62	LV01-128B	LV01-97	LV01-133C	W01-3	SV01-3	SV01-35	SV01-46	LV01-102	SV01-35	SV01-39
SiO2	80.545	73.553	66.575	76.042	56.675	68.798	98.739	99.948	99.636	98.553	69.726	61.624	40.843	65.814	84.509	40.843	23.915
TiO2	1.541	0.793	1.553	1.663	2.002	1.940	0.014	0.006	0.002	0.023	0.218	0.633	0.320	0.725	0.989	0.320	0.613
Al2O3	11.466	7.439	11.424	12.915	13.422	14.994	0.330	0.120	0.130	0.629	14.975	15.055	3.803	17.319	8.361	3.803	21.238
Fe2O3	0.610	10.591	13.614	2.340	14.987	5.607	0.659	0.429	0.420	0.979	2.122	13.689	13.593	5.728	0.956	13.593	42.045
MnO	0.008	0.053	0.075	0.024	0.111	0.083	0.005	0.004	0.006	0.008	0.019	0.044	0.210	0.080	0.008	0.210	0.449
MgO	0.128	3.598	2.384	1.077	6.234	1.594	<0.05	<0.07	<0.07	<0.04	1.651	3.184	28.348	2.498	0.325	28.348	4.184
CaO	0.521	<0.05	0.446	0.274	0.191	0.010	<0.07	<0.08	<0.08	<0.08	<0.05	<0.04	4.388	<0.06	<0.07	4.388	<0.03
Na2O	0.177	<0.03	0.087	0.059	<0.04	0.019	0.010	<0.06	<0.04	<0.11	0.098	0.106	0.232	0.029	0.039	0.232	<0.02
K2O	3.276	0.135	0.857	4.046	1.613	4.442	0.115	0.052	0.072	0.211	10.214	2.201	0.201	4.626	2.720	0.201	0.007
P2O5	0.443	0.008	0.412	0.274	0.202	0.155	0.003	0.003	0.002	0.003	0.070	0.018	0.032	0.084	0.012	0.032	0.036
SO3	<0.001	0.045	0.035	0.004	<0.003	<0.006	<0.011	<0.008	<0.003	<0.008	<0.011	0.001	<0.002	0.001	<0.004	<0.002	0.022
NiO	0.001	0.075	0.004	0.012	0.007	0.009	0.005	<0.001	<0.001	0.013	0.005	0.028	0.208	0.004	0.004	0.208	0.075
Cr2O3	<0.001	0.384	<0.001	0.009	0.010	0.009	0.004	0.004	0.001	0.013	0.005	0.003	0.801	0.009	0.846	0.801	0.535
H2O-	0.082	0.040	0.039	0.008	0.010	0.037	0.020	0.020	0.008	0.027	0.048	0.026	0.037	0.222	0.056	0.037	0.002
LOI	1.591	2.965	3.086	2.092	4.529	2.804	0.123	0.123	0.076	0.082	1.706	3.792	6.990	3.365	1.347	6.990	6.365
Total	100.388	99.679	100.589	100.839	99.992	100.499	100.026	100.709	100.353	100.541	100.857	100.404	100.006	100.503	100.174	100.006	99.486
Mo	<0.61	<0.73	<0.77	0.81	<0.82	<0.72	1.55	1.5	<0.59	2.31	0.91	<0.81	<0.8	<0.71	0.85	<0.8	<1.12
Nb	8.34	3.54	7.96	5.14	5.46	5.52	<0.53	<0.55	<0.55	0.74	5.31	8.24	1.02	9.33	3.34	1.02	4.74
Zr	203.86	51.67	189.91	121.84	132.42	140.91	3.59	2.54	1.97	4.74	135.55	163.52	17.65	190.26	48.94	17.65	85.27
Y	54.63	11.87	57.25	59.75	27.59	35.95	0.76	<0.64	<0.63	0.78	16.84	17.2	6.24	13.85	17.11	6.24	11.9
Sr	6.62	5.48	10.05	5.31	7.35	9.12	0.95	1.12	<0.59	1.37	34.18	20.86	5.56	14.44	15.64	5.56	2.28
U	<1.33	<1.63	<1.75	<1.46	<1.86	<1.6	<1.25	<1.27	<1.28	<1.31	2.19	<1.81	<1.81	<1.56	<1.38	<1.81	<2.58
Rb	72.76	3.24	19.86	89.43	45.72	116.1	2.13	1.35	0.87	4.72	158.67	59.15	5.19	119.71	88.33	5.19	<1.24
Th	1.71	<1.72	<1.84	<1.54	<1.95	<1.68	<1.31	<1.34	<1.34	<1.37	4.28	4.35	<1.9	3.64	<1.46	<1.9	3.81
Pb	<1.81	2.46	<2.38	<1.98	5.6	2.61	<1.7	2.67	2.43	4.28	7.07	2.45	2.86	<2.11	2.67	2.86	12.02
Zn	14.92	100.31	110.46	18.73	111.5	122.35	50.6	1.5	1.16	204.59	142.43	60.15	101.32	43.94	111.38	101.32	56.36
Cu	13.52	18.93	11.28	18.8	30.46	73.64	62.04	4.24	4.83	58.45	14.95	7.02	73.31	14.94	11.52	73.31	43.84
Ni	18	438.45	38.24	81.92	47.79	97.99	454.45	9.81	5.14	99.18	141.29	68.87	1982.14	30.47	44.69	1982.14	397.32
Co	5.03	37.47	17.64	26.62	34.95	28.85	71.98	<1.21	<1.35	15.7	3.31	<3.07	123.73	<2.21	11.76	123.73	135.14
Mn	42.96	420.55	507.87	139.93	886.64	585.09	1429.5	29.43	29.91	65.45	104.96	376.05	1460.07	663.95	19.77	1460.07	3207.43
Cr	8.37	3451.7	7.93	50.75	61.06	65.73	2458.51	18.4	13.51	81.14	26.47	28.46	5317.38	39.8	6520.36	5317.38	5336.96
V	6.78	158.64	7.96	293.57	405.24	341.26	127.91	2.93	<1.15	4.54	5.56	55.24	80.25	57.66	181.21	80.25	286.82

Concentrations of the major elements are given in wt%.
Concentrations of minor and trace elements are given in ppm.

Appendix B
Table 3c: Results of the ICP-MS analyses

	shallow intusives from area I		*consolidated ash or tuff from area I*	*interlocking felsic rocks from area II*				*quartz porphyries from area I*					
	LV01-140	LV01-ON99T1	LV01-109B	LV01-11	LV01-13B	LV01-141	LV01-142	LV01-122	LV01-125A	LV01-125B	LV01-127	LV01-127C	LV01-129
Ga	22.9	23	18.4	21.4	19.8	21.8	22	15.6	17	13.8	13.2	16.3	13.1
Rb	58.4	39.8	150	16.2	22	116	143	160	99.3	71.9	78.2	80.8	86.1
Sr	95.1	55.5	3.89	279	191	53.3	26	6.17	3.3	5.71	6.75	15.7	1.71
Y	7.29	4.81	3.28	2.86	3.01	4.36	3.68	2.89	3.49	4.14	3.5	2.48	2.15
Zr	111	123	134	121	113	93.8	95.5	120	114	71	66.2	61.9	63
Nb	5.24	4.98	5.28	5.2	4.8	4.35	4.39	4.41	4.66	3.01	2.57	3.05	2.74
Cs	1.71	1.24	3.18	0.47	0.82	2.51	5.67	2.38	1.86	1.24	2.02	1.51	2.83
Ba	314	294	64.4	247	175	247	314	131	92.7	83.6	102	172	61.9
La	15.4	14.8	13.2	6.6	5.61	14.6	12	10.2	12.7	6.49	8.78	8.59	8.52
Ce	24.7	25.9	23.5	15.2	12.4	27.2	23.3	19.3	23.9	11.5	16.5	16.5	15.4
Pr	2.82	2.87	2.44	1.59	1.34	2.88	2.4	1.93	2.23	1.15	1.76	1.74	1.52
Nd	10.7	11	9.09	6.23	5.57	10.5	8.87	7.22	8.25	4.15	6.64	6.49	5.46
Sm	1.81	1.84	1.49	1.1	1.08	1.77	1.54	1.1	1.36	0.74	1.21	1.16	0.87
Eu	0.58	0.52	0.43	0.35	0.38	0.53	0.49	0.29	0.49	0.29	0.39	0.34	0.29
Gd	1.7	1.34	1.03	0.85	0.91	1.33	1.2	0.81	1.01	0.69	0.95	0.89	0.65
Tb	0.21	0.18	0.13	0.12	0.12	0.17	0.15	0.11	0.14	0.11	0.13	0.12	0.08
Dy	1.17	0.93	0.67	0.61	0.58	0.88	0.78	0.56	0.73	0.67	0.74	0.59	0.47
Ho	0.23	0.17	0.12	0.12	0.12	0.16	0.14	0.1	0.15	0.14	0.15	0.11	0.08
Er	0.66	0.48	0.36	0.33	0.34	0.43	0.37	0.29	0.39	0.43	0.43	0.29	0.24
Tm	0.09	0.07	0.05	0.05	0.05	0.06	0.05	0.04	0.06	0.06	0.06	0.04	0.03
Yb	0.61	0.45	0.35	0.33	0.32	0.39	0.35	0.29	0.38	0.44	0.41	0.24	0.22
Lu	0.1	0.06	0.05	0.04	0.05	0.06	0.05	0.04	0.05	0.07	0.06	0.03	0.04
Hf	2.77	3.05	3.31	3	2.8	2.38	2.5	2.95	2.88	1.71	1.69	1.6	1.6
Ta	0.6	0.55	0.6	0.52	0.53	0.51	0.51	0.45	0.53	0.35	0.29	0.35	0.27
Pb	3.94	70.6	1.58	10.3	5.63	4.19	2.77	4.98	3.61	1.61	1.6	4.23	1.69
Th	3.78	3.37	3.2	2.41	2.27	3.92	3.67	2.6	3.44	2.27	2.21	2.31	2.12
U	1.17	1	1.31	0.99	0.88	1.45	1.27	1.22	1.28	0.82	0.76	1	0.71
Sc	--	--	--	--	--	--	--	--	--	--	--	--	--
V	--	--	--	--	--	--	--	--	--	--	--	--	--
Cr	--	--	--	--	--	--	--	--	--	--	--	--	--
Co	--	--	--	--	--	--	--	--	--	--	--	--	--
Ni	--	--	--	--	--	--	--	--	--	--	--	--	--
Cu	--	--	--	--	--	--	--	--	--	--	--	--	--

All concentrations are give in ppm.
-- = not determined

Appendix B
Table 3c: Results of the ICP-MS analyses

	felsic lavas from area I		*felsic lavas from area II*		*Stolzburg Pluton*			*(ultra-) mafic rocks*							
	LV01-124C	LV01-128A	LV01-23	LV01-144A	LV01-131A	LV01-131B	LV01-132	LV01-56	LV01-68	LV01-82	LV01-94	LV01-124A	LV01-124D	LV01-128C	LV01-143
Ga	5.15	21.5	17.6	19.8	40.7	43.4	27.7	--	10.4	24.7	14.3	21.1	22.8	22.6	--
Rb	21	67	108	121	49.6	104	59.9	9.67	7.65	83.8	6.87	81.7	43.2	31	6.42
Sr	4.98	8.04	9.61	10.1	416	255	452	5.22	63.3	12.7	0	2.75	3.92	8.6	173
Y	3.42	8.08	2.14	3.86	1.31	1.1	1.75	9.32	17.3	25	18.6	9.34	8.23	24.2	53.3
Zr	15	92.1	116	119	31.9	16.6	78.4	99.9	66.4	129	0	113	65.5	131	79.6
Nb	0.79	5.86	4.37	4.86	1.99	2.16	2.47	8.05	4.18	5.91	2.31	6.48	3.88	5.98	6.4
Cs	0.35	1.45	2.03	2.37	1.03	1.39	1.09	0.21	1.53	2.15	0.25	1.38	0.99	0.65	0.32
Ba	103	342	121	192	1288	1414	471	48.9	34.7	158	22.7	230	306	70.9	133
La	5.05	8.45	9.89	17.1	2.77	13.7	9.38	4.24	5.05	6.85	2.42	2.23	3.52	3.71	7.05
Ce	4.36	20.6	21.4	22.1	5.33	27.2	19.4	13.6	12.7	20.5	7.01	9.53	9.83	12.2	16.8
Pr	1.48	2.65	1.98	3.13	0.59	2.71	2.04	1.7	1.96	2.83	1.06	1.04	1.33	1.5	2.66
Nd	6.95	12.3	7.21	11	2.33	9.13	7.89	8.12	9.92	14.4	5.67	5.25	6.47	7.69	13.9
Sm	1.5	2.84	1.11	1.86	0.51	1.2	1.27	2.18	2.67	4.08	1.81	1.5	1.77	2.25	4.23
Eu	0.43	0.83	0.3	0.5	0.28	0.35	0.42	0.76	0.95	1.39	0.68	0.39	0.5	0.74	1.47
Gd	1.52	2.14	0.75	1.41	0.33	0.58	0.88	2.36	3.16	4.98	2.54	1.89	2.11	3.39	6.85
Tb	0.2	0.28	0.09	0.18	0.05	0.06	0.09	0.36	0.49	0.79	0.44	0.31	0.33	0.59	1.07
Dy	1.07	1.74	0.44	0.85	0.23	0.21	0.43	2.29	3.1	5.08	3.16	2.11	2.03	4.21	7.23
Ho	0.17	0.36	0.08	0.16	0.04	0.04	0.07	0.46	0.61	1.05	0.68	0.45	0.4	0.96	1.57
Er	0.43	1.03	0.21	0.37	0.14	0.11	0.14	1.29	1.68	3.03	2.05	1.33	1.12	2.9	4.34
Tm	0.05	0.15	0.03	0.05	0.02	0.01	0.02	0.18	0.23	0.44	0.3	0.19	0.16	0.42	0.56
Yb	0.34	1	0.21	0.33	0.11	0.09	0.14	1.21	1.41	2.8	1.99	1.24	1.06	2.72	3.38
Lu	0.05	0.15	0.03	0.04	0.02	0.01	0.02	0.18	0.21	0.42	0.3	0.18	0.16	0.41	0.52
Hf	0.37	2.31	2.93	3.06	0.96	0.85	2.07	2.53	1.57	3.17	1.16	2.56	1.74	3.18	2.08
Ta	0.07	0.47	0.39	0.51	0.28	0.35	0.25	0.9	0.34	0.4	0.18	0.42	0.27	0.4	0.84
Pb	0.83	2.19	0.94	3.61	9.25	16.1	13.35	1.45	6.1	0.58	0.6	2.97	1.16	1.39	0.91
Th	0.27	1.06	2.26	3.53	1.32	4.08	1.6	0.36	0.46	0.53	0.19	0.28	0.43	0.52	0.5
U	0.16	0.32	1.27	1.31	0.53	0.78	0.67	0.19	0.13	0.14	0.05	0.14	0.26	0.14	0.14
Sc	--	--	--	--	--	--	--	27.6	--	--	--	--	--	--	31.1
V	--	--	--	--	--	--	--	420	--	--	--	--	--	--	312
Cr	--	--	--	--	--	--	--	5443	--	--	--	--	--	--	116
Co	--	--	--	--	--	--	--	256	--	--	--	--	--	--	52.8
Ni	--	--	--	--	--	--	--	2326	--	--	--	--	--	--	89.5
Cu	--	--	--	--	--	--	--	316	--	--	--	--	--	--	96.8

All concentrations are give in ppm.
-- = not determined

Appendix B
Table 3c: Results of the ICP-MS analyses

	silicified basalts						*cherts*				*px/amph porphyries*				*others*		
							sedimentary		massive								
	LV01-47	LV01-48A	LV01-49	LV01-100B	LV01-100D	LV01-100E	LV01-62	LV01-128B	LV01-97	LV01-133C	W01-3	SV01-1	SV01-3	SV01-46	LV01-102	SV01-35	SV01-39
Ga	18.6	16	20.3	18.2	20.8	24.7	1.15	22.6	0.67	2.33	19.4	32.6	19.9	23.5	22.4	5.66	19.4
Rb	69	3.09	20.7	89.9	39.8	108	2.38	31	1.33	4.73	142	32.9	50.6	114	90.9	5.45	0.03
Sr	4.88	5.42	9.94	3.6	6.63	6.72	0.94	8.6	0.46	1.6	27.5	259	4.44	5.2	11.2	6.01	1.08
Y	38.8	9.53	42	28.6	17.4	15.9	0.55	24.2	0.21	0.52	7.78	34.5	7.45	7.35	11.5	6.01	3.63
Zr	186	49.3	183	113	128	131	3.23	131	1.88	4.04	129	346	152	173	45.6	17.9	88.6
Nb	6.36	3.52	7.81	3.68	5.81	5.67	0.34	5.98	0.09	0.4	5.25	35.4	7.96	8.79	2.31	0.57	4.82
Cs	1.7	0.17	0.79	1.41	0.84	2	0.12	0.65	0.05	0.16	1.62	0.62	1	1.74	2.85	1.52	0.01
Ba	105	44.6	41.5	128	107	202	15.8	70.9	9.37	23.8	219	648	69.1	140	176	5.64	1.1
La	8	9.37	8.71	7.59	3.15	4.05	1.11	3.71	0.25	1.27	27.7	299	18.8	23	3.93	0.75	1.65
Ce	23.9	21.5	25.7	23.4	11.2	15.1	2.11	12.2	0.41	2.61	25.8	616	43	55	8.77	2.01	3.88
Pr	3.58	2.8	3.68	3.39	1.4	1.84	0.22	1.5	0.05	0.29	5.98	67.7	5	6.32	1.27	0.3	0.36
Nd	18.7	12.7	19.1	17.5	7.35	9.63	0.82	7.69	0.18	1.08	22.6	246	19.9	27	6.6	1.74	1.36
Sm	5.54	2.52	5.59	4.7	2.29	2.8	0.11	2.25	0.04	0.2	3.64	32.2	3.19	4.91	1.82	0.65	0.38
Eu	1.63	0.74	1.98	1.55	0.71	0.9	0.03	0.74	0.01	0.04	0.91	6.98	0.85	1.07	0.71	0.29	0.17
Gd	7.33	1.91	7.13	5.71	3.06	3.41	0.07	3.39	0.04	0.12	2.71	19.2	2.27	3.73	1.79	0.94	0.59
Tb	1.19	0.28	1.18	0.96	0.5	0.55	0.01	0.59	0.01	0.02	0.32	2.11	0.3	0.42	0.29	0.16	0.11
Dy	7.99	1.83	8.15	6.32	3.39	3.64	0.09	4.21	0.04	0.1	1.63	8.58	1.65	1.99	2.08	1.08	0.8
Ho	1.63	0.42	1.74	1.28	0.75	0.76	0.02	0.96	0.01	0.02	0.29	1.35	0.3	0.3	0.46	0.22	0.19
Er	4.61	1.26	5.14	3.35	2.3	2.19	0.07	2.9	0.02	0.07	0.78	3.34	0.87	0.71	1.43	0.64	0.67
Tm	0.63	0.2	0.76	0.42	0.35	0.32	0.01	0.42	0	0.01	0.1	0.38	0.12	0.08	0.22	0.09	0.11
Yb	3.87	1.38	5.06	2.47	2.38	2.13	0.09	2.72	0.02	0.08	0.62	2.13	0.8	0.47	1.41	0.56	0.83
Lu	0.57	0.22	0.78	0.32	0.38	0.31	0.02	0.41	0	0.01	0.09	0.28	0.12	0.06	0.21	0.08	0.13
Hf	4.67	1.29	4.67	2.78	3.14	3.23	0.07	3.18	0.03	0.1	2.99	5.75	3.6	4.03	1.19	0.46	2.12
Ta	0.4	0.27	0.54	0.22	0.39	0.38	0.03	0.4	0.01	0.04	0.52	1.05	0.5	0.54	0.17	0.06	0.36
Pb	1.13	4.8	3.04	0.46	3.83	0.72	0.67	1.39	2.07	4.44	5.51	16.55	1.01	1.36	2.4	2.72	12
Th	0.77	0.31	0.8	0.4	0.46	0.46	0.28	0.52	0.07	0.32	2.63	16.33	2.35	3.13	0.27	0.05	1.25
U	0.21	0.2	0.17	0.22	0.14	0.16	0.18	0.14	0.26	0.15	1.15	3.08	0.76	0.92	0.42	0.02	0.55
Sc	--	--	--	--	--	--	--	--	--	--	--	--	--	--	--	--	--
V	--	--	--	--	--	--	--	--	--	--	--	--	--	--	--	--	--
Cr	--	--	--	--	--	--	--	--	--	--	--	--	--	--	--	--	--
Co	--	--	--	--	--	--	--	--	--	--	--	--	--	--	--	--	--
Ni	--	--	--	--	--	--	--	--	--	--	--	--	--	--	--	--	--
Cu	--	--	--	--	--	--	--	--	--	--	--	--	--	--	--	--	--

All concentrations are give in ppm.
-- = not determined

Appendix C: XRF versus ICP-MS

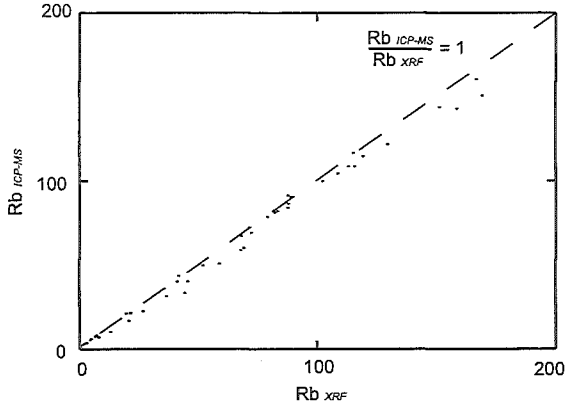

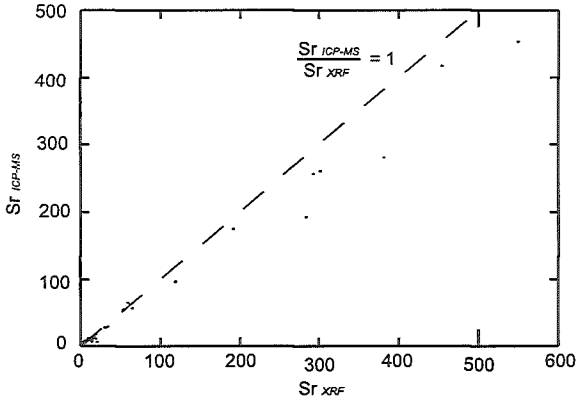

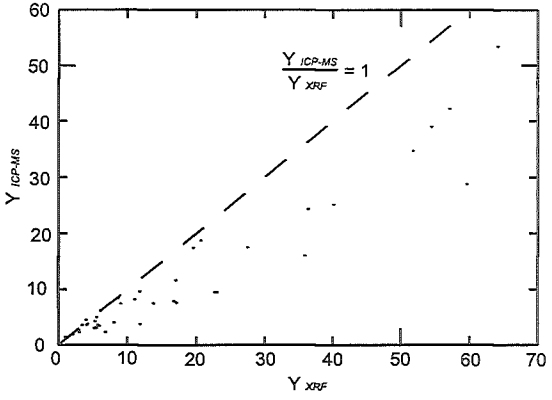

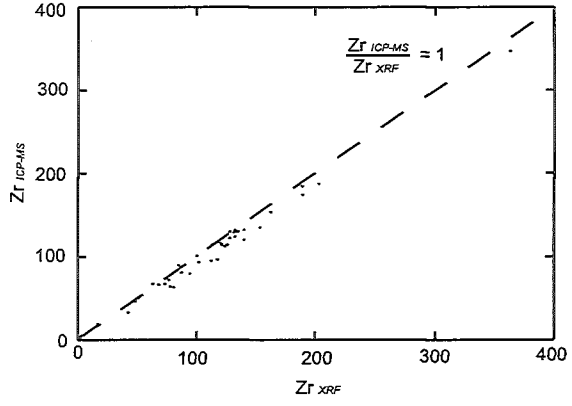

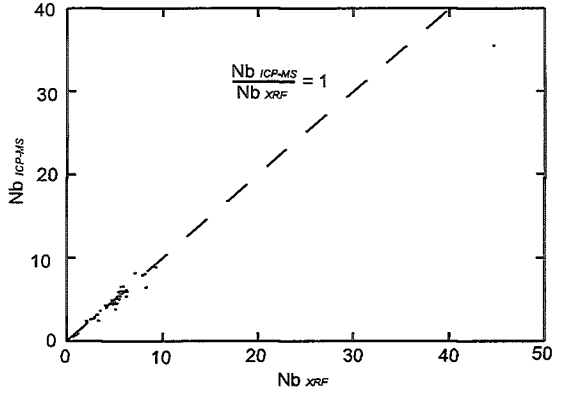

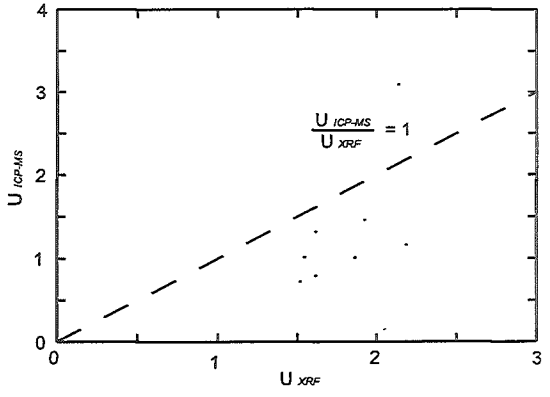

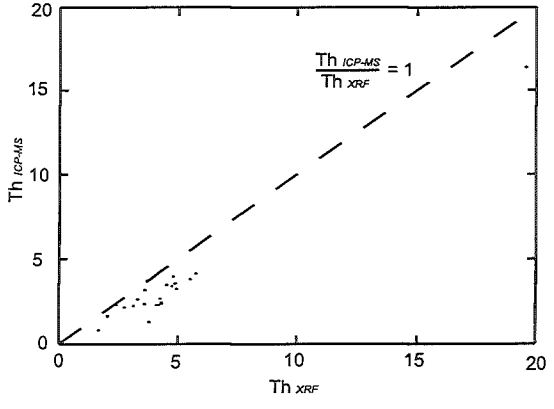

In all cases the element ICP-MS/element XRF ratio is equal to or below 1. Nice linear trends exist for Rb, Sr, Zr, and Nb with ratios ~1. For Y the scattering is the most variable with ratios between 0.3 and 1. U (ratios between 0.5 and 1) and Th (mean ratio 0.75) levels are below detection limit of the XRF for most or many of the samples. Their trends in the diagrams above are less reliable but also show that in general the method of XRF indicates lower concentrations of trace elements relative to the XRF method.

Accuracy of both methods is dependant on calibration of the instruments against rock reference materials (a.o. Hawaiian basalt BHVO-1) and internal standards. For the geochemical plots presented in this report trace elemental data from the ICP-MS were used whenever data was available from both analyses because of the often lower detection limits of the ICP-MS and to reduce variations due to instrumental effects (e.g. drift), which may be different for the two methods.